General Disclaimer

One or more of the Following Statements may affect this Document

- This document has been reproduced from the best copy furnished by the organizational source. It is being released in the interest of making available as much information as possible.

- This document may contain data, which exceeds the sheet parameters. It was furnished in this condition by the organizational source and is the best copy available.

- This document may contain tone-on-tone or color graphs, charts and/or pictures, which have been reproduced in black and white.

- This document is paginated as submitted by the original source.

- Portions of this document are not fully legible due to the historical nature of some of the material. However, it is the best reproduction available from the original submission.

Produced by the NASA Center for Aerospace Information (CASI)

FINAL REPORT

September 15, 1968 - September 15, 1969

A SPACE COMMUNICATIONS STUDY

for

National Aeronautics and Space Administration

Electronic Research Center

under

NASA GRANT NGR-33-006-020

Prepared by

Donald L. Schilling, Associate Professor
Raymond L. Pickholtz, Associate Professor
Kenneth K. Clark, Professor

PIBEE 69-006

1969

DEPARTMENT OF ELECTRICAL ENGINEERING
POLYTECHNIC INSTITUTE OF BROOKLYN

N70-154[illegible] (ACCESSION NUMBER) (THRU)
101 (PAGES) 1 (CODE)
CR-107456 (NASA CR OR TMX OR AD NUMBER) 07 (CATEGORY)
FACILITY FORM 602

A SPACE COMMUNICATIONS STUDY

Final Report

PIBEE 69-006

September 15, 1968 - September 15, 1969

Prepared for

National Aeronautics and Space Administration

Electronic Research Center

Under

NASA GRANT NGR-33-006-020

Donald L. Schilling,
Associate Professor
Principal Investigator

Raymond L. Pickholtz,
Associate Professor
Co-Principal Investigator

Kenneth K. Clarke,
Professor,
Co-Principal Investigator

DEPARTMENT OF ELECTRICAL ENGINEERING
POLYTECHNIC INSTITUTE OF BROOKLYN

TABLE OF CONTENTS

Introduction

This final report summarizes all of the research sponsored by the National Aeronautics and Space Administration under the Grant NGR-33-006-020 for the period 15 September 1968 through 15 September 1969. The research supported by this grant encompasses the problems of receiving analog and digital signals which have been transmitted through a noisy channel. Frequency modulation is emphasized, with particular attention focused on the problem of threshold extension. Throughout the study, theory and experiment were worked hand-in-hand with approximately equal effort expended on each.

Part I of this report discusses Threshold Extension. The distinction between Spikes and Cycle Slips are first discussed. A discussion of the FMFB follows. The canonical equations are presented along with some results regarding extreme-case operation. Then some experimental results are presented concerning "clicks" in the FMFB.

Part II considers Single Sideband FM - and why not to use it, and optimum preemphasis. Here it is shown that 2dB or more can be gained by using an optimum preemphasis network.

Part III considers a Slow Scan Digital TV System. Here a complete computer controlled system is presented which transfers information from a photographic slide into a stored digital form. Measurements and Coding are possible.

Part IV deals with a recursive second order gradient algorithm.

The results of this grant represent a significant step forward in the theory of operation of FM systems. This grant has also served to support the publication of a large number of papers, as well as many masters and PhD dissertations.

Participating in this program were:

Professors - R. Boorstyn

K. Clarke

D. Hess

J. Oberst

R. Pickholtz

H. Schachter

D. Schilling

Messrs. - E. Hoffman

A. Snider

F. Cassara

The final report was prepared by

Professors - D. L. Schilling

R. L. Pickholtz

K. K. Clarke

I. Threshold Extension

1.1 Spikes and Cycle Slips in the Phase Locked Loop

In 1961 Rice[1] showed that the output of an FM discriminator could be represented near threshold by 3 terms: the modulating signal m(t); a smooth noise term, commonly called the FM noise having a power spectral density proportional to f^2; and an impulsive noise term having an approximately "white" power spectral density.

In 1963 Schilling[2] proposed an identical model for the Phase Locked Loop (PLL) and the Frequency Demodulator Using Feedback (FMFB). It was later learned, in private correspondence with S. O. Rice, that Rice's original model was for the FMFB and the FM discriminator was merely a special case of that system when the feedback was equal to zero.

At approximately the same time Viterbi[3], using a procedure developed by Tikonov, obtained the phase distribution at the output of a PLL when the input is an unmodulated carrier embedded in white Gaussian noise. Viterbi showed that the PLL "slips cycles" in the presence of the noise.

It is important to note that while Schilling and Viterbi both studied the PLL, the use and hence the design is quite different. Schilling considered a PLL demodulator to demodulate an FM signal in noise with low distortion. This application requires a relatively "wideband" PLL preceded by an IF filter of comparable bandwidth. Viterbi, Lindsey, and others have considered using the PLL for carrier tracking. In this application we are interested in the VCO output not its input. The PLL employed is a narrowband device preceded by an IF filter of much wider bandwidth (the input noise is white compared to the PLL). In the demodulator application we consider "spike (impulsive)" noise, while in the carrier tracking application "cycle slipping" is considered. It is the purpose of this report to compare cycle slipping and the spikes.

To compare cycle slipping and spikes we choose an example which is fictional, but has the advantage that it can be calculated by hand without needing a digital computer.[4] Figure 1 shows a 1st-order PLL, having an input

$$v_i(t) = R(t) \sin(\omega_o t + \phi(t)) \tag{1}$$

To simplify our problem we consider a phase detector having the characteristic shown in Fig. 2. Then if the error phase ψ:

$$\psi = \phi - G_o \int_{-\infty}^{t} v_o(\lambda)\, d\lambda \tag{2}$$

is less, in magnitude, than $\pi/2$,

$$v_o(t) = \frac{2}{\pi} \psi(t) = \frac{2}{\pi} \left[\phi(t) - G_o \int_{-\infty}^{t} v_o(\lambda)\, d\lambda \right] \tag{3a}$$

or

$$\dot{v}_o(t) + \frac{2G_o}{\pi} v_o(t) = \frac{2}{\pi} \dot{\phi}(t) \tag{3b}$$

and

$$\psi(t) = \frac{\pi}{2} v_o(t) \quad . \tag{4}$$

If, however, $\frac{\pi}{2} \leq \psi \leq \frac{3\pi}{2}$, then

$$v_o(t) = 2 - \frac{2}{\pi} \psi(t) = 2 - \frac{2}{\pi} \left[\phi(t) - G_o \int_{-\infty}^{t} v_o(\lambda)\, d\lambda \right] \tag{5a}$$

or

$$\dot{v}_o(t) - \frac{2G_o}{\pi} v_o(t) = -\frac{2}{\pi} \dot{\phi}(t) \tag{5b}$$

and

$$\psi(t) = \frac{\pi}{2} (2 - v_o(t)) \ . \tag{6}$$

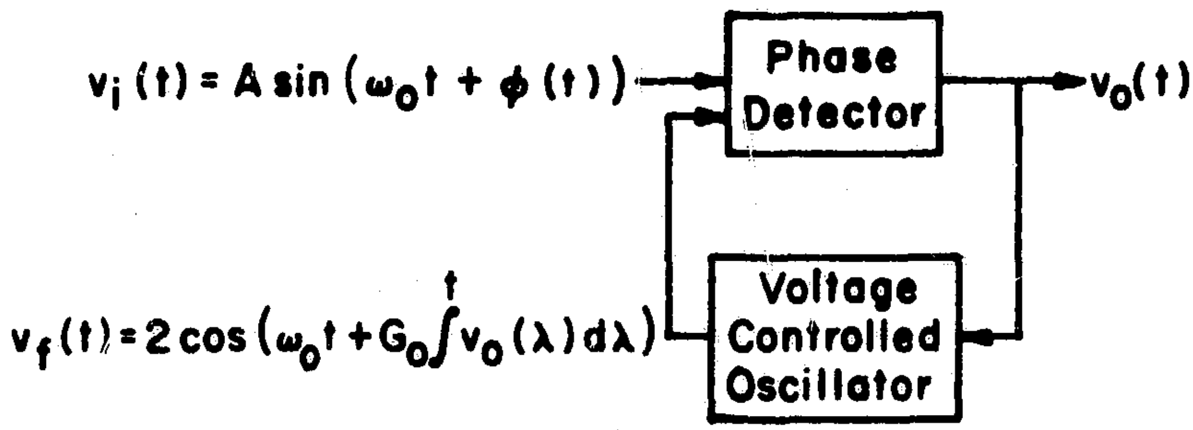

Fig. 1 A Phase Locked Loop

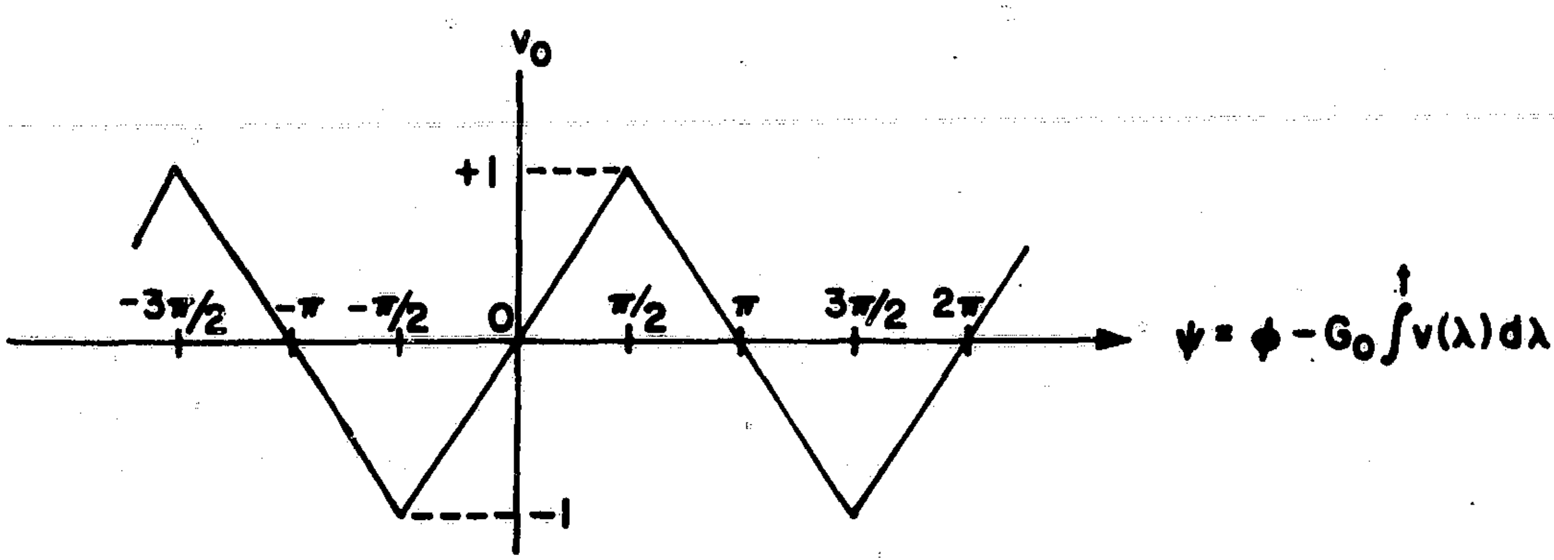

Fig. 2 Phase Detector Characteristic

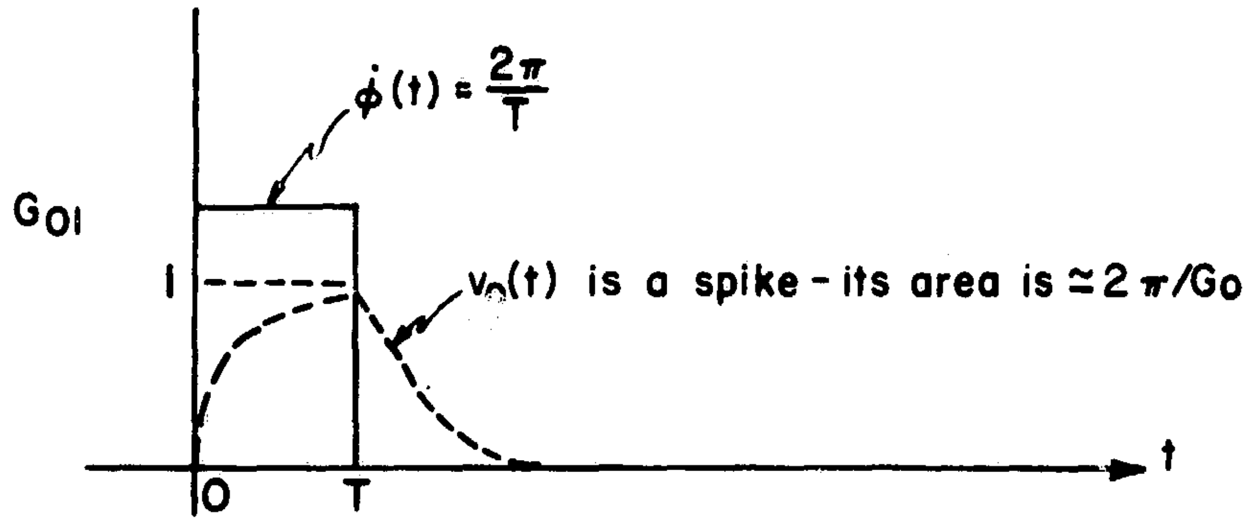

(a) ν_0 (t) is a spike, $|\psi(t)| < \frac{\pi}{2}$

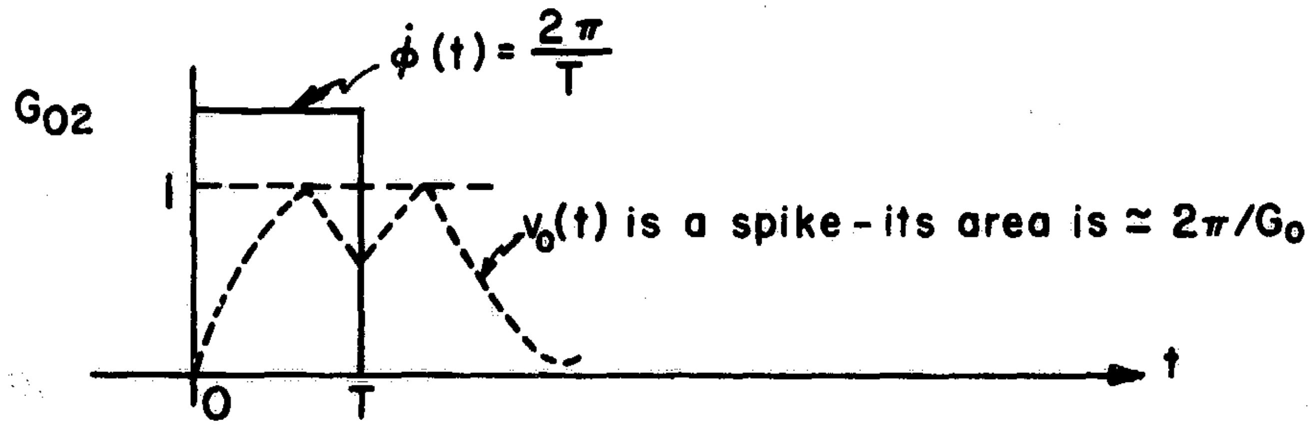

(b) ν_0 (t) is a spike, $|\psi(t) < \pi$.

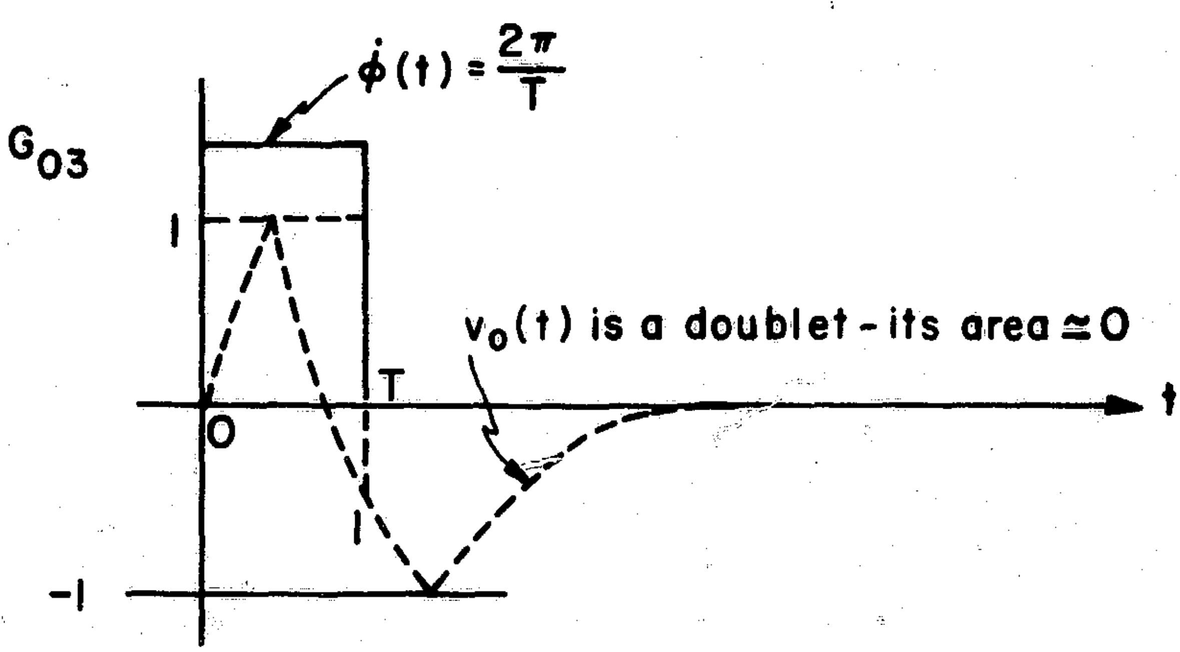

(c) ν_0 (t) is a doubles, ψ(t) goes to 2π.

Fig. 3 $G_{01} > G_{02} > G_{03}$ Conditions for a Spike and Doublet

Let us now consider that $v_i(t)$ in Eq. 1 represents an unmodulated carrier embedded in noise. Then R(t) is the envelope of the carrier amplitude and the noise, and $\phi(t)$ is the phase rotation of the envelope due to the noise. The output of an FM discriminator is $\dot{\phi}(t)$. Let us now assume that at $t = 0$, $\phi(t)$ changes by 2π; i.e., that the noise causes a 2π rotation of the envelope R(t) about the real axis. The discriminator produces a spike under these conditions. We will now determine the response of the PLL.

To analyze this problem simply we will assume that $\phi(t)$ rotates 2π radians in a linear manner:

$$\phi(t) = \begin{cases} \frac{2\pi}{T} t & 0 \leq t \leq T \\ 0 & \text{elsewhere} \end{cases} \tag{7}$$

<u>Case 1.</u> $G_o > \frac{2\pi}{T}$

Using Eq. 3b we have

$$v_o(t) = \begin{cases} \frac{2\pi}{TG_o}\left(1 - e^{-\frac{2G_o}{\pi}t}\right) & 0 \leq t \leq T \\ \frac{2\pi}{TG_o}\left(1 - e^{-\frac{2G_oT}{\pi}}\right) e^{-\frac{2G_ot}{\pi}} & t > T \end{cases} \tag{8}$$

In this case $v_o(t)$ is always less than unity. Hence

$$|\psi(t)| < \frac{\pi}{2} \tag{9}$$

Thus, for a "large" gain G_o, ψ remains less than $\frac{\pi}{2}$ and there is no cycle slipping. However, $v_o(t)$ "follows" $\dot{\phi}(t)$ and hence a spike is produced. Note that the area of $v_o(t)$ is approximately $2\pi / G_o$. This is illustrated in Fig. 3a.

<u>Case 2.</u> $G_o < \frac{2\pi}{T}$

In this case $v_o(t)$ reaches unity and hence $\psi(t)$ reaches $\frac{\pi}{2}$ when $t = T_1 << T$. Eqs. (5) and (6) must then be employed to finish the calculation for $v_o(t)$. Referring to Eq. (5b), and letting $v_c(t_1) = 1$, we have

$$v_o(t) = \frac{2\pi}{T G_o}\left(1 - e^{\frac{2G_o}{\pi}[t - T_1]}\right) + 1\, e^{\frac{2G_o}{\pi}(t - T_1)} \qquad (10)$$

$$T_1 < t < T$$

Two possibilities now exist. The first possibility is that, although $v_o(t)$ is decreasing from +1 to -1, $v_o(T) > 0$ ($\frac{\pi}{2} \leq \psi < \pi$). In this case (see Fig. 2) one can easily show that for $t > T$, $v_o(t)$ increases again to +1 and then decreases to zero. Thus $\psi(t)$ decreases from its maximum value attained at $t = T$ (note that this value is less than π) to 0. The result, shown in Fig. 3b, is a spike.

The second possibility is that at time $t = T$, $v_o(T) < 0$. In this case (see Fig. 2) $v_o(t)$ continues to decrease to -1 and then increase to zero. Thus, $\psi(t)$ continues to increase to 2π. This result is shown in Fig. 3c. Note that the "doublet" occurs when $\psi(t)$ moves through 2π radians; i.e., the PLL <u>slips a cycle.</u> Note also that the cycle slip results for the smallest of the three gains: $G_{03} < G_{02} < G_{01}$ as shown in Fig. 3.

Conclusion

We have demonstrated for the simple case of an unmodulated carrier the simple case of an unmodulated carrier in noise that if there is an FM discriminator spike, then there will be a PLL spike if there is no cycle slip, but if a cycle is slipped no PLL spike results. We have shown furthermore that to avoid a spike the gain G_o should be made as small as possible. However, decreasing G_o decreases the PLL bandwidth and therefore increases distortion. Thus a compromise must be made between pike rejection and distortion.

References

1. Rosenblatt, M. Time Series Analysis, Chapt 25, J. Wiley and Sons Inc., 1963.
2. Schilling, D. L. and Billig, J., " On the Threshold Extension Capability of the PLL and the FMFB, Proc. IEEE, May 1964.
3. Viterbi, A. " Phase Locked Loop Dynamics by Fokker Planck Techniques", Proc. IEEE, Dec. 1963.
4. Taub, H. and Schilling, D. L., " Principles of Communication Systems, Chapt 10, McGraw-Hill Book Co. 1970.

1.2 The Frequency Demodulator Using Feedback

1.2.1 Canonical Equations and Limiting Conditions

Introduction

Although the Frequency Demodulator with Feedback (FMFB) has been the subject of much discussion and debate since the late 1930's, the fundamental equations governing its operation under arbitrary inputs, and the solution of these equations have not been published.

In this paper we present these fundamental equations of operation for a first order FMFB and for a second order FMFB with a baseband filter. It is shown that the equations may be extended, using the basic technique employed here to describe the operations of higher order loops of any order.

The asymptotic operations of the FMFB at the extreme values of its parameters are then derived. It is demonstrated that for a large feedback gain G, or for a wide IF bandwidth α, the operation of the FMFB approaches that of the FMD. For very small feedback gain G, the FMFB again reduces to an FMD which is preceded by the IF filter.

Fundamental Equations

The FMFB to be analyzed is shown in Fig. 1. The input to the RF filter is composed of the sum of the RF signal and additive white gaussian noise of two-sided spectral density $\eta / 2$. The output of the RF filter (which is the input to the FMFB) is a phasor, e_{in}, which may be decomposed along orthogonal components of the unmodulated signal as shown in Fig. 2.

We define:

ω_o = signal carrier frequency

$\phi_m(t)$ = signal modulation angle

$x(t)$ = in-phase component of noise at RF filter output

$y(t)$ = quadrature component of noise at RF filter output.

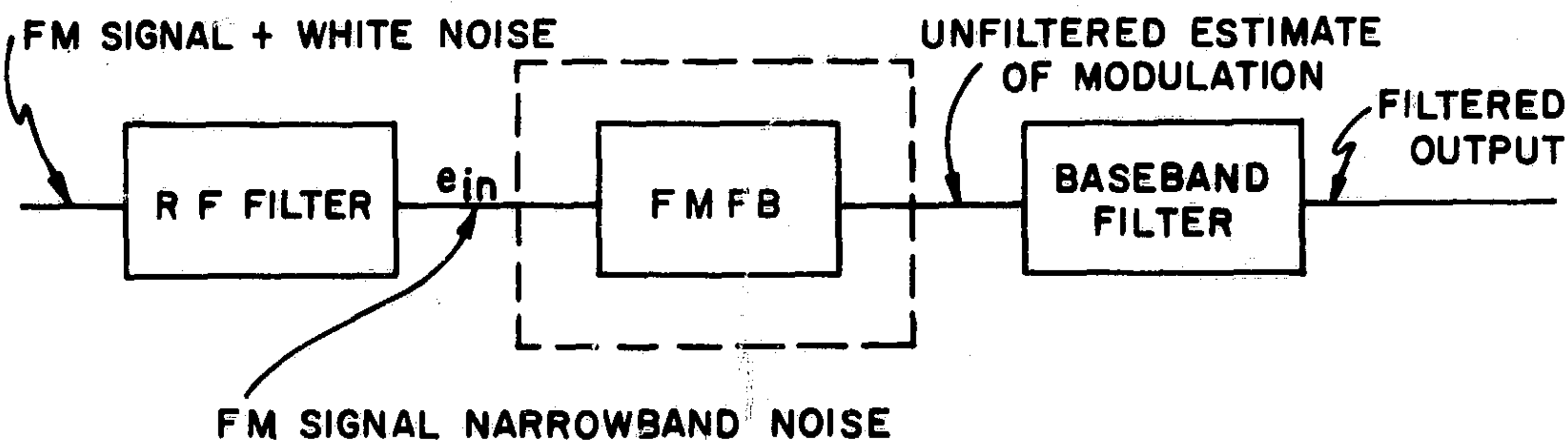

Fig. 1. FMFB used to Demodulate FM Signal

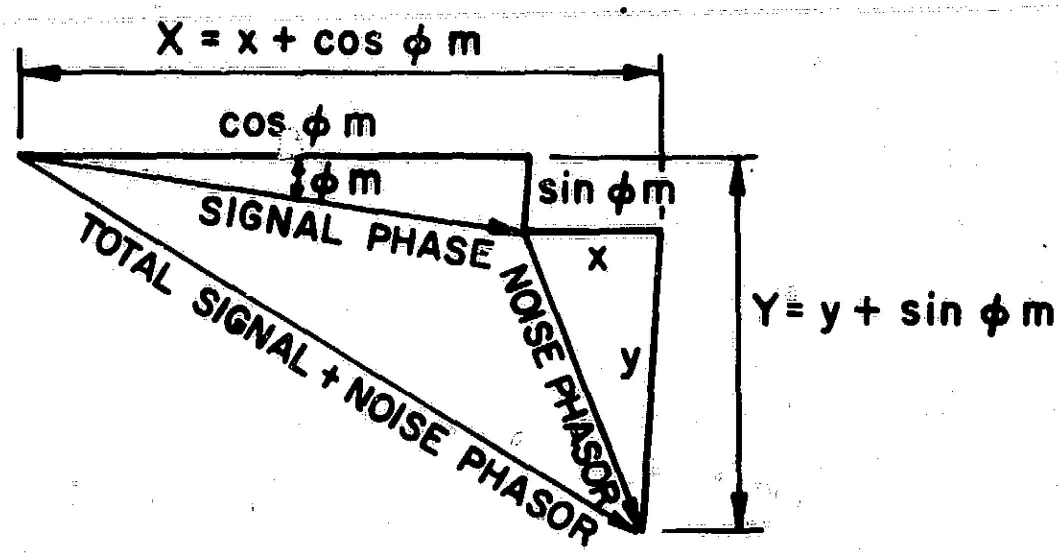

Fig. 2. Input Phasor Modulated Signal and Noise

Hence,

$$e_{in} = X(t) \cos \omega_o t - Y(t) \sin \omega_o t \qquad (1)$$

where

$$X(t) = x(t) + \cos \phi_m(t) \qquad (2)$$

and

$$Y(t) = y(t) + \sin \phi_m(t) \qquad (3)$$

An unmodulated signal of unity amplitude is assumed.

The block diagram of the FMFB is shown in Fig. 3. The input signal plus noise is applied to the multiplier whose output is e_m. The second input to the multiplier is e_{VCO}, the output of the Voltage Controlled Oscillator (VCO). The VCO is centered quiescently at $(\omega_o + \omega_1)$, while e_{in}, in accordance with Eq. (1), is centered at ω_o. The multiplier output e_m feeds the IF filter in the loop which is centered at the difference frequency, ω_1. The IF filter output, e_f, is applied to an ordinary FMD which is assumed to have an ideal amplitude limiter and thereby acts as a differentiator of the phase of e_f. The output of the FMD is fed to a baseband filter, in the case of the higher order FMFB.

We consider first the simplest case, that of a first order FMFB and thus connect the FMD output directly to an amplifier of gain G. The output of this amplifier is $\dot{\phi}$ and is directly proportional to the frequency of the VCO. Since the FMD eliminates all amplitude information, e_f is of the form $A \cos(\omega_1 t + \frac{\phi}{G})$, where A is the time varying envelope of the input to the ideal limiter. The gain constants of the FMD and VCO are assumed to be unity. When this is not the case, these gains may be lumped into G.

The output of the FMFB demodulator $\dot{\psi}$ is obtained by amplifying the demodulated signal by a gain (G + 1) which serves to restore the gain constant, from input to output under ordinary demodulation, to unity.

We denote the output of the VCO as:

$$e_{VCO} = 2 \left[\cos (\omega_o + \omega_1)t + \phi(t)\right] \tag{4}$$

The amplitude of e_{VCO} may be chosen arbitrarily, since the FMD possesses an ideal limiter. The value of 2 is chosen for simplicity. The multiplier output is:

$$e_m = (e_{in})(e_{VCO}) \tag{5}$$

When eq. (1) and eq. (4) are substituted in eq. (5) and standard trigonometric identities are applied, we get:

$$\begin{aligned} e_m &= X \cos (\omega_1 t + \phi(t)) + Y \sin (\omega_1 t + \phi(t)) \\ &\quad + X \cos ([2\omega_o + \omega_1] t + \phi(t)) - Y \sin ([2\omega_o + \omega_1] t + \phi(t)) \end{aligned} \tag{6}$$

The IF filter for the first order FMFB is an RLC with a 3 dB half bandwidth α and a low pass equivalent transfer function $H(\omega)$ given by:

$$H(\omega) = \frac{\alpha}{S + \alpha} \tag{7}$$

Since the IF filter is centered at ω_1, a sufficiently large carrier frequency ω_o will insure the validity of the use of the low-pass equivalent of the filter. This results in neglecting of the last two terms of the right hand side of eq. (6) because terms at $(2\omega_o + \omega_1)$ are greatly attenuated by the IF filter. The baseband equivalent of the loop may therefore be utilized, which results in the IF filter input and output as shown in Fig. 4.

For the RLC type IF filter shown we have:

$$\alpha e_m = \alpha e_f + \frac{d}{dt} e_f \tag{8}$$

With e_m and e_f as shown in Fig. 4, and using eq. (8) we obtain:

$$\alpha[X \cos \phi + Y \sin \phi] = (\alpha A + \dot{A}) \cos \frac{\phi}{G} - \frac{A\dot{\phi}}{G} \sin \frac{\phi}{G} \tag{9}$$

One recognizes that the right hand side of eq. (9) is a phasor expressed in terms of quadrature components along the angle $\frac{\phi}{G}$. The left hand side is a phasor expressed in terms of components relative to an angle ϕ. We endeavor to project the left hand side along the orthogonal components of the angle ϕ/G. To do this we first define the parameter γ:

$$\gamma = \frac{G+1}{G} \tag{10}$$

Then substituting eq. (10) into eq. (9), we obtain:

$$\alpha\left[Y \sin(\gamma\phi - \frac{\phi}{G}) + X \cos(\gamma\phi - \frac{\phi}{G})\right] = (\dot{A} + \alpha A) \cos \frac{\phi}{G} - \frac{\dot{\phi} A}{G} \sin \frac{\phi}{G} \tag{11}$$

or:

$$\alpha\left[Y \sin\gamma\phi \;\gamma\; X \cos\gamma\phi\right]\cos \frac{\phi}{G} + \alpha\left[- Y \cos\gamma\phi + X \sin\gamma\phi\right]\sin \frac{\phi}{G}$$
$$= (\dot{A} + \alpha A) \cos \frac{\phi}{G} - \frac{\dot{\phi} A}{G} \sin \frac{\phi}{G} \tag{12}$$

In eq. (12), the components along each orthogonal projection must be equal. Then:

$$\dot{\phi} = \frac{G\alpha}{A}\left[Y \cos\gamma\phi - X \sin\gamma\phi\right] \tag{13}$$

and

$$\dot{A} = \alpha\left[Y \sin\gamma\phi + X \cos\gamma\phi\right] - \alpha A \tag{14}$$

The external amplifier to the loop, of gain (G + 1) establishes the relation between the FMD output $\dot{\phi}/G$ and the demodulator output $\dot{\psi}$:

$$\dot{\psi} = (G+1) \frac{\dot{\phi}}{G} \tag{15}$$

If one assumes negligible delay within the loop,

$$\psi = \frac{(G+1)}{G} \phi \tag{16}$$

We substitute eq. (16) into eq. (13) and eq. (14) to get:

$$\dot{\psi} = [\, Y \cos \psi - X \sin \psi \,] \frac{G + 1)\alpha}{A} \tag{17}$$

and

$$\dot{A} = \alpha \,[\, Y \sin \psi \gamma X \cos \psi] - \alpha A \tag{18}$$

Eq. (17) and Eq. (18) are the fundamental equations of the first order FMFB. They are given in a canonical form which make them readily available to computer solution. In general, one is interested in the statistics of $\dot{\psi}$ when X and Y are composed of an arbitrary modulation and gaussian noise. A closed form solution of eq. (17) and eq. (18) under these conditions is not available. However, the use of the "Most-Likely Trajectory" of the noise has provided a deterministic noise model for which a computer solution has been obtained.

Higher order loops may be obtained by insertion of a baseband filter in the feedback loop or by utilization of IF filters of higher degree. This distinction is not trivial, since the effect of the filtering in the two cases is quite different. Combinations of the two kinds of higher degree loops are also feasible but subject to stability considerations.

When a baseband filter is inserted in the feedback path as shown in Fig. 5, the operating equations may be derived in a manner similar to that of the first order loop up to the point where e_f is related to e_m. We now write:

$$\alpha\,[X \cos \phi + Y \sin \phi] = (\dot{A} + \alpha A) \cos \frac{\lambda}{G} - \frac{\dot{\lambda} A}{G} \sin \frac{\lambda}{G} \tag{19}$$

where $\frac{\dot{\lambda}}{G}$ is the output of the FMD.

Rewriting the left hand side of eq. (19) we obtain:

$$\alpha[X \cos[(\phi + \frac{\lambda}{G}) - \frac{\lambda}{G}] + Y \sin[(\phi + \frac{\lambda}{G}) - \frac{\lambda}{G})] = (\dot{A} + \alpha A) \cos \frac{\lambda}{G} - $$

$$- \frac{\dot{\lambda} A}{G} \sin \frac{\lambda}{G} \tag{20}$$

Using trigonometric identities and equating coefficients of the orthogonal projections we get, as in eq. (13) and eq. (14)

$$\dot{\lambda} = \frac{G\alpha}{A}\left[Y \cos\left(\frac{\lambda}{G} + \phi\right) - X \sin\left(\frac{\lambda}{G} + \phi\right)\right] \tag{21}$$

and

$$\dot{A} = \alpha\left[Y \sin\left(\frac{\lambda}{G} + \phi\right) + X \cos\left(\frac{\lambda}{G} + \phi\right)\right] - \alpha A \tag{22}$$

The relationship between λ and ϕ is obtained from the baseband filter characteristics.

Consider a first order baseband filter, which correspond to a second order FMFB. The zero of the filter is located at γ and the pole at B. Let the d-c transfer function be unity. We then obtain:

$$\frac{\dot{\phi}}{B}\ \gamma\,\phi = \frac{\dot{\lambda}}{\gamma} + \lambda \tag{23}$$

In order to restore the scale factor to unity we insert an external amplifier of gain (G + 1) as shown in Fig. 5. The following relationships are then established:

$$\frac{\theta}{G+1} = \frac{\lambda}{G} \tag{24}$$

and

$$\frac{\varphi}{G+1} = \frac{\phi}{G} \tag{25}$$

Using eq. (24) and eq. (25) in eq. (21), eq. (22) and eq. (23), we obtain:

$$\dot{\theta} = \frac{G+1\,\alpha}{A}\left\{ Y \cos\left[\frac{\theta}{G+1} + \frac{G\varphi}{G+1}\right] - X \sin\left[\frac{\theta}{G+1} + \frac{G\varphi}{G+1}\right]\right\} \tag{26}$$

$$\dot{A} = \alpha\left\{ Y \sin\left[\frac{\theta}{G+1} + \frac{G\varphi}{G+1}\right] + X \cos\left[\frac{\theta}{G+1} + \frac{G\varphi}{G+1}\right]\right\} - \alpha A \tag{27}$$

and

$$\dot{\psi} = B\left\{\theta - \varphi + \frac{\dot{\theta}}{\gamma}\right\} \tag{28}$$

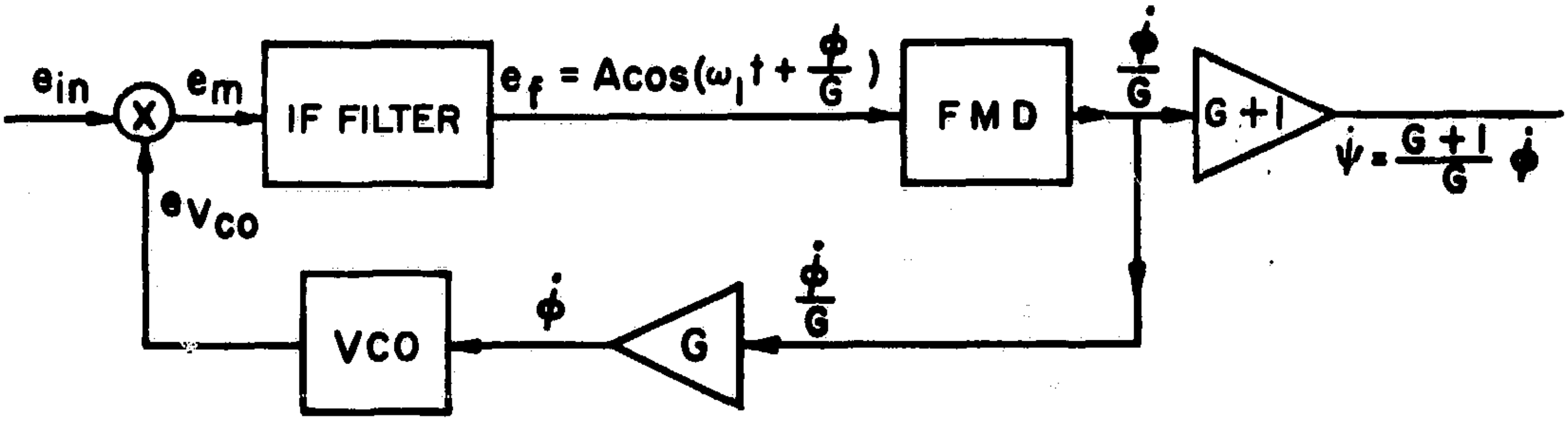

Fig. 3. First Order FMFB Block Diagram

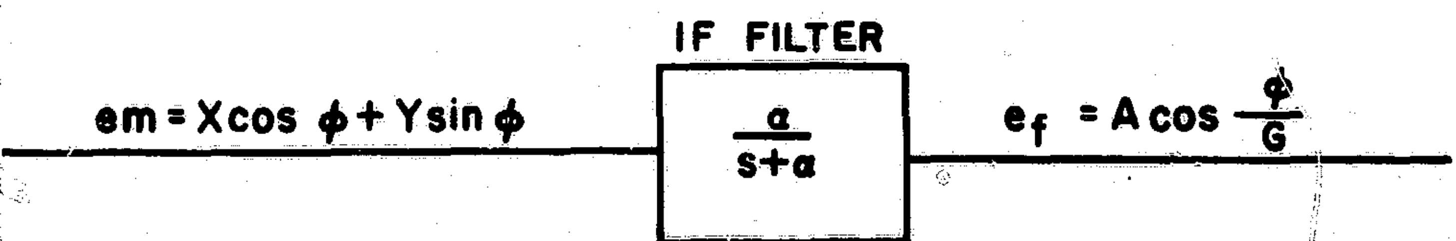

Fig. 4. Baseband Equivalent of IF Filter

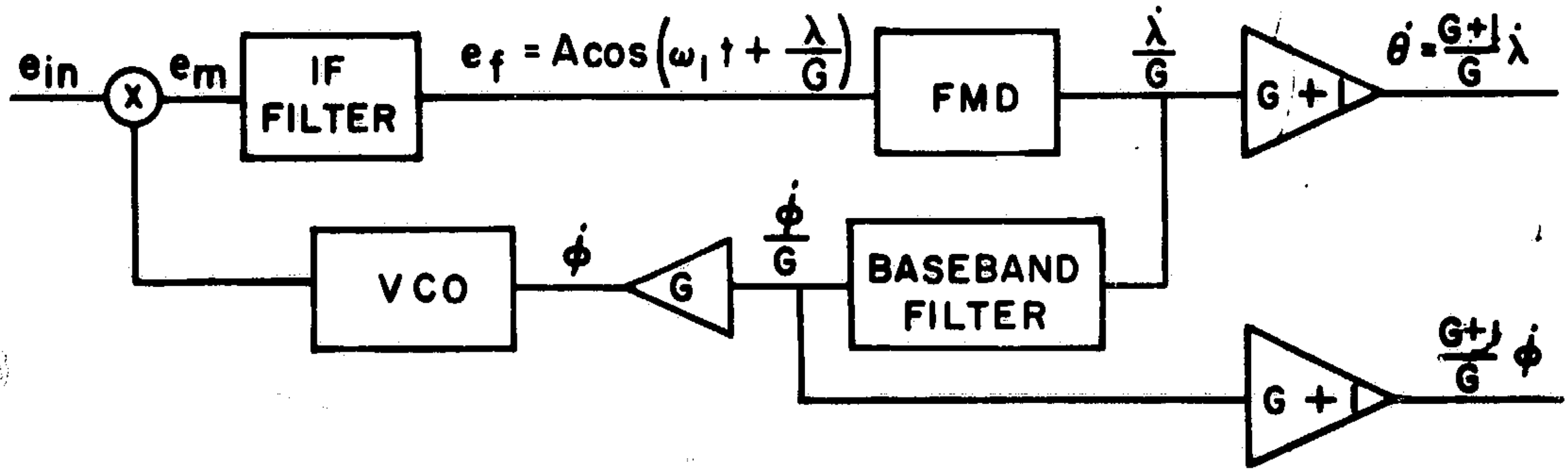

Fig. 5. Higher Order FMFB - Block Diagram

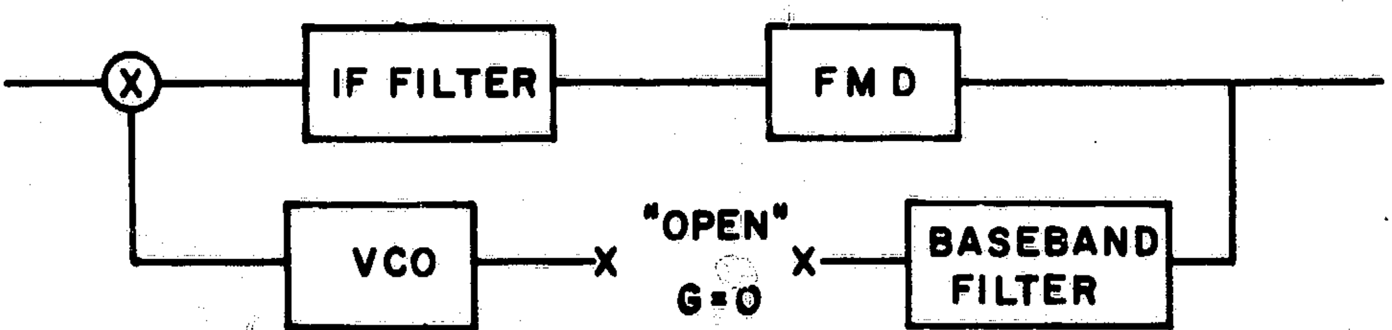

Fig. 6. FMFB Reduces to FMD Preceded by IF Filter when G = 0

Eq. (28) may be rewritten, using eq. (26), as:

$$\dot{\varphi} = B\left\{\theta - \omega + \frac{G+1}{\gamma A}\alpha \left[Y\cos\left(\frac{\theta}{G+1} + \frac{G\varphi}{G+1}\right) - X\sin\left(\frac{\theta}{G+1} + \frac{G\varphi}{G+1}\right)\right]\right\} \tag{29}$$

Equations (26), (27) and (29) represent the canonical form of the fundamental equations for the second order FMFB, with the state variables chosen as θ, φ and A.

For the Nth order loop, equations (26) and eq. (27) remain unchanged. It is merely required to state the relationship between the filter input and output (i.e., $\frac{\dot{\lambda}}{G}$ and $\frac{\dot{\phi}}{\phi}$) corresponding to eq. (23). With the use of eq. (24) and eq. (25), the equivalent of eq. (29) for the Nth order loop is then obtained. The canonical form may again be derived by proper selection of the state variables.

When, instead of a baseband filter, a higher order IF filter is used, the new differential equation relating e_m to e_f must be specified. The technique employed in solving for the fundamental equations employs a projection of e_f along ϕ/G as was done for the first order FMFB.

Asymptotic Operation at Extreme Values of the Parameters.

Since an exact solution to the fundamental equations under arbitrary conditions is not available, it is instructive to determine the behavior of the FMFB under extremely large and small values of its parameters.

CASE I - α approaches infinity; any G, First Order FMFB

The behavior of this FMFB is equivalent to one without an IF filter. From eq. (17) of the fundamental equations, for the first order FMFB:

$$\lim_{\alpha \to \infty} \frac{A\dot{\psi}}{(G+1)\alpha} = 0 = Y\cos\psi - X\sin\psi \tag{30}$$

Hence, $$\tan\psi = \frac{Y}{X} \tag{31}$$

This relationship shows that operation is identical to that of the FMD since the output angle is identical to the input angle to the FMFB. From eq. (18) we obtain:

$$A = Y \sin \psi + X \cos \psi \tag{32}$$

Using eq. (31) and eq. (32) we obtain:

$$A = Y \frac{Y}{\sqrt{X^2 + Y^2}} + X \frac{X}{\sqrt{X^2 + Y^2}} = \sqrt{X^2 + Y^2}$$

The input amplitude A to the FMD, internal to the FMFB, is simply the input amplitude to the loop. With no IF filter present, this is precisely the expected intuitive result.

__2nd Order FMFR__

In the second order loop, we define the angle u as,

$$u = \frac{\theta}{G+1} + \frac{G\phi}{G+1} \tag{33}$$

Since θ and ϕ are linearly related, the angle u is proportional to the input phase angle, and the second order loop acts as an FMD with additional filtering in the output. It is worth noting that although elimination of the IF filter reduces the system to an FMD, elimination of the baseband filter rather than the IF filter does not have the same effect.

__CASE II__ - G approaches infinity; finite α

From eq. (17) we obtain:

$$\lim_{G \to \infty} \frac{A\dot{\psi}}{(G+1)\alpha} = 0 = Y \cos \psi - X \sin \psi \tag{32}$$

hence,

$$\tan \psi = \frac{Y}{X} \tag{33}$$

Thus, we again have FMD-like operation as in case 1, with α approaching infinity.

From eq. (18) and eq. (33) we have:

$$\dot{A} + \alpha A = \alpha \left[X \cos \psi + Y \sin \psi \right] = \alpha \sqrt{X^2 + Y^2}$$

Thus, the effect of the IF filter is reflected in amplitude information only, which is lost in the limiter of the FMD.

Here, as in the case when α approaches infinity, the second order loop acts as a "filtered" FMD.

<u>CASE III</u> - G approaches zero

The case where G approaches zero is equivalent to an "opened" feedback path, as illustrated in Fig. 6. This case is equivalent to simple heterodyning of the input signal to the IF filter center frequency. Thus, operation is identical to an ordinary FMD preceded by the IF filter. Hence the FMD may be treated as a special case of the FMFB with G approaching zero.

Conclusions

The fundamental equations of the FMFB, for the first and second order case have been presented in canonical form. It was shown that the basic technique employed in the derivation may be extended to higher order loops.

The asymptotic operation of the FMFB was found to approach the performance of the ordinary FMD for very large values of feedback gain G, or IF filter bandwidth α. For very small G, the FMFB reduces to an FMD preceded by an extra IF filter.

These results have been used to calculate IM and harmonic distortion in the FMFB and the FMD, and to determine the threshold characteristics of these devices.

I. 2. 2 Noise " Clicks" in the FM Demodulator with Feedback

Introduction

It is well known[1] that the limiter discriminator, phase-locked loop (PLL), frequency locked loop (FLL), [2] and frequency demodulator with feedback (FMFB) may be employed as FM detectors. The most rewarding technique to predict the FM noise threshold of these demodulators focuses its attention on FM noise " clicks". For those devices which experience the cycle slipping phenonemon[3] (e.g., PLL and FMFB) experimental studies indicate two types of " clicks" of the first and second kind exist. [4] The expected number of " clicks" per second appearing at the output of a limiter discriminator and PLL excited by a carrier plus narrow band noise has been determined by Rice[5] and Hess[4] respectively. Rice solves the discriminator problem for both the unmodulated and modulated carrier cases. Hess concerns himself with the calculation of " clicks" of the first kind and hence solves the PLL problem for the unmodulated carrier case only.

Very little literature exists on the computation of the expected number of " clicks" per second appearing at the FMFB output. Hess[6] has established the equivalence between the FMFB (without a limiter in the loop), PLL, and FLL. In particular, he demonstrates that the defining equations of the FMFB degenerate into the equations for the FLL and PLL as the loop IF filter bandwidth of the FMFB approaches infinity and zero respectively.

One of the objectives of this report is to establish the equivalence between the FMFB (with a limiter in the loop), limiter-discriminator, and a PLL type structure. Specifically, it will be shown that as the internal IF filter bandwidth is reduced to zero the defining equation of the FMFB degenerates into a PLL type equation (not the same PLL that the FMFB without limiter degenerates to). Conversely, as the bandwidth increases without bound the equations for the FMFB and limiter discriminator become identical.

The merit in drawing such equivalences is apparent when we consider the physical insight into the FMFB operation that is obtained; moreover, the equivalences provide us with the expected number of "clicks" per second appearing at the output of an FMFB excited by a carrier (unmodulated) plus narrow band noise. Although this technique provides an accurate expression for the expected number of "clicks" only for the two special cases of an FMFB with a very small and very large IF bandwidth, an experimental study made on the first order FMFB indicates that the expression to be derived predicts reasonably well the actual number of "clicks" even for intermediate values of IF bandwidth.

Equivalence Between FMFB (with limiter), PLL, and Limiter Discriminator

The block diagram of a PLL is shown in Figure 1.

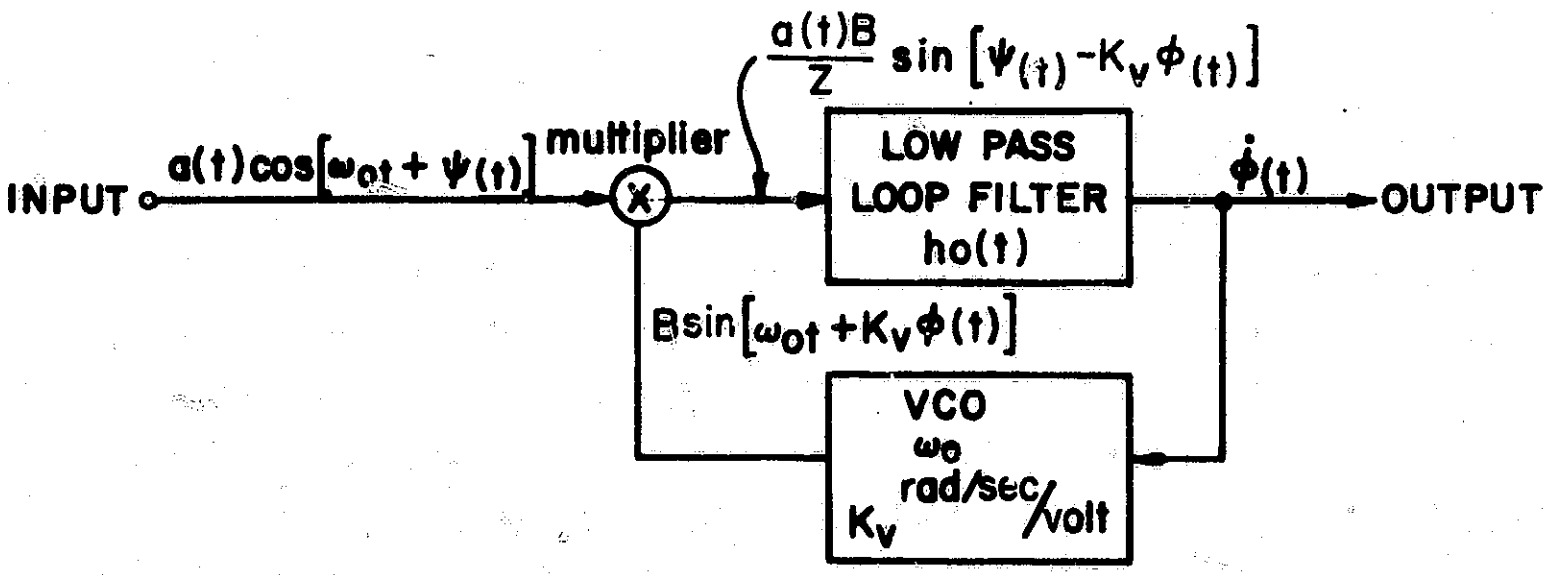

Fig. 1. Block Diagram of Phase Locked Loop

The input is taken to be a carrier of frequency ω_o and amplitude A plus narrow band noise n(t). Such an input signal may be written as

$$a(t) \cos[\omega_o t + \psi(t)] \ .$$

If the output of the loop is designated $\dot{\phi}(t)$ and the voltage controlled oscillator (VCO) constant is taken to be K_v $^{rad/sec}/$volt the VCO output may be written as $B \sin[\omega_o t + K_v \phi(t)]$. The multiplier output is simply

$$\frac{a(t)B}{2} \sin[\psi(t) - K_v \phi(t)] + \text{second harmonic terms.}$$

Assuming the low pass loop filter rejects the second harmonic terms appearing at the multiplier output the defining equation of the PLL becomes

$$\dot{\phi}(t) = \left\{ \frac{a(t)\,B}{2} \sin[\psi(t) - K_v \phi(t)] \right\} * h_o(t) \tag{1}$$

where $h_o(t)$ is the impulse response of the low pass loop filter.

If we define the phase error by $\theta(t) = \psi(t) - K_v \phi(t)$ and the closed loop bandwidth by $\omega_{L,\,PLL} = \frac{AB}{2}$, Equation (1) takes the alternate form

$$\dot{\psi}(t) = \dot{\theta}(t) + \left\{ \frac{a(t)}{A} \omega_{L,\,PLL} \sin\theta(t) \right\} * h_o(t) \tag{2}$$

For the first order PLL, the transfer function of the low pass loop filter is

$$H_o(s) = \mathcal{L}[h_o(t)] = 1 \ .$$

Assuming the second harmonic terms are still rejected, equation (2) reduces to

$$\psi(t) = \dot{\theta}(t) + \frac{a(t)}{A} \omega_{L,\,PLL} \sin\theta(t) \tag{3}$$

Using a model for carrier plus narrow band noise, Hess[4] computes the expected number of "clicks" per second $N_{\pm}$ appearing at the output of a first order PLL. His result is

$$N_{\pm} = \gamma/\pi \;\; \mathrm{erfc}\left[\sqrt{2}\;\; \mathrm{CNR}\left(1 + \frac{1.04\gamma}{\omega_{L,\,PLL}}\right)\right] \tag{4}$$

where, the input voltage carrier to noise ratio is defined by

$$\mathrm{CNR} = A/\sqrt{2N} \tag{5}$$

and $N = E\{n^2(t)\}$ is the total input noise power.

The radius of gyration of the input noise is defined by

$$\gamma = \sqrt{\frac{\int_{-\infty}^{\infty} G_L(\omega)\,\omega^2\, d\omega}{\int_{-\infty}^{\infty} G_L(\omega)\, d\omega}} \tag{6}$$

and $G_L(\omega)$ is the power spectrum of the low pass equivalent of the input noise, and finally,

$$\mathrm{erfc}\; y = 1/\sqrt{2\pi} \int_{y}^{\infty} \epsilon^{-x^2/2}\, dx \tag{7}$$

The differential equation of the FMFB will now be derived. The general case will be considered first. We will then specialize to the case of an FMFB with a very narrow loop IF filter and demonstrate that the defining differential equation of the loop degenerates into a PLL type equation. Some interesting observations will also be pointed out. We then turn to the case of an FMFB with a very broad loop IF filter and demonstrate that its performance is identical to a limiter discriminator.

The block diagram of an FMFB is shown in Figure 2.

For the loop driven by a carrier plus narrow band noise we again write the input as $a(t) \cos [\omega_o t \;\gamma\; \psi(t)]$. If we designate the output by $\dot{\phi}(t)$ and let the VCO constant be K_v $^{\mathrm{rad/\,sec}}/\mathrm{volt}$ the VCO output takes the form $B \cos [\omega_1 t + K_v \phi(t)]$. The multiplier output simply becomes

$$\frac{a(t)\,B}{2} \cos [\omega_2 t + \theta(t)] + \text{second harmonic terms}$$

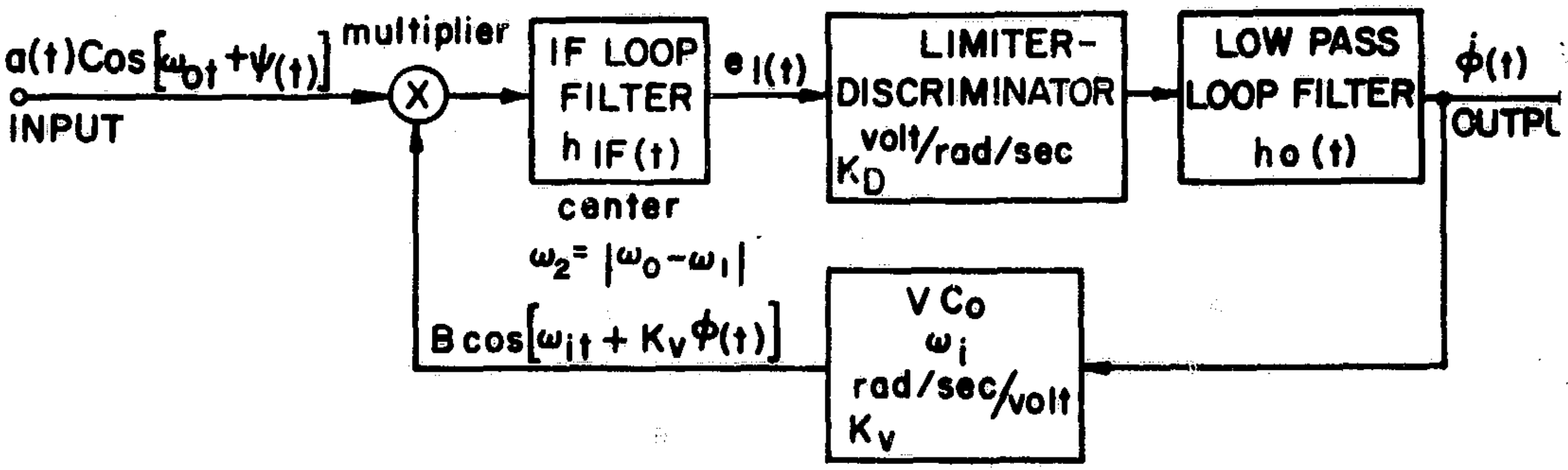

Fig. 2. Block Diagram of Frequency Demodulator with Feedback

where

$$\omega_2 = |\omega_o - \omega_1|$$

and

$$\theta(t) = \psi(t) - K_v\phi(t) \tag{8}$$

Denoting the impulse response of the loop IF filter by $h_{IF}(t)$, the IF output $e_1(t)$ may be written as

$$e_1(t) = \left\{ \frac{a(t)\,B}{2} \cos\left[\omega_2 t + \theta(t)\right] \right\} * h_{IF}(t) \tag{9}$$

Assuming the second harmonic terms in the vicinity of $2\,\omega_2$ are rejected.

Letting $h_L(t)$ be the impulse response of the low pass equivalent of the IF filter we may expand Equation (9) and rewrite in the form

$$e_1(t) = \left[\left\{\frac{a(t)\,B}{2}\cos\theta(t)\right\} * h_L(t)\right]\cos\omega_2 t - \left[\left\{\frac{a(t)\,B}{2}\sin\theta(t)\right\} * h_L(t)\right]\sin\omega_2 t \tag{10}$$

Equation (10) may be rearranged further to yield

$$e_1(t) = (C + c)\cos\omega_2 t - (D + d)\sin\omega_2 t \tag{11}$$

where C and D are the average (dc) values of the coefficients of $\cos \omega_2 t$ and $\sin \omega_2 t$ respectively and c(t) and d(t) are coefficients of $\cos \omega_2 t$ and $\sin \omega_2 t$ less their average values respectively. If the RF filter preceding the loop is symmetric about ω_o and if $\overline{\phi(t)} = 0$, then from symmetry considerations $\overline{\psi(t)} = 0$ and $\overline{a(t) \sin [\psi(t) - K_v \phi(t)]} = 0$; hence D = 0 and

$$d(t) = \left\{ \frac{a(t)\, B}{2} \sin \theta(t) \right\} * h_L(t) \tag{12}$$

Equation (11) now reduces to

$$e_1(t) = \sqrt{(C + c)^2 + d^2} \cos [\omega_2 t + \tan^{-1} d/C + c] \tag{13}$$

Denoting the impulse response of the low pass loop filter by $h_o(t)$ and letting the discriminator constant be K_D volts/rod./sec., the differential equation of the FMFB loop becomes

$$\phi (t) = K_D \tan^{-1} (d/C + c) * h_D(t) * h_o(t) \tag{14}$$

where $h_D(t)$ designates the differentiation operation of the discriminator.

Using Equation (8) and defining the dc feedback factor $F = 1 + K_v K_D$, the defining equation for the FMFB may be written in general as

$$\dot{\psi}(t) = \dot{\theta}(t) + (F - 1) \tan^{-1} (d/C + c) * h_D(t) * h_o(t) \tag{15}$$

We now consider the special case of a narrow IF filter. As the IF bandwidth is reduced to zero C becomes much greater than c(t) and d(t) since more and more of the ac component is filtered out while the dc component remains unchanged. Hence, for this special case of a narrow IF filter we may use the approximation

$$\tan^{-1} d/C + c \doteq d/C \tag{16}$$

Using Equations (16) and (12) Equation (15) may be rewritten as

$$\dot{\psi}(t) = \dot{\theta}(t) + (F - 1)\left\{\frac{a(t)\,B}{2C}\sin\theta(t)\right\} * h_D(t) * h_L(t) * h_o(t) \tag{17}$$

It is interesting to note here that the filtering operations provided by the loop IF filter and the low pass loop filter are completely interchangeable provided the IF bandwidth is narrow enough to make the approximation in Equation (16) a valid one.

To compute $C = \overline{\left\{\frac{a(t)\,B}{2}\cos\theta(t)\right\} * h_L(t)}$ we recognize that for the limiting case of zero IF bandwidth C is just the peak value of the IF carrier, i. e., $e_1(\omega_2)$ peak. This is simply one-half the product of the peak value of the VCO carrier and the input carrier. The peak value of the input carrier is simply A. To determine the peak value of the carrier of the phase modulated signal appearing at the VCO output we use a result of Schwartz, Bennett, and Stein[1] (pp. 167-168). If we consider the phase modulation of the VCO output to be gaussian with zero mean and mean square value much less than one we may write the peak value of VCO carrier as

$$\sqrt{B^2 \exp(-R_{K_v\phi}(0))} = B\exp\left(-\frac{1}{2}R_{K_v\phi}(0)\right)$$

where

$$R_{K_v\phi}(0) = E\left\{[K_v\phi(t)]^2\right\} \ll 1 \tag{18}$$

Hence,

$$C = \frac{AB}{2}\exp\left\{-\frac{1}{2}R_{K_v\phi}(0)\right\}$$

Equation (17) now takes on the form of a PLL equation

$$\dot{\psi}(t) = \dot{\theta}(t) + (F - 1)\exp\left(\frac{1}{2}R_{K_v\phi}(0)\right)\left\{\frac{a(t)}{A}\sin\theta(t)\right\} * h_D(t) * h_L(t) * h_o(t) \tag{19}$$

If the loop IF filter is a single pole RLC circuit, the transfer function of its low pass equivalent may be taken as

$$H_L(s) = \mathcal{L}\,[h_L(t)] = \frac{\omega_{IF}}{s + \omega_{IF}} \quad .$$

In the limiting case as ω_{IF} approaches zero,

$$h_L(t) \longrightarrow \omega_{IF} \int^t (\cdot)\, dt$$

Thus the integration and differentiation operators cancel and Equation (19) may be written as

$$\dot{\psi}(t) = \dot{\theta}(t) + (F-1)\,\omega_{IF} \exp\left(\tfrac{1}{2} R_{K_v\phi}(0)\right) \left\{ \frac{a(t)}{A} \sin\theta(t) \right\} * h_o(t) \qquad (20)$$

Clearly, Equation (20) takes on the same form as the PLL Equation (2) if we relate $\omega_{L,\,PLL}$ to $(F-1)\,\omega_{IF} \exp\left\{\frac{1}{2} R_{K_v\phi}(0)\right\}$. Hence, the equivalence between the FMFB (with limiter) and PLL has been demonstrated.

It is interesting to note here that the FMFB with limiter in the loop does not reduce to the same PLL as the FMFB without limiter. The difference is only slight however, since the term $\exp\left(\frac{1}{2} R_{K_v\phi}(0)\right)$ is near one in order for the assumption in Equation (18) to be valid. It will be shown below that the term $R_{K_v\phi}(0)$ is a function of the input carrier to noise ratio as well as the loop parameters. Another interesting observation that can be made at this point is that like the FMFB without limiter in the loop the FMFB with limiter can have an arbitrarily narrow loop IF filter and still successfully demodulate an FM signal.

We will now compute $R_{K_v\phi}(0)$ for the specific example of the first order FMFB, i.e., when the transfer function of the low pass loop filter $H_o(s) = 1$. From the theory of power spectra

$$R_{K_v\phi}(0) = \int_{-\infty}^{\infty} S_{K_v\phi}(\omega)\, df = \int_{-\infty}^{\infty} S_\psi(\omega)\, |H_c(j\omega)|^2\, df \qquad (21)$$

where $S_\psi(\omega)$ is the power spectral density of $\psi(t)$ and $|H_c(j\omega)|$ is the magnitude of the closed loop transfer function between input of loop and VCO output. If we express the input narrow band gaussian noise with symmetric power spectrum about ω_o by[1]

$$n(t) = x(t)\cos\omega_o t - y(t)\sin\omega_o t \tag{22}$$

then x(t) and y(t) are zero mean statistically independent gaussian processes. If the predetection RF bandwidth is rectangular in shape, symmetric about ω_o, and total bandwidth $B\omega$, then

$$S_x(\omega) = S_y(\omega) = \begin{cases} N/B\omega & |\omega| \le \frac{2\pi\ B\omega}{2} \\ 0 & |\omega| > \frac{2\pi\ B\omega}{2} \end{cases} \tag{23}$$

where $N = E\{n^2(t)\}$ is the total input noise power. $\psi(t)$ may then be written as $\tan^{-1} y/A + x$ where A is the carrier amplitude and for high carrier to noise ratios may be approximated by the gaussian, zero mean, process y/A.

Thus

$$S_\psi(\omega) = \begin{cases} \frac{N}{B\omega\ A^2} & |\omega| \le \frac{2\pi\ B\omega}{2} \\ 0 & |\omega| > \frac{2\pi\ B\omega}{2} \end{cases} \tag{24}$$

To compute $|H_c(j\omega)|$ for the first order FMFB we use the linearized baseband version of the FMFB shown in Figure 3.

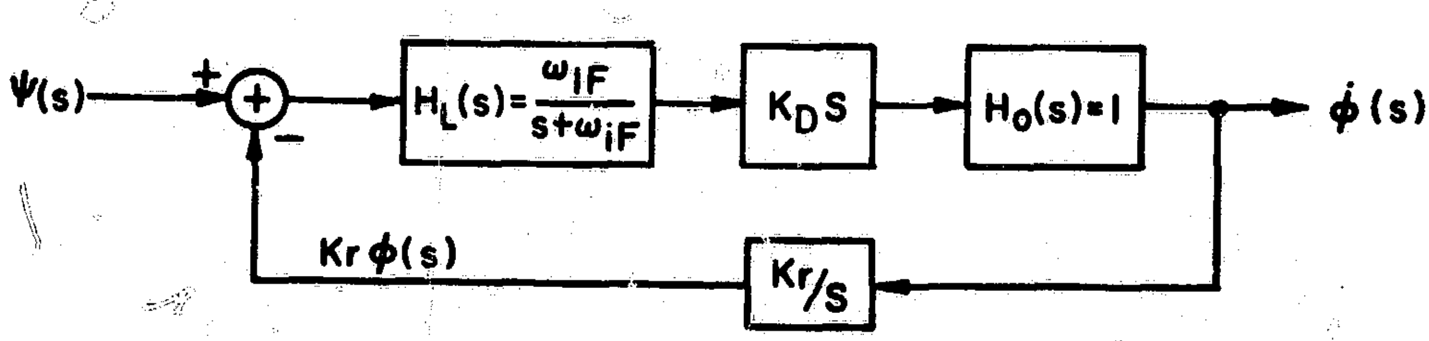

Fig. 3. Linearized Baseband Version of First Order FMFB

Clearly,

$$|H_c(j\omega)|^2 = \left| \frac{K_v K_D \frac{\omega_{IF}}{j\omega + \omega_{IF}}}{1 + K_v K_D \frac{\omega_{IF}}{j\omega + \omega_{IF}}} \right|^2 = \left| \frac{K_v K_D \,\omega_{IF}}{j\omega + \omega_{IF} (1 + K_v K_D} \right|^2 \qquad (25)$$

using the definition $F = 1 + K_v K_D$ and $\omega = 2\pi f$, Equation (25) reduces to

$$|H_c(j\omega)|^2 = \frac{(F-1)^2 f_{IF}{}^2}{f^2 + (f_{IF} F)^2} \qquad (26)$$

Substitution of Equations (24) and (26) into Equation (21) yields,

$$R_{K_v \phi}(0) = \int_{-\frac{B\omega}{2}}^{\frac{B\omega}{2}} \frac{N}{A^2 B\omega} \left[\frac{(F-1)^2 f_{IF}{}^2}{f^2 + (f_{IF} F)^2} \right] df = \frac{N}{A^2} \left(\frac{F-1}{F} \right)^2 \left(\frac{F f_{IF}}{B\omega} \right) \int_{-\frac{B\omega}{2}}^{\frac{B\omega}{2}} \frac{F f_{IF}}{f^2 + (F f_{IF})^2} df \qquad (27)$$

which readily integrates to

$$R_{K_v \phi}(0) = \frac{N}{A^2} \left(\frac{F-1}{F} \right)^2 \left(\frac{2F f_{IF}}{B\omega} \right) \tan^{-1} \left(\frac{B\omega}{2F f_{IF}} \right) \qquad (28)$$

Simple computation will show that $R_{K_v \phi}(0) << 1$ for a carrier to noise ratio in the threshold region, hence the original assumption of Equation (18) is valid.

In summary, the differential equation for the first order FMFB loop reduces to the first order PLL equation

$$\dot{\psi}(t) = \dot{\theta}(t) + (F-1)\,\omega_{IF} \exp\left(\frac{1}{2} R_{K_v \phi}(0) \right) \frac{a(t)}{A} \sin\theta(t) \qquad (29)$$

where, for a loop preceded by a rectangular RF filter of total bandwidth $B\omega$, $R_{K_v \phi}(0)$ is given by Equation (28).

If we now allow the bandwidth of the loop IF filter to become large compared to the band of frequencies occupied by

$$\frac{a(t)\,B}{2}\cos\left[\omega_2 t + \psi(t) - K_v\phi(t)\right],$$

the output of the IF filter becomes simply

$$e_1(t) = \frac{a(t)\,B}{2}\cos\left[\omega_2 t + \psi(t) - K_v\phi(t)\right]$$

(assuming the second harmonic terms in the vicinity of $2\,\omega_2$ are still rejected).

Hence, for the first order FMFB

$$\dot{\phi}(t) = K_D\left[\psi(t) - K_v\dot{\phi}(t)\right]$$

or,

$$\dot{\phi}(t) = \frac{K_D}{F}\,\dot{\psi}(t) = (\text{constant})\,\dot{\psi}(t) \tag{30}$$

which is identical to the defining equation of a limiter discriminator if the input to the limiter discriminator is again taken as $a(t)\cos\left[\omega_o t + \psi(t)\right]$ and its output is designated by $\dot{\phi}(t)$. Consequently, the equivalence between the FMFB and limiter discriminator has been demonstrated.

Expected Number of FMFB Noise "Clicks"

By applying the techniques already developed for the PLL and limiter discriminator, the expected number of " clicks" per second appearing at the output of an FMFB excited by a carrier (unmodulated) plus narrow band noise can now be simply obtained. Although the result will be strictly valid for the two cases of an FMFB with a very small or very large IF filter bandwidth, experimental results on the first order FMFB indicate that this simple technique predicts reasonably well the actual number of " clicks" even for intermediate values of IF bandwidth.

For the FMFB with small IF bandwidth the expected number of "clicks" per second $N\pm$ is found using Hess' result Equation (4). It has been demonstrated that the FMFB is equivalent to a PLL with equivalent closed loop bandwidth $(F-1)\,\omega_{IF} \exp\left[\frac{1}{2} R_{K_v\phi}(0)\right]$.

Hence,

$$N_{\pm}\ \text{FMFB (narrow IF)} = \frac{\gamma}{\pi}\ \text{erfc}\left[\sqrt{2}\ \text{CNR}\left(1 + \frac{1.04\,\gamma}{(F-1)\omega_{IF}\exp\left[\frac{1}{2}R_{K_v\phi}(0)\right]}\right)\right] \tag{31}$$

where CNR, γ, and erfc are defined by Equations 5, 6, and 7 respectively and $R_{K_v\phi}(0)$ is given by Equation (28) for a rectangular RF filter.

For the FMFB with large IF bandwidth the expected number of "clicks" per second approaches Rice's result[5] for the limiter discriminator which

$$N_{\pm}\ \text{FMFB (wide IF)} = \frac{\gamma}{\pi}\ \text{erfc}\left[\sqrt{2}\ \text{CNR}\right] \tag{32}$$

where γ, CNR, and erfc have the same meaning as above.

The region of validity of the expressions is determined from an experimental study discussed in the following section.

Experimental Results

An experimental first order FMFB was constructed to operate with an input carrier frequency of 455 kHz and a loop IF center frequency of 174 kHz. A block diagram of the experimental set-up appears in Figure 4. The RF filter used was a Collins mechanical filter rectangular in shape, symmetric about 455 kHz, and 13 kHz in bandwidth. The loop IF filter was a single tuned RLC circuit. Its bandwidth was changed by varying its Q. The General Radio GR1142-A frequency discriminator was used for the loop limiter discriminator. The VCO used was an astable multivibrator whose square wave output operated a switching transistor which served as the multiplier. The loop gain was adjusted by varying the VCO constant. The input 455 kHz carrier was obtained from a Wavetek Model 111 variable frequency generator and the input noise was obtained from a General Radio GR 1390-B Noise Generator.

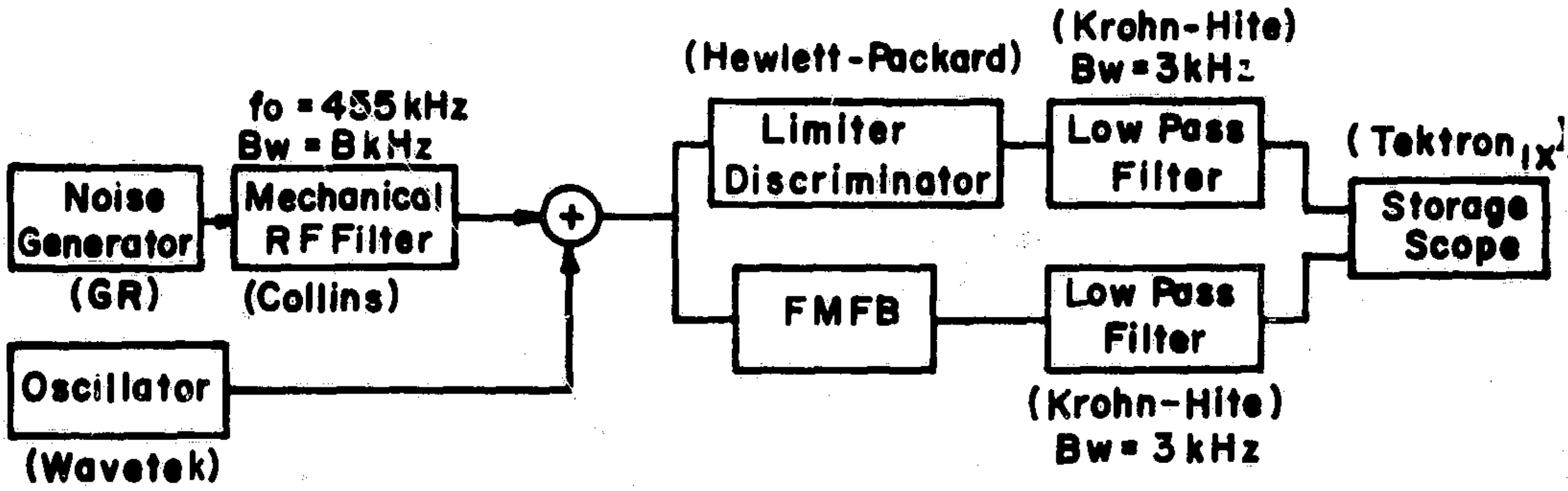

Fig. 4. Experimental Set-Up

The input carrier to noise ratio $A/\sqrt{2N}$ was varied by adjusting the output of the noise generator. A limiter discriminator and FMFB were driven simultaneously with the same carrier plus narrow band noise. The purpose of this is to ensure that all the clicks counted in the FMFB output are clicks of the first kind. The outputs of the limiter discriminator and FMFB were passed through low pass filters to make the " clicks" readily recognizable on a storage oscilloscope.

Assuming the output of the noise generator flat over of the rectangular pass band of the RF filter the radius of gyration of the input noise becomes

$$\gamma = \frac{2\pi B\omega}{2\sqrt{3}} \tag{33}$$

where $B\omega$ is the total bandwisth of the RF filter. Substituting Equation (33) into Equations (31) and (32), the expected number of " clicks" per second appearing at the output of the first order FMFB is

$$N_{\pm}\,\text{FMFB(narrow IF)} = \frac{B\omega}{\sqrt{3}}\,\text{erfc}\left[\sqrt{2}\;\text{CNR}\left(1+\frac{0.6}{(F-1)\frac{2f_{IF}}{B\omega}\exp\left(\frac{1}{2}R_{K_v\phi}(0)\right)}\right)\right] \tag{34}$$

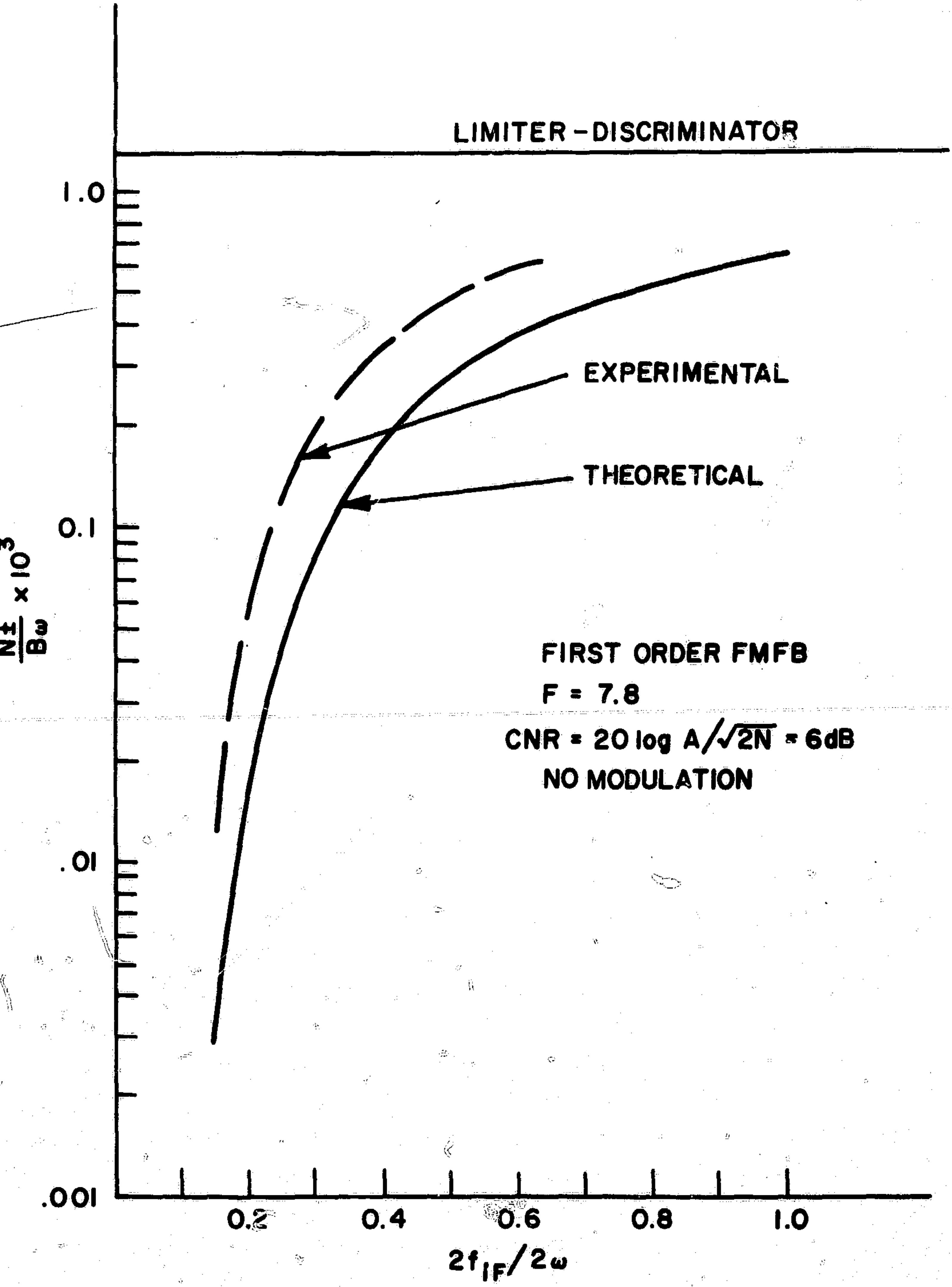

LIMITER-DISCRIMINATOR
1.0
0.1
.01
.001
EXPERIMENTAL
THEORETICAL
FIRST ORDER FMFB
F = 7.8
CNR = 20 log A/√2N = 6dB
NO MODULATION
0.2
0.4
0.6
0.8
1.0
2f_IF/2ω

Fig. 5.

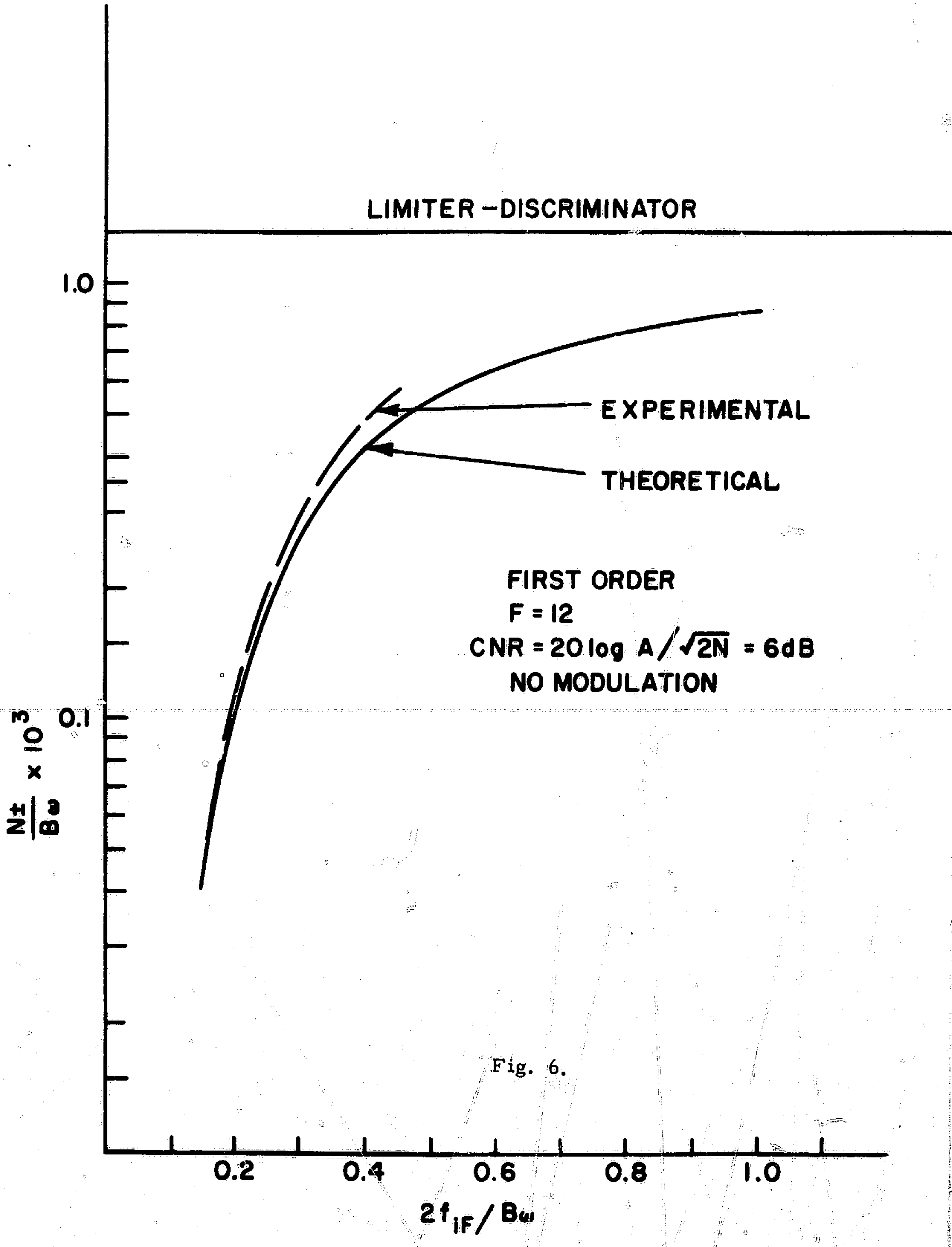

LIMITER – DISCRIMINATOR
1.0
0.1
EXPERIMENTAL
THEORETICAL
FIRST ORDER
F = 12
CNR = 20 log A/√2N = 6dB
NO MODULATION
$\frac{N\pm}{B\omega} \times 10^3$
0.2
0.4
0.6
0.8
1.0
$2f_{IF}/B\omega$

Fig. 6.

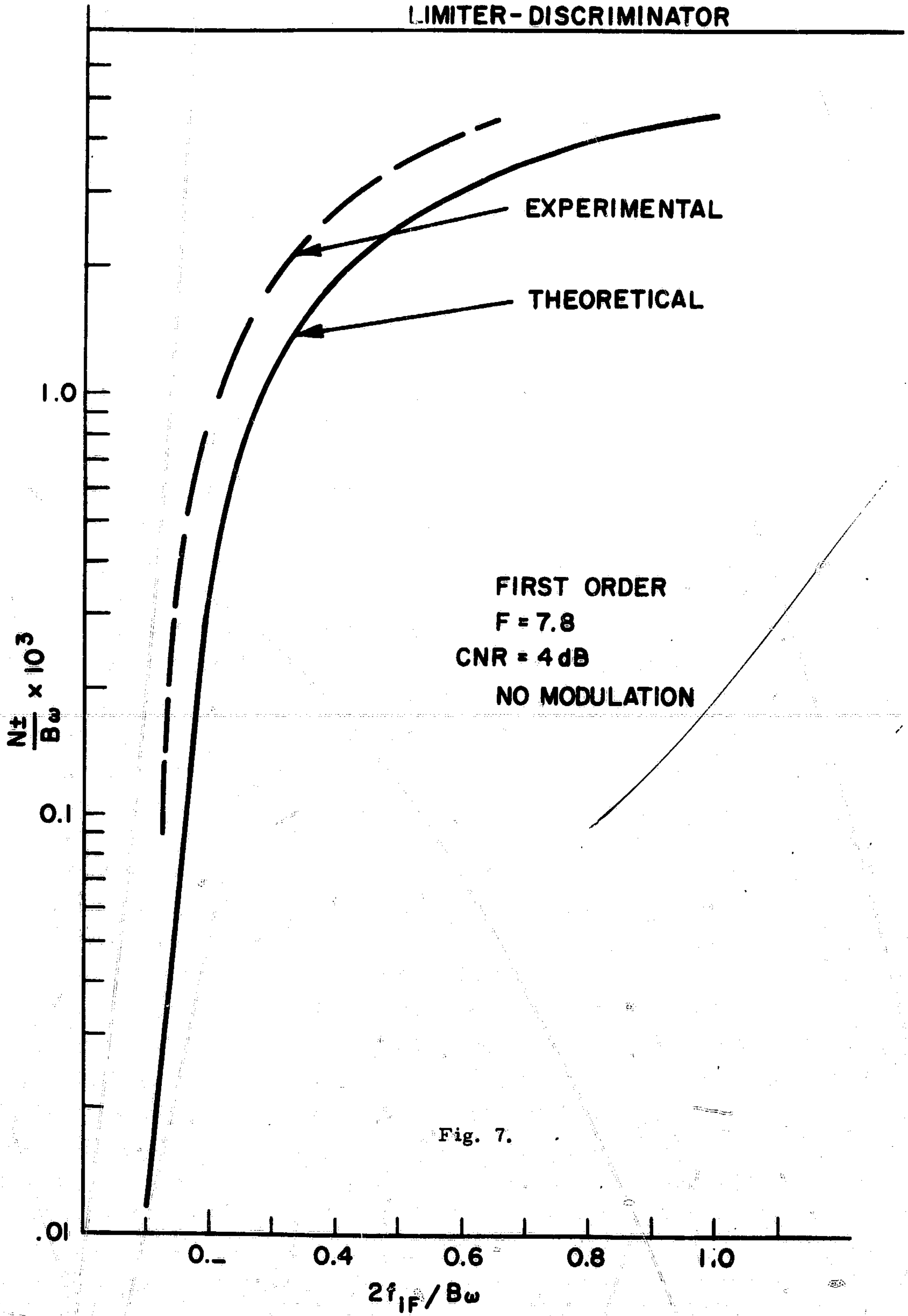
LIMITER-DISCRIMINATOR
EXPERIMENTAL
THEORETICAL
FIRST ORDER
F = 7.8
CNR = 4 dB
NO MODULATION
1.0
0.1
.01
$\frac{N\pm}{B\omega} \times 10^3$
0._
0.4
0.6
0.8
1.0
$2f_{IF}/B\omega$

Fig. 7.

where $R_{K_v\phi}(0)$ is given by Equation (28)

$$N_{\pm\,FMFB(\text{wide IF})} = \frac{B\omega}{\sqrt{3}} \operatorname{erfc}\left[\sqrt{2}\ CNR\right] \tag{35}$$

Using Equation (34) plots of $N_{\pm} / B\omega$ vs. $\frac{2 f_{IF}}{B\omega}$ with CNR and F as parameters are presented in Figures 5, 6, and 7 along with experimentally obtained data. The experimental results indicate that the FMFB essentially behaves as a limiter discriminator when its internal IF bandwidth exceeds two or three times its rectangular RF bandwidth and acts very much like a PLL when its IF bandwidth is less than one or two tenths the rectangular RF bandwidth. More importantly Equation (34) predicts reasonably well the expected number of FMFB "clicks" even for intermediate values of IF bandwidth.

Conclusion

It has been shown that the defining equation of the FMFB with limiter in the loop degenerates into the equations of a limiter-discriminator and a PLL type structure as the loop IF filter bandwidth of the FMFB approaches infinity and zero respectively. It was observed that when the internal IF bandwidth is narrow the filtering operations performed by the loop IF filter and low pass loop filter are completely interchangeable. Moreover, by drawing these equivalences a simple technique was made available to compute the expected number of "clicks" per second, appearing at the output of an FMFB excited by a carrier plus narrow band noise. Although the resulting expression for the expected number of "clicks" is strictly valid for the special case of an FMFB with a very narrow or very wide IF filter, experimental results on the first order FMFB indicate that the expression is useful in predicting the actual number of "clicks" for intermediate values of IF bandwidth (expecially for large feedback factors).

Continued research in this area is under way to include an extension of similar analyses to higher order frequency demodulators with feedback as well as an extensive study of modulation induced "clicks", i.e., "clicks" of the second kind. Given specifications of the received signal, a design procedure to obtain the optimum FMFB, i.e., the FMFB which minimizes the total number of "clicks" of the first and second kind, is sought. The maximum threshold extension realizable with this optimum FMFB will then be determined. In addition, since equivalences have been established between many of the FM threshold extension demodulators in existence today a general unification of the treatment of FM threshold extension techniques will also be sought.

<u>References</u>

(1) M. Schwartz, W. R. Bennett, and S. Stein, "Communication Systems and Techniques," McGraw-Hill, 1966,

(2) K. K. Clarke and D. T. Hess, "Frequency Locked Loop FM Demodulator," IEEE Trans. on Comm. Tech., Vol. Com-15, August 1967, pp. 518-524.

(3) A. J. Viterbi, "Principles of Coherent Communication," McGraw-Hill, 1966, Chapter 4.

(4) D. T. Hess, "Cycle Slipping in First Order Phase Locked Loops," IEEE Trans. on Comm. Tech., April 1968, pp. 255-260.

(5) S. O. Rice, "Noise in FM Receivers," Time Series Analysis, M. Rosenblatt, Ed., New York: Wiley, 1963, Chapter 25.

(6) D. T. Hess, "Equivalence of FM Threshold Extension Receivers," IEEE Trans. on Comm. Tech., Vol. Com-16, October 1968, pp. 476-478.

II. Characteristics of FM

II.I Single Sideband FM

Review of Results - Old and New

In the last report we discussed the origin of SSB-FM and some of its bandwidth properties. Also we have shown that a quasi SSB-FM signal of the form $a\, e^{-\alpha \sin \omega_m t} \cos(\omega_o t + \beta \cos \omega_m t)$ with α less than β, occupies approximately the same bandwidth as a true SSB-FM signal does. The former is preferable to the latter since the output of a discriminator receiving this signal will contain fewer clicks, at the same input signal to noise ratio, than when an SSB-FM signal is received.

An SSB-FM generator was constructed and threshold tests were performed on a quasi SSB-FM waveform with sine wave modulation, Fig. 1 shows the experimental set up. The results were verified theoretically. When the click rates shown in Fig. 2, 3, 4 and 5 are compared to those occurring in the FM case it is seen that threshold occurs at much higher input signal to noise ratios for SSB-FM than for FM. One would not expect that the results for gaussian modulation would be significantly better especially since for rms phase deviations greater than 1, SSB-FM has a larger bandwidth than FM.

The ratio of the output signal to noise ratio to the input signal to noise ratio vs. rms frequency deviation was calculated for the case of gaussian modulation with an exponential baseband power spectrum.

Expected Number of Clicks

Rice[1] has discussed completely the theory behind the threshold phenomenon in FM. In particular it was shown that for the case of constant offset carrier, N_+, the expected number of positive 2π jumps in the received signal phase during a one second interval is given by:

[redacted]

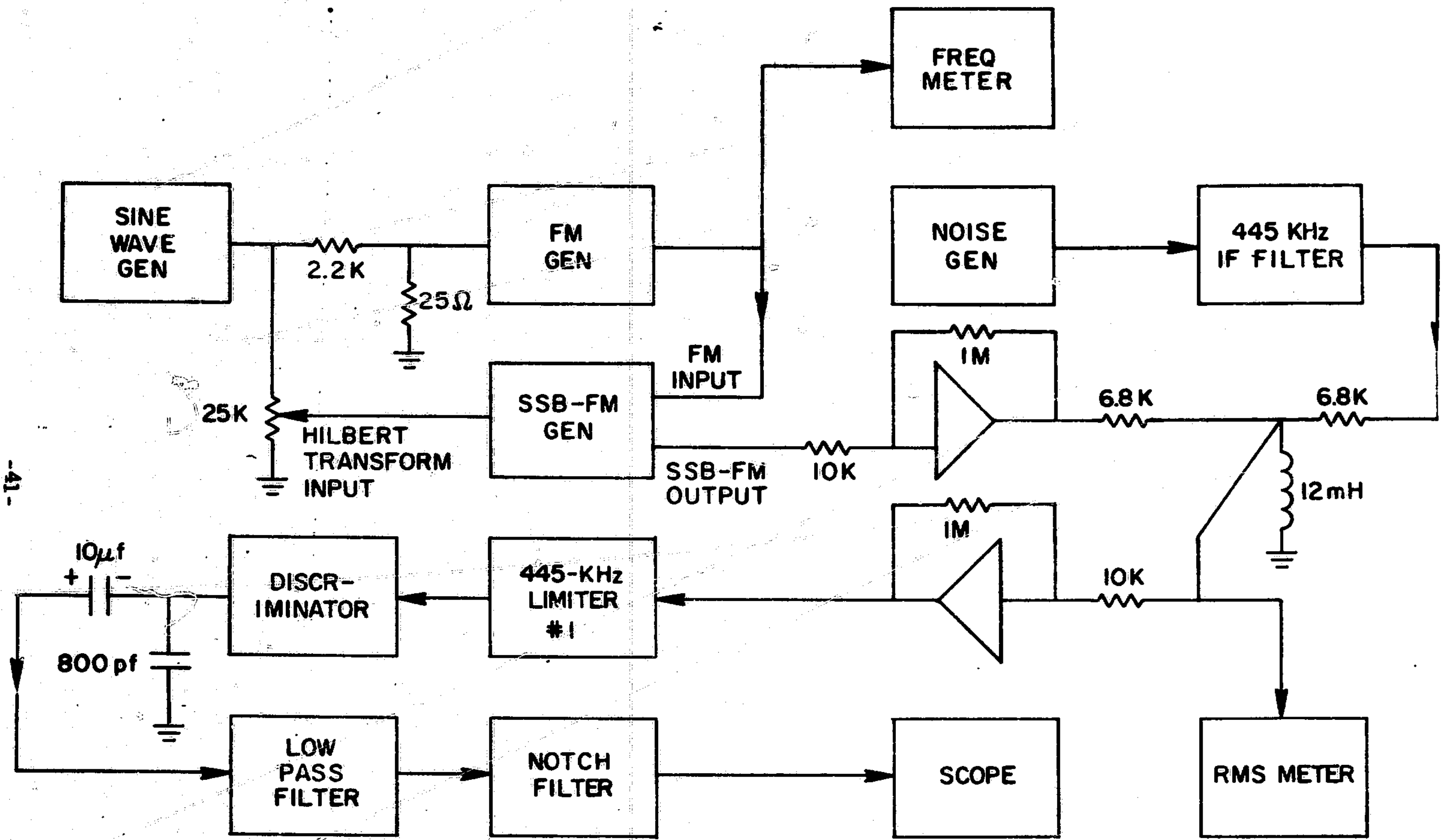

Fig. 1 Block Diagram of Experimental Set-Up

$$N_+ = \frac{1}{2}\left\{ (r^2 + f_o^2)^{1/2} \left[1 - \operatorname{erf}\left(\rho + \rho f_o^2 r^{-2}\right)^{1/2}\right] - f_o e^{-\rho}\left[1 - \operatorname{erf}\left(f_o r^{-1} \rho^{1/2}\right)\right]\right\} \tag{1}$$

The expected number of negative jumps, N_- is given by:

$$N_- = N_+ + f_1 e^{-\rho} \tag{2}$$

where f_1 is the offset frequency in hertz from the carrier frequency, f_o, ρ is the input carrier to noise ratio and r is the rms bandwidth of the r. f. filter.

Returning to SSB-FM we see that we are dealing with an FM wave that has peaks and valleys in its instantaneous amplitude, A(t).

$$\begin{aligned} V_{SSB-FM} &= a\, e^{-\hat{x}(t)} \cos(\omega_o t + x(t)) \\ A(t) &= a\, e^{-\hat{x}(t)} \end{aligned} \tag{3}$$

Since during the time duration of a click occurance the modulation waveform changes only slightly one should be able to calculate N_+ and N_- by averaging over all values of f_1 and $\rho = A^2(t)/2\sigma_N^2$. We may simplify our calculations by recalling that our carrier frequency f_o, lies at the upper end of the r. f. filter passband. Therefore even with no modulation N_- will be several orders of magnitude larger than N_+. Since we expect clicks only in the valleys of A(t) where the instantaneous frequency is larger than f_o we can neglect all terms associated with N_+. In fact positive clicks were so rare an event that only a few were observed even at the lowest input signal to noise ratios. Since we are dealing with a deterministic signal we calculate N_- from (2) as:

$$N_- = \lim_{T \to \infty} \frac{1}{2\pi} \int_{-T}^{T} |\dot{\phi}(t)|\, e^{-\rho(t)}\, dt. \tag{4}$$

$$N_- = \frac{1}{2\pi} \int_0^{2\pi} |1/2\, f_1 + \Delta f \cos\theta|\, e^{-\rho'}\, e^{-2\alpha\cos\theta}\, d\theta \tag{5}$$

This integral was evaluated on a computer and the results plotted along with the experimental data in Fig. 2, 3, 4, and 5. The values for f_1, Δf and α where those used experimentally. In the case Fig. 3, 4, and 5 the value of α had to be modified to account for the fact that in the region of $v_{in} > 2$ volts the exponential circuit did not give a true exponential output. This fact only slightly affects the single sided nature of the modulated signal spectrum but greatly affects the click rate since it is in this region that all the clicks occur.

Output S/N Above Threshold

Consider an SSB-FM signal of the form:

$$A\, e^{\hat{D}(t)} \cos(\omega_o t + D(t)) \tag{6}$$

corrupted by additive gaussian noise.

$$n(t) = r(t) \cos(\omega_o t + \theta(t)) \tag{7}$$

where n(t) is derived by passing white noise with autocorrelation function $\frac{n_o}{2}\,\delta(t)$ through the r.f. filter used in the receiver.

Suppressing the ω_o term the received signal phase ϕ is given by:

$$\phi = D + \tan^{-1} \frac{r \sin(\theta - D)}{A e^{\hat{D}} + r \cos(\theta - D)} \tag{8}$$

For high signal to noise ratios

$$\phi_N = \phi - D = \frac{e^{-\hat{D}}}{A}\, r \sin(\theta - D)$$

$$= \frac{e^{-\hat{D}}}{A}\, r\, [\sin(\theta) \cos(D) - \sin(D) \cos(\theta)]$$

$$\underbrace{r \sin(\theta)}_{y}\, \frac{e^{-\hat{D}}}{A} \cos(D) - \underbrace{r \cos(\theta)}_{x}\, e^{-\hat{D}} \sin(D)$$

Since the noise is onesided about ω_o and we are using the lower sideband,

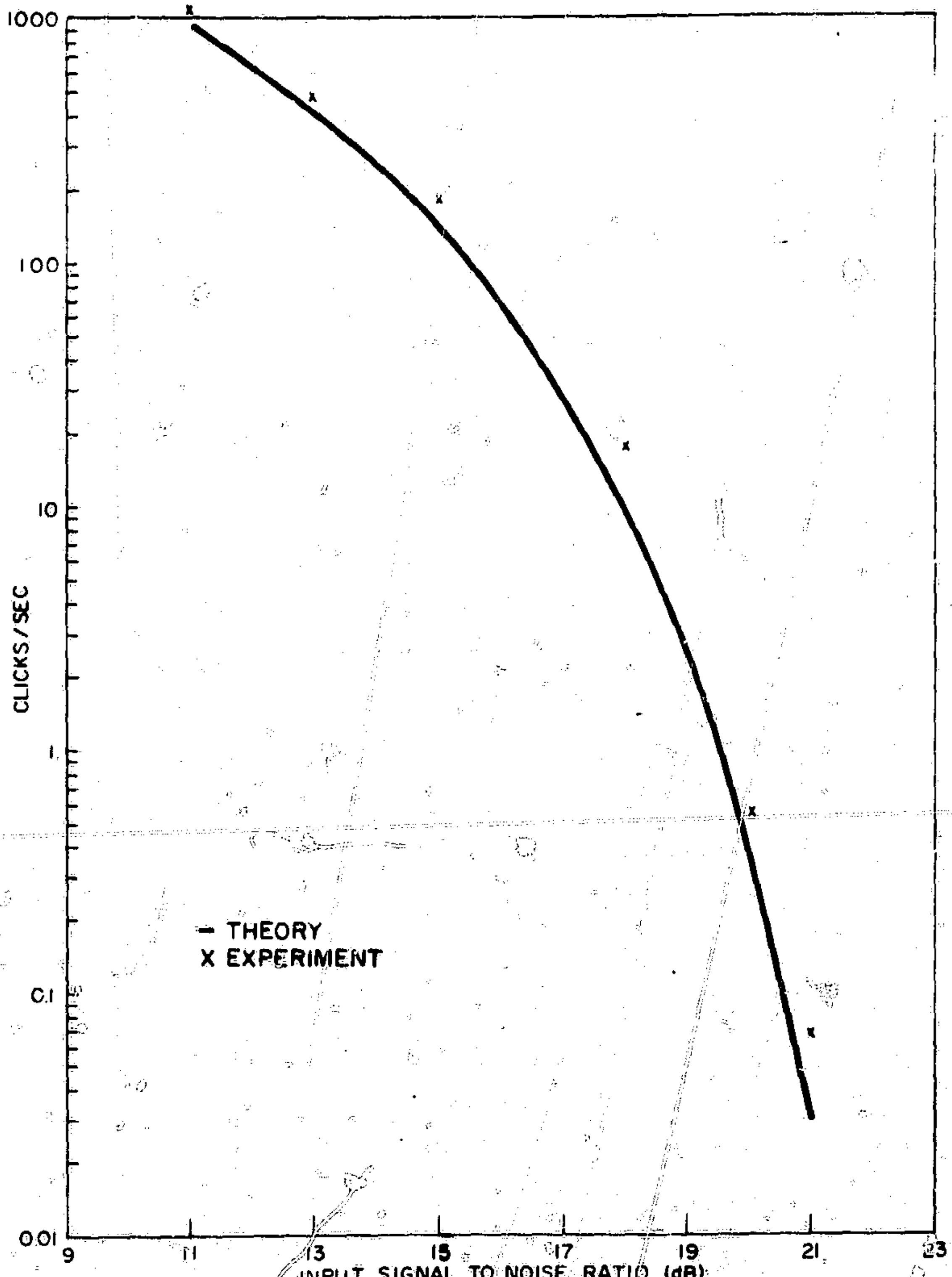

Fig. 2. Click Rate vs. Input Signal to Noise Ratio for Quasi SSB-FM Signal $\exp[-\alpha \cos \omega_m t] \cos(\omega_o t + \beta \sin \omega_m t)$

$\alpha = .82$ $\beta =$ [illegible]1 $f_m = 5.3$ KHz

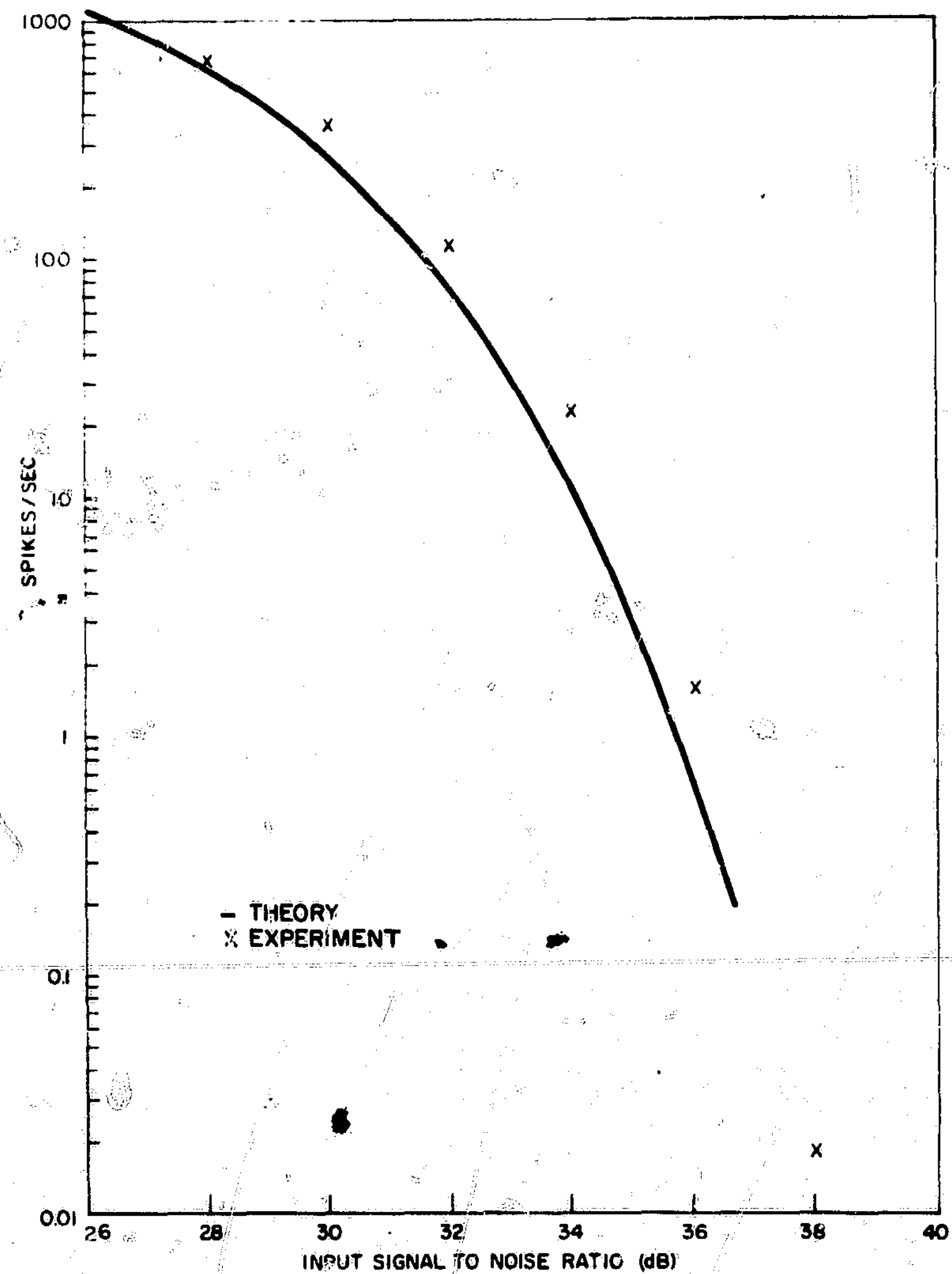

Fig. 3. Click Rate vs. Input Signal to Noise Ratio for Quasi SSB-FM Signal $\exp[-\alpha \cos \omega_m t] \cos(\omega_o t + \beta \sin \omega_m t)$

$\alpha = 2.1$ $\beta = 2.33$ $f_m = 3KHz$

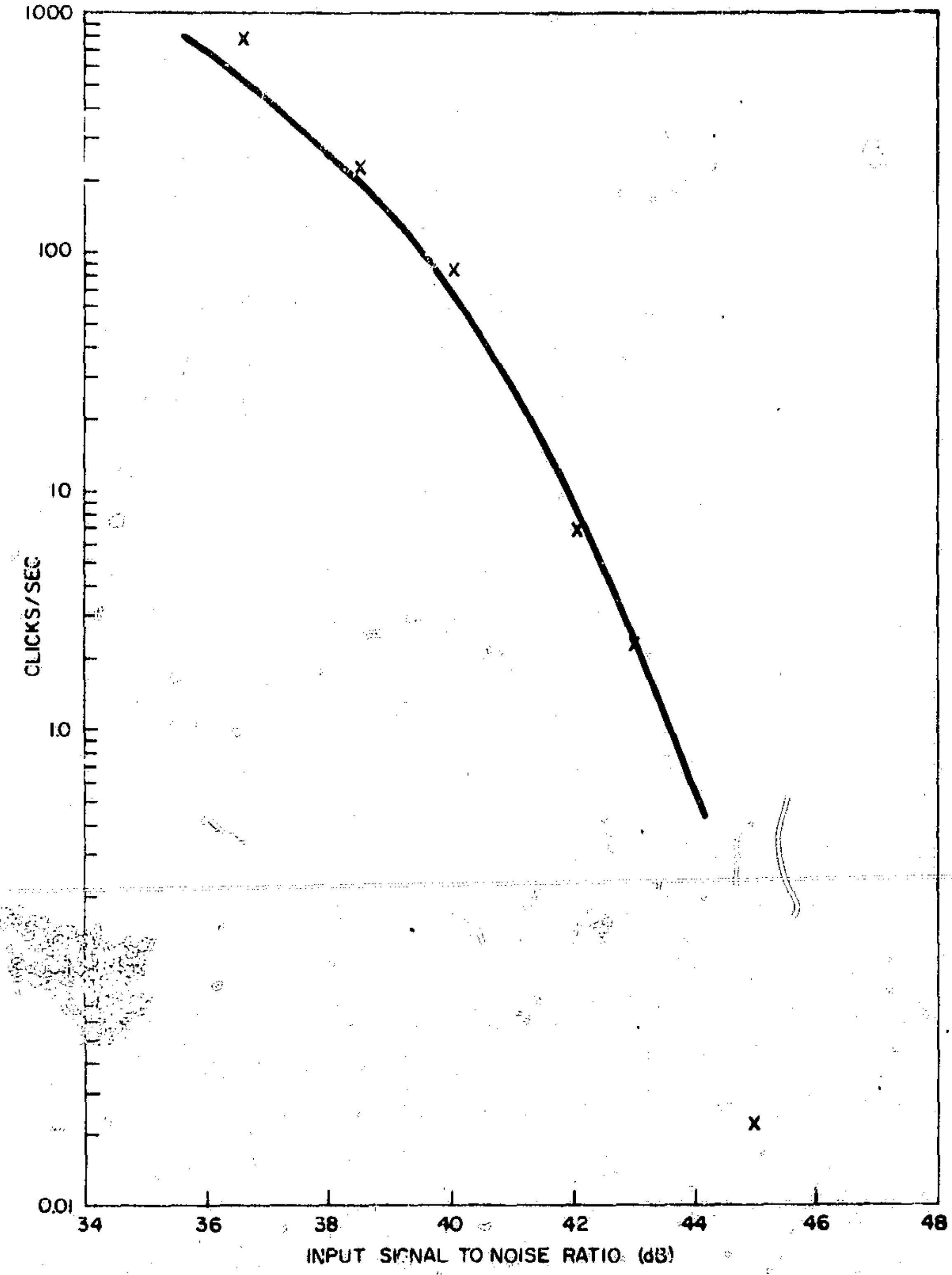

Fig. 4. Click Rate vs. Input Signal to Noise Ratio for Quasi SSB-FM Signal $\exp[-\alpha \cos \omega_m t] \cos(\omega_o t + \beta \sin \omega_m t)$

$\alpha = 3.0 \quad \beta = 8.55 \quad f_m = 1.29$ KHz

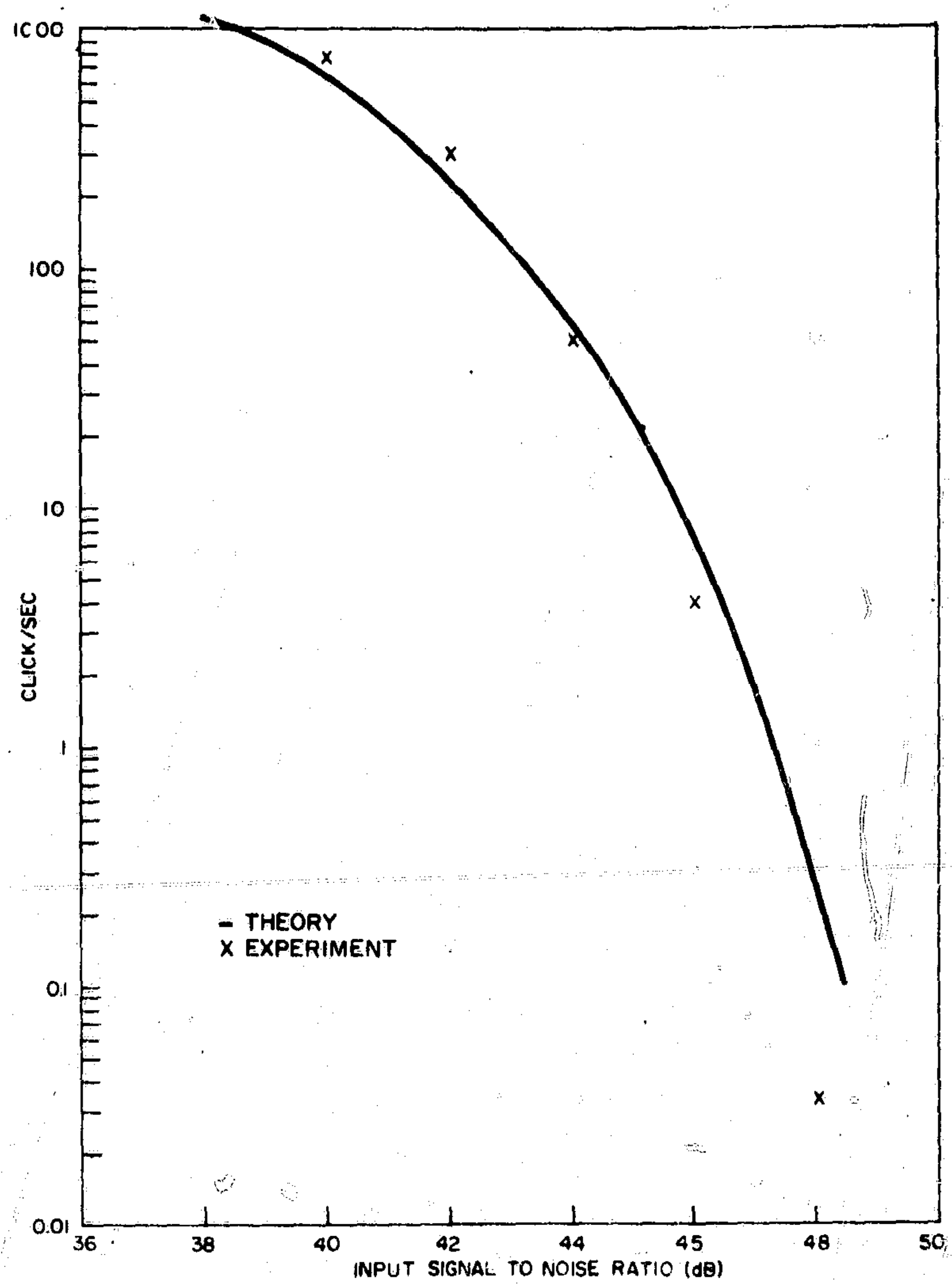

Fig. 5. Click Rate vs. Input Signal to Noise Ratio for Quasi SSB-FM Signal $\exp[-\alpha \cos \omega_m t] \cos(\omega_o t + \beta \sin \omega_m t)$

$\alpha = 4.4 \quad \beta = 12 \quad f_m = 1$ KHz

$$n(t) = x \cos \omega_o t - y \sin \omega_o t = x \cos \omega_o t + x \sin \omega_o t$$

$$\phi_N = - [\hat{x} \frac{e^{-\hat{D}}}{A} \cos (d) + x \frac{e^{-\hat{D}}}{A} \sin (D)] \tag{10}$$

$$R_{\phi_N} = E \{ \phi_N(t + \tau) \phi_N(t) \}$$

Since the noise is assumed independent of the modulation:

$$\begin{aligned} R_{\phi_N}(\tau) &= R_x(\tau) E \left\{ \frac{e^{-\hat{D}(t+\tau) - \hat{D}(t)}}{A^2} \cos (D(t+\tau) - D(t) \right\} \\ &- \hat{R}_x(\tau) E \left\{ \frac{e^{-\hat{D}(t+\tau) - \hat{D}(t)}}{A^2} \sin (D(t+\tau) - D(t) \right\} \end{aligned} \tag{11}$$

Consider:

$$\epsilon = E \{ \exp [- \hat{D}(t+\tau) - \hat{D}(t) + i D(t+\tau) - i D(t)] \} \tag{12}$$

Thus the first term above is

$$\frac{1}{A^2} R_x(\tau) \operatorname{Re}(\epsilon)$$

and the second term is

$$\frac{1}{A^2} \hat{R}_x(\tau) I_m(\epsilon) \tag{13}$$

However, ϵ is just the complex autocorrelation function of the SSB-FM signal, therefore:

$$\begin{aligned} R_{\phi_N}(\tau) &= \frac{1}{A^2} R_x(\tau) e^{2 R_D(\tau)} \cos 2 \hat{R}_D(\tau) \\ &- \frac{1}{A^2} \hat{R}_x(\tau) e^{2 R_D(\tau)} \sin 2 \hat{R}_D(\tau) \\ &= \frac{1}{A^2} \operatorname{Re} \left\{ [R_x(\tau) + i \hat{R}_x(\tau)] e^{2[R_D(\tau) + i \hat{R}_D(\tau)]} \right\} \end{aligned} \tag{14}$$

Our next step is to find $S_{\phi_N}(\omega)$ the Fourier Transform of $R_{\phi_N}(\tau)$.

$$R_{\phi_N}(\tau) = \mathrm{Re}\,\frac{1}{A^2}\left\{[R_x(\tau) + i\,\hat{R}_X(\tau)]\exp\,(2R_D(\tau) + 2i\,\hat{R}_D(\tau))\right\}$$
$$= \frac{1}{A^2}\,\mathrm{Re}\left\{R_c(\tau)\right\} \tag{15}$$

We will now show that it is sufficient to consider only $R_c(\tau)$ whose Fourier Transform we denote as $S_c(\omega)$. Since each factor of $R_c(\tau)$ is an analytic signal $S_c(\omega)$ is a one sided spectrum. The real part of $R_c(\tau)$ is even and its imaginary part is odd therefore $S_{\phi_N}(\omega)$ is the even part of $S_c(\omega)$. But as $S_c(\omega)$ is one sided it is twice $S_{\phi_N}(\omega)$ for positive frequencies. Thus if we consider only positive frequencies our calculations will be simplified.

To find $S_c(\omega)$ we note that the term in brackets of (15) transforms to the equivalent low pass complex noise power spectrum evaluated at $\omega = -\omega$. (Recall that we started out with the lower sideband the above autocorrelation function corresponds to the upper sideband). The exponential is related by a constant of proportionality to the autocorrelation function of an upper sideband SSB-FM signal.

From now on we specialize to the case where the r.f. and baseband filters are rectangular with unity gain. Their bandwidths are ω_c and ω_ℓ respectively. The former is chosen to be three times the rms bandwidth of the input signal whereas the latter is chosen to pass 98% of the modulation power. The modulation spectrum will be assumed exponential thus we may take advantage of the previously calculated analytic expression for the SSB-FM spectrum.

$$S_D(\omega) = \pi\,\sigma_D^2\,e^{-|\omega|}$$
$$R_D(\tau) = \sigma_D^2/1+\tau^2 \tag{16}$$

$$S_{SSB\text{-}FM}(\omega) = \frac{\delta(\omega)}{A^2} + \frac{4\pi\sigma_D^2\,I_1(2\sqrt{2\sigma_D^2}\,\omega)\,e^{-\omega}}{A^2\sqrt{2\sigma_D^2}\,\omega} \qquad \omega > 0 \tag{17}$$

Thus:

$$S_c(\omega) = \frac{\eta_o}{A^2}\left[1 + 4\pi\,\sigma_D^2 \int_{\omega-\omega_c}^{\omega} \frac{I_1\left(2\sqrt{2\sigma_D^2 x}\right)}{\sqrt{2\sigma_D^2 x}}\, e^{-x}\, dx\right] \tag{18}$$

Recall:

$$I_1(z) = \left(\frac{1}{2} z\right) \sum_{k=0}^{\infty} \frac{\left(\frac{1}{4} Z^2\right)^k}{k!\,\Gamma(k+2)} \tag{19}$$

Let:

$$Z = 2\sqrt{2\sigma_D^2 x} \tag{20}$$

Then:

$$S_c(\omega) = \frac{\eta_o}{A^2}\left[1 + 4\pi\,\sigma_D^2 \int_{\omega-\omega_c}^{\omega} \sum_{k=0}^{\infty} \frac{(2\sigma_D^2 x)^k}{k!\,\Gamma(k+2)}\, e^{-x}\, dx\right] \tag{21}$$

We can confine our attention to frequencies $0 < \omega < \omega_c$ since $\omega_\ell < \omega_c$ and $S_{SSB-FM}(\omega) = 0\ \omega < 0$. Therefore

$$S_c(\omega) = \frac{\eta_o}{A^2}\left\{1 + 4\pi\,\sigma_D^2 \sum_{k=0}^{\infty} \frac{(2\sigma_D^2)^k}{(k+1)!}\left[\frac{1}{\Gamma(k+1)} \int_0^{\omega} x^k e^{-x}\, dx\right]\right\} \tag{22}$$

The term in brackets is known as the incomplete gamma function $\Gamma(R+1,\ \omega)$.

$$S_c(\omega) = \frac{\eta_o}{A^2}\left[1 + 4\pi\,\sigma_D^2 \sum_{k=0}^{\infty} \frac{(2\sigma_D^2)^k}{(k+1)!}\,\Gamma(k+1,\omega)\right] \tag{23}$$

To find $\sigma_{\phi_N}^2$ we integrate $\frac{1}{2\pi}\, S_{\phi_N}(\omega)$ between the limits $\omega = 0$ and $\omega = \omega_\ell$

$$\sigma_{\phi_N}^2 = \frac{\eta_o}{2\pi A^2}\,\frac{\omega_\ell^3}{3} + \frac{2\sigma_D^2 \eta_o}{A^2} \int_0^{\omega_\ell} \sum_{k=0}^{\infty} \frac{2\sigma_D^2}{(k+1)!}\, \omega^2\, \Gamma(k+1,\omega)\, d\omega \tag{24}$$

However:

$$\Gamma(k+1,\omega) = e^{-\omega} \sum_{n=k+1}^{\infty} \frac{\omega^n}{\eta!} = 1 - e^{-\omega} \sum_{n=0}^{k} \frac{\omega^n}{\eta!} \tag{25}$$

Therefore the integral in (24) becomes

$$\frac{2\sigma_D^2 \eta_o}{A^2} \sum_{k=0}^{\infty} \int_0^{\omega_\ell} \frac{(2\sigma_D^2)^k}{(k+1)!}\left[\omega^2 - e^{-\omega} \sum_{n=0}^{k} \frac{\omega^{n+2}}{\eta!}\right] d\omega \tag{26}$$

Thus:

$$\sigma^2_{\dot{\phi}_N} = \frac{\eta_o \omega_\ell^3}{6\pi A^2} + \frac{2\sigma_D^2 \eta_o}{A^2} \sum_{k=0}^{\infty} \frac{2\sigma_D^2}{(k+1)!} \left[\frac{\omega_\ell^3}{3} - \sum_{n=0}^{k} \frac{\gamma\,(n+3,\ \omega_\ell)}{\eta\,!} \right] \tag{27}$$

where $\gamma\,(n, x) = \int_0^x e^{-y}\, y^{n-1}\, dy$

and is a tabulated function.

Recalling that the r.f. filter bandwidth was chosen to be three times the SSB-FM rms bandwidth, we see through the use of Chebychev's inequality that this filter must pass at least 90% of the transmitted signal power. Since $< P_{SSB\text{-}FM} > = \frac{A^2}{2} e^{2\sigma_D^2}$ the input signal power is $.45\, A^2 e^{2\sigma_D^2}$ and as the input noise power is $3\, B_{SSB\text{-}FM}\, \eta_o$ the input signal to noise ratio is:

$$SNR_I = \frac{.15\, A^2 e^{2\sigma_D^2}}{B_{SSB\text{-}FM}\, \eta_o} \tag{28}$$

On the other hand for the baseband spectrum chosen the modulation power is $2\,\sigma_D^2$ dividing this term by (28) gives the output signal to noise ratio:

$$SNR_o = \frac{2\,\sigma_D^2}{\frac{\eta_o \omega_\ell^3}{6\pi A^2} + \frac{2\sigma_D^2 \eta_o}{A^2} \sum_{k=0}^{\infty} \frac{(2\sigma_D^2)^k}{(k+1)!} \left[\frac{\omega_\ell^3}{3} - \sum_{n=0}^{k} \gamma\,[(n+3),\ \omega_\ell] \right]} \tag{29}$$

These expressions were evaluated with the aid of an IBM 360/50 digital computer. The ratio SNR_o / SNR_I vs. σ_D is plotted in Fig. 6.

Conclusion

It appears that SSB-FM will not find broad practical application since it is both difficult to generate and does not perform as well as FM does.

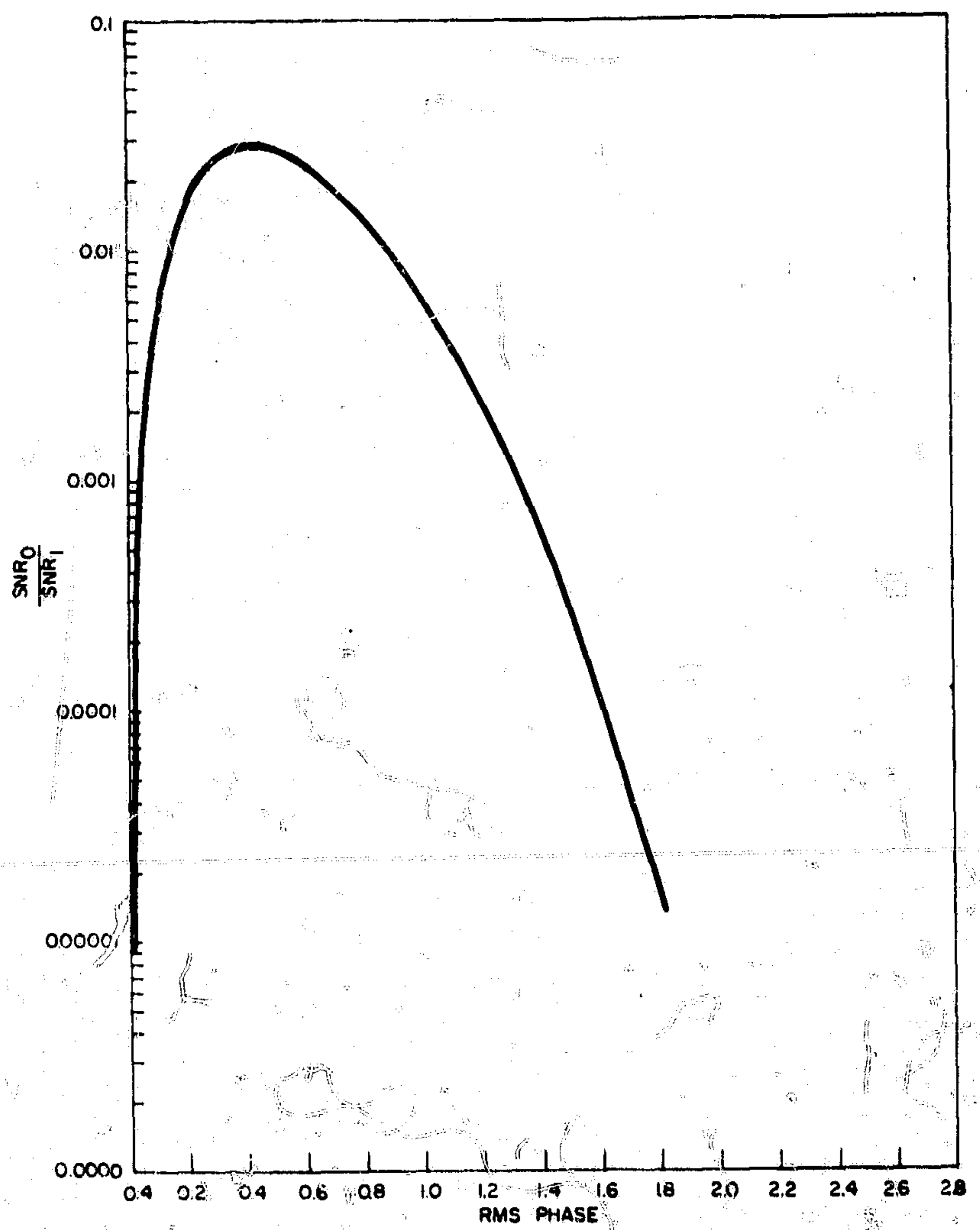

Fig. 6. **Output Signal to Noise Ratio, SNR_o, Divided by Input Signal to Noise Ratio, SNR_I vs. RMS Phase, σ_D**

References

(1) S. O. Rice, "Noise in FM Receivers," Times Series Analysis, M. Rosenblatt, Ed., New York: Wiley, 1963, Chapter 25.

(2) M. Schwartz, W. R. Bennett, and S. Stein, "Communication Systems and Techniques," McGraw-Hill, 1966.

II. 2. Optimum Preemphasis in FM

The purpose of this report is to show the advantage in using an optimum preemphasis network instead of the RC filter usually employed, or a whitening filter.

If a signal m(t) frequency modulates an FM carrier, the output SNR of the demodulated signal, when measured above threshold is,

$$\frac{S_o}{N_o} = \frac{3}{4\pi^2} \left(\frac{\overline{m^2(t)}}{f_M^2} \right) \frac{S_i}{\eta f_M} \tag{1}$$

where $\frac{S_o}{N_o}$ is the output SNR

S_i is the received input signal power

η is the power spectral density of the input noise (one-sided)

f_M is the bandwidth of the modulation, m(t)

and

$\overline{m^2(t)}$ is the power contained in the modulating signal. This value is also equal to the mean square deviation.

If a preemphasis network is employed to filter the signal before modulation, and a deemphasis network placed after the FM demodulator, then the output SNR is increased. Since the deemphasis network is, in principle, the inverse of the preemphasis network (see Fig. 1), the filtered output signal is independent of the preemphasis employed. Thus, the improvement achieved by preemphasis is due to the filtering by the deemphasis network of the demodulated "FM noise".

The power spectral density of the demodulated noise is

$$G_n(f) = \frac{2\pi^2 \eta}{S_i} f^2 \qquad |f| \le \frac{B}{2} \tag{2}$$

where B is the IF bandwidth employed. If preemphasis is not employed the output noise power, N_o is

$$N_o = \int_{-f_M}^{f_M} G_n(f)\, df = \frac{4\pi^2}{3} \frac{\eta f_M^3}{S_i} \tag{3}$$

If, however, a preemphasis network having a transfer function $H_p(f)$, is employed, the deemphasis network has a transfer function $\frac{1}{H_p(f)}$, and the output noise power is now,

$$N_{op} = \int_{-f_M}^{f_M} G_n(f) \frac{1}{|H_p(f)|^2}\, df = \frac{4\pi^2 \eta}{S_i} \int_0^{f_M} \frac{f^2}{|H_p(f)|^2}\, df \tag{4}$$

Before comparing N_{op} with N_o we note that there is a constraint on the selection of $H_p(f)$. The constraint is that the <u>same</u> bandwidth B be required in both cases. Since the bandwidth B is proportional to the rms frequency deviation of the FM signal we have

$$\int_0^{f_M} G_m(f)\, df = \int_0^{f_M} G_m(f)\, |H_p(f)|^2\, df \tag{5}$$

where $G_m(f)$ is the power spectral density of the modulating signal. It should be noted that if Eq. 5 is not satisfied, the frequency deviation of the FM carrier would differ in each case. In this case we could adjust B to be different in each case. This in turn results in different noise powers being received at the demodulator input. Thus, the constraint provided by Eq. 5 insures that the input noise power $N_i = \eta B =$ constant.

The optimum preemphasis network is found by minimizing N_{op} (Eq. 4) subject to the constraint of Eq. 5. The minimization is accomplished by combining Eqs. 4 and 5 to form a new integral, I:

$$I = \int_0^{f_M} \left\{ \frac{4\pi^2 \eta}{S_i} \left(\frac{f^2}{|H_p(f)|^2} \right) + \lambda \left(|H_p(f)|^2 - 1 \right) G_m(f) \right\} df \tag{6}$$

where λ is a Lagrange multiplier. Minimizing I results in minimizing Eq. 4 subject to the constraint of Eq. 5. From the calculus of variations we know that I is a minimum when

$$\frac{\partial}{\partial y} \left\{ \frac{4\pi^2\eta}{S_i} \left(\frac{f^2}{y} \right) + \lambda (y - 1) G_m(f) \right\} df = 0$$

where $y \equiv |H_p(f)|^2$ (7)

Solving Eq. 7 yields

$$|H_p(f)|^2 = \frac{f}{\sqrt{G_m(f)}} \; \frac{\int_0^{f_M} G_m(f)\, df}{\int_0^{f_M} f\sqrt{G_m(f)}\; df} \tag{8}$$

and

$$N_{op} = \frac{4\pi^2 \eta f_M^3}{S_i} \; \frac{\left[\int_0^1 x\sqrt{G_m(x)}\; dx \right]^2}{\int_0^1 G_m(x)\, dx} \tag{9}$$

where the dummy variable $x = \dfrac{f}{f_M}$.

The improvement obtained depends solely on the power spectral density $G_m(f)$. To determine this improvement and to compare our results with the improvement obtained using several sub-optimum preemphasis networks we choose several examples.

1. <u>The RC High-Pass Filter</u>

In this case

$$|H_{RC}(f)|^2 = K_1 \left[1 + \left(\frac{f}{f_1} \right)^2 \right] \tag{10}$$

where K_1 is found from Eq. 5 to be

$$K_1 = \frac{\int_0^1 G_m(x)\, dx}{\int_0^1 \left[1 + \frac{x}{x_o}\right)^2 G_m(x)\, dx} \tag{11}$$

and $x_o = \frac{f_1}{f_M}$.

Eq. 4 now becomes

$$N_{O_{RC}} = \frac{4\pi^2 \eta f_M^3}{S_i} \frac{\int_0^1 [1 + (\frac{x}{x_o})^2] G_m(x)\, dx}{\int_0^1 G_m(x)\, dx} \cdot \int_0^1 \frac{x^2\, dx}{1 + (\frac{x}{x_o})^2} \tag{12}$$

The im rovement obtained when using the optimum filter is therefore

$$\frac{N_{OP}}{N_{O_{RC}}} = \frac{[\int_0^1 x \sqrt{G_m(x)}\, dx]^2}{\int_0^1 [1 + (\frac{x}{x_o})^2] G_m(x)\, dx \int_0^1 \frac{x^2\, dx}{1 + (\frac{x}{x_o})^2}} \tag{13}$$

2. <u>The Whitening Preemphasis Network</u>

In this case

$$|H_W(f)|^2 = \frac{K_2}{G_m(f)} \tag{14}$$

where K_2 is found from Eq. 5 to be

$$K_2 = \int_0^1 G_m(x)\, dx \tag{15}$$

Eq. 4 now becomes

$$N_{OW} = \frac{4\pi^2 \eta f_M^3}{S_i} \frac{\int_0^1 x^2 G_m(x)\, dx}{\int_0^1 G_m(x)\, dx} \tag{16}$$

The improvement obtained now when using the optimum preemphasis network is

$$\frac{N_{OP}}{N_{OW}} = \frac{[\int_0^1 x \sqrt{G_m(x)}\, dx]^2}{\int_0^1 x^2 G_m(x)\, dx} \tag{17}$$

It is interesting to prove that the ratios $\frac{N_{OP}}{N_{O_{RC}}}$ and $\frac{N_{OP}}{N_{OW}}$ are indeed less than or equal to unity. To prove $\frac{N_{OP}}{N_{O_{RC}}} \leq 1$ we employ the Schwarz Inequality:

$$\int_0^1 \frac{x^2 dx}{1 + (\frac{x}{x_o})^2} \int_0^1 [1 + (\frac{x}{x_o})^2] G_m(x)\, dx \geq [\int_0^1 x\sqrt{G_m(x)}\, dx]^2 \quad (18a)$$

The equal sign holds only when

$$G_m(f) = C \frac{f^2}{[1 + (\frac{f}{f_1})^2]^2} \quad (18b)$$

To prove that $\frac{N_{OP}}{N_{OW}} \leq 1$ we let $x\sqrt{G_m(x)} = V(x)$. Then

$$\int_0^1 (V(x) - \int_0^1 V(x)\, dx)^2\, dx \geq 0 \quad (19a)$$

Expanding we have:

$$\int_0^1 V^2(x)\, dx - 2[\int_0^1 V(x)\, dx]^2 + [\int_0^1 V(x)\, dx]^2 \geq 0 \quad (19b)$$

or

$$\int_0^1 x^2 G_m(x)\, dx \geq [\int_0^1 x\sqrt{G_m(x)}\, dx]^2 \quad (20a)$$

The equal sign applies when

$$V(x) = \int_0^1 V(x)\, dx \quad (20b)$$

or

$$V(x) = x\sqrt{G_m(x)} = \text{constant} \quad (20c)$$

Hence,

$$G_m(f) = C_1 \cdot f^2 \quad (21)$$

Thus, it is seen that the RC high pass filter is optimum when the power spectral density of the modulation is given by Eq. 18b, and the whitening network is optimum when $G_m(f)$ is given by Eq. 21. For any other $G_m(f)$ the optimal network results in an output noise reduction and hence an output SNR increase.

Examples

1. $G_m(f) = \dfrac{1}{1 + \left(\dfrac{f}{f_1}\right)^2}$

This is an often used representation of the modulation. One assumes that m(t) is a sample function of a white Gaussian process which has been filtered by an RC low pass filter having a 3dB frequency f_1. In this case it is easily shown that

$$\frac{N_{OP}}{N_{O_{RC}}} = \frac{N_{OP}}{N_{OW}} = \frac{\left[\int_0^1 \frac{x\,dx}{1+(x/x_o)^2}\right]^2}{\left[\int_0^1 \frac{x^2\,dx}{1+(x/x_o)^2}\right]} = \frac{\left[1 + \left(\frac{f_1}{f_M}\right)^2 - \frac{f_1}{f_M}\right]^2}{\left[1 - \frac{f_1}{f_M}\cot^{-1}\frac{f_1}{f_M}\right]} \tag{22}$$

for example, if $\dfrac{f_1}{f_M} = 0.25$, $\dfrac{N_{CP}}{N_{O_{RC}}} = \dfrac{N_{OP}}{N_{OW}} = 0.92$. A 0.36 dB improvement in output SNR results.

2. $G_m(f) = 2\sqrt{\pi}\ t^2 e^{-t^2}$

The functional form of $G_m(f)$ was chosen to represent the spectrum of speech. The constant $2\sqrt{\pi}$ was chosen so that $\int_{-\infty}^{\infty} G_m(f)\,df$ is the same in examples 1 and 2. The results obtained are

$$\frac{N_{OP}}{N_{O_{RC}}} = \frac{\left[\sqrt{\frac{\pi}{2}}\ \frac{f_1}{f_M}\ \mathrm{erf}\left(\frac{f_M}{\sqrt{2}\,f_1}\right) - \exp\left(-\frac{f_M^2}{2 f_1^2}\right)\right]^2}{\left[1 - \frac{f_1}{f_M}\tan^{-1}\frac{f_M}{f_1}\right]\left[\frac{5\sqrt{\pi}\,f_1}{3 f_M}\ \mathrm{erf}\left(\frac{f_M}{f_1}\right) - \left(\frac{5}{4} + \frac{f_M^2}{2 f_1^2}\right)\exp\left(-\frac{f_M^2}{f_1^2}\right)\right]} \tag{23}$$

If $\dfrac{f_1}{f_M} = 0.25$, $\dfrac{N_{OP}}{N_{O_{RC}}} \approx 0.53$. Hence a 2.8 dB improvement results.

Using the whitening filter yields

$$\frac{N_{OP}}{N_{OW}} = \frac{\left[\sqrt{\frac{\pi}{2}}\ \frac{f_1}{f_M}\ \mathrm{erf}\left(\frac{f_M}{\sqrt{2}\, f_1}\right) - \exp\left(-\frac{f_M^2}{2 f_1^2}\right)\right]^2}{\left[\frac{3\sqrt{\pi}\, f_1}{8 f_M}\ \mathrm{erf}\ \frac{f_M}{f_i} - \left(\frac{3}{4} + \frac{f_M^2}{2 f_1^2}\right) \exp\left(-\frac{f_M^2}{f_1^2}\right)\right]} \tag{24}$$

If $\frac{f_1}{f_M} = 0.25$, $\frac{N_{OP}}{N_{OW}} \simeq 0.59$. Hence a 2.2 dB improvement results.

Conclusions

In conclusion we reiterate our thesis that the optimum preemphasis network will, in general, result in substantial SNR improvement as compared to the simple and more often used networks. Since, in many communication problems 2 - 3 dB is of considerable importance it seems worthwhile to determine the benefits derived by using an optimum preemphasis network.

III. A Slow Scan Digital TV System

This section outlines a complete computer controlled system that transfers information from a photographic slide into a stored digital form, that allows detailed bit by bit measurements of this data, that allows both linear and non-linear manipulations and/or "transformations" of this data, and that allows the reconversion of either the original or of any "transformed" version of the original data back into a photographic form.

The system utilizes an assembly language programmed Digital Equipment Company, PDP8 computer with a magnetic tape storage unit in conjunction with a laboratory constructed flying-spot scanner and a modified version of a Tektronix 541A oscilloscope.

System Input

The system input is provided by scanning the desired slide with a laboratory constructed flying spot scanner and converting this analog signal into a digital form. After intermediate storage in the core storage unit of the PDP8 this digital information is transferred to magnetic tape for permanent storage.

To some extent the system design has been tailored to suit the computer's idiosyncrasies. For example, the PDP8 core storage and magnetic tape storage units handle information in the form of "pages" of 128, 12 bit words. A total of 4096 words or 32 pages of core storage is available. Since the program that is causing the "recording," "manipulating," or "playing out" of the data must also be in the core storage and it may be convenient to have several other auxiliary programs also available in the core storage one normally wishes to design so that not more than half of the available core memory is used for data storage.

While more than 6 bits [64 levels] are rarely discernible in an outputed video signal the system is simplified by utilizing one word per video sample. An existing narrow band TV system in the laboratory has shown that a 100 x 100 matrix of points is sufficient to reproduce a picture with adequate detail for our purposes. Hence while a 128 x 128 matrix would be just as compatible with the computer memory organization we employ 100 samples/line and 100 lines/frame. With a photographic output no benefit is derived from frame interleaving and it is not employed.

Figure 1 illustrates a block diagram of the recording system.

Since the total number of programs related to the digital video system now totals more than 25 it is convenient to store these programs on magnetic tape in both their machine language and in their binary forms. Both forms are desirable since machine language is the only form that is understandable to the human operator and the only form in which constants may be inserted or routines modified, while the binary form is the form upon which the machine actually operates. If the binary form is not stored permanently then before every run one must go through a routine of having the machine translate the machine language program into the binary form all over again.

Since the scanning routine is known (it may be horizontal or vertical or may proceed in either direction) no addressing of individual points is required.

While it is perfectly possible to operate upon the data before storage, we have chosen not to do this but to store directly in an unperturbed fashion. This allows one to have the "original" picture available for playback and comparison with any modified version. [Such comparison may be either in an output video form or may be done on a bit-by-bit basis within the machine itself.]

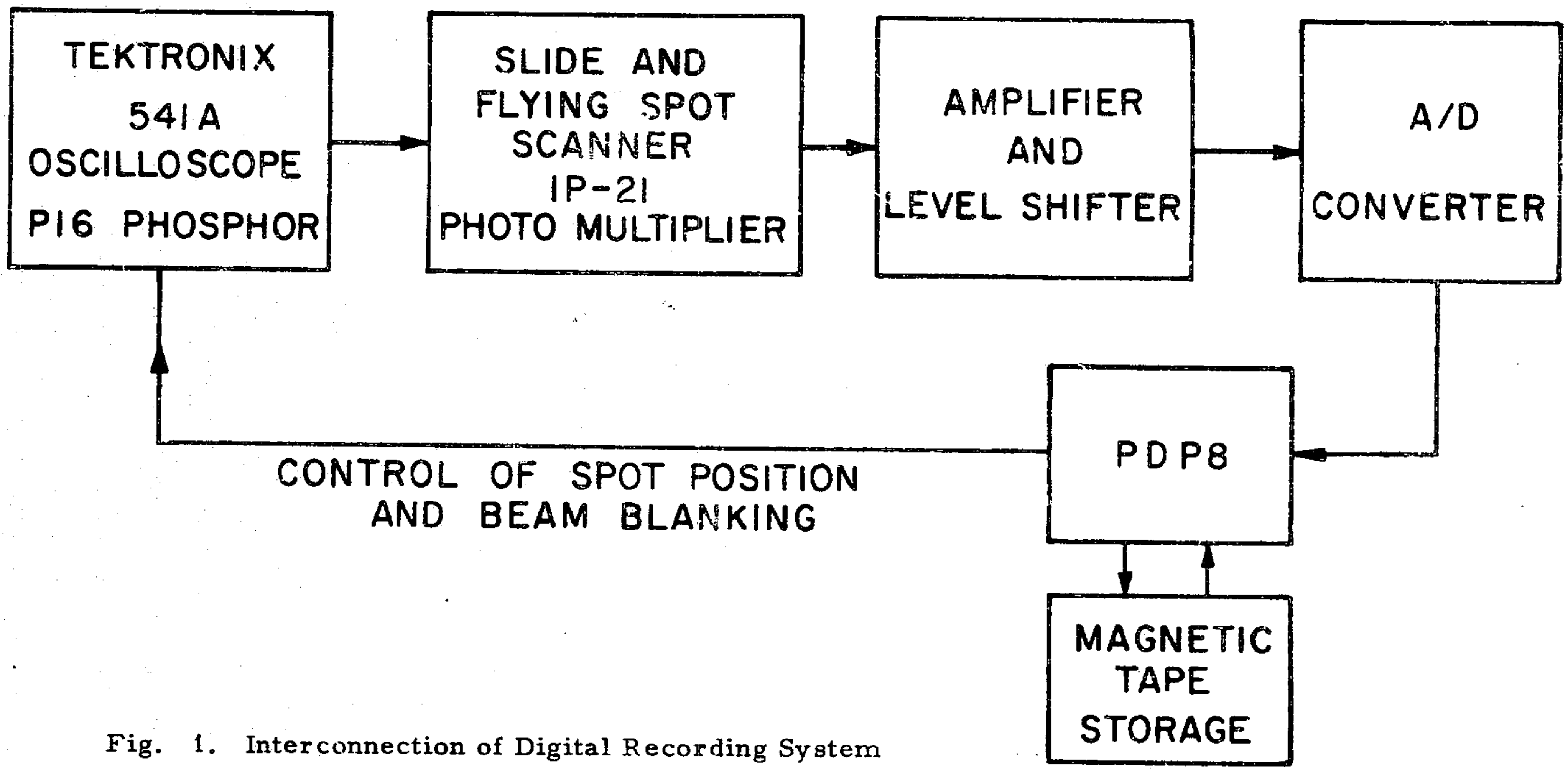

Fig. 1. Interconnection of Digital Recording System

With computer control there is no need to scan by the line at all since one could just as well scan spirally or in N x N squares [N < 100] or otherwise. So far we have found it convenient to do the initial scanning in a linear fashion even though subsequent operations may deal with N x N square of points. [A real time system that chose to handle data in N x N squares would of course want a N x N scan to reduce its buffer storage problems.]

System Output

To return the data to video form one must first switch tapes back to the program tape and transfer the binary form of PLAY, and LIN into the core storage. After standardization the flying spot scanner is replaced by an oscilloscope camera. [A experimental determination of the "optimum" f stop for a given film speed is necessary for any given system,] and the PLAY program has its internal data seeking address changed so that it reads the appropriate video data. The camera shutter is now opened and the PLAY program is started to print out the video data.

The print out is accomplished by varying the unblanking time of the constant intensity beam while it is shifted successively through the 10^4 data points. This duration modulation scheme removes the effect of phosphor nonlinearities. The P16 phosphor has a decay time to 10% of its initial brightness in 100 nsec. Thus from the phosphor viewpoint if the maximum duration at any one point is 1 μsec or more then the apparent intensity will be proportional to duration.

The actual system has 128 "duration increments" of 4.5 μsec each thus it is capable of presenting a 128 level gray scale. In practice we normally divide the total range into only 64 or 32 levels. Since "white" produces an exposure of 576 μsec/sample and "black" produces no exposure the "normal" picture takes about 3 seconds to print out.

Actually a linear variation of duration with intensity does not lead to a linear picture since while the phosphor nonlinearity has been removed the film nonlinearity remains. The LIN program has a table look-up capability that translates any "linear" sample level into a new level along a desired nonlinear scale that may be used both for film gamma correction and if desired to perform an "expansion" function.

Picture Manipulation and Measurement Programs

Among the programs that have been developed are:

(a) Overall picture level probability density programs.

(b) Programs for the probability densities for the averages of adjacent squares of 2 x 2, 3 x 3, and 4 x 4 samples.

(c) Programs to reduce the average transmission time by a number of simple manipulations.

(1) Skip transmission of alternate points.

(A) Use amplitude of first point of the pair.

(B) Use amplitude of average of the two points of a linear pair.

(2) Extend to three points or more in row.

(3) Extend to squares of 2 x 2, 3 x 3, and 4 x 4 points.

(4) Modify (3) by transmitting the average for say a 3 x 3 matrix as well as a two bit signal for each sample that indicates the sign of the depatrure as well as whether the departure from the average is less than one unit or more than one unit.

(d) Programs that contain samples of random noise and that allow randomization of the quantization noise component of the stored digital signal.

(e) Programs that contain nine, sixteen, and thirty-two level linear gray scales for test and adjustment purposes.

(f) Programs that allow the real time transmission and subsequent reception and storage of twelve lines at a time of video data. One program allows transmission and reception in analog form while another transmit the signal in binary form. In either case the transmission and reception are under the control of an external clock. These programs allow the transmission of the stored or compressed data through a real or simulated channel so that the effect of the channel may be studied. The twelve lines at a time limitation is imposed by the limited core storage available in the computer. Obviously further transmission is possible after an interval that allows for the transfer of the received data back to the tape and the transfer of another 12 lines from the tape into the core storage.

Results

Figure 2 is a picture after complete transmission through the system. In the original photograph from the oscilloscope face it is possible to distinguish individual picture elements. For reproduction purposes these pictures have been enlarged by a factor of three times. [The output picture size in our system is limited by the deflection capabilities of the particular oscilloscope employed.] For monitoring and visual read-outs other oscilloscopes with much larger available areas have been employed. Since single picture elements may be monitored, one is able to note the effects of digital errors upon each particular portion of the picture.

Figure 3 and 4 show flow charts for the RECORD and PLAY programs respectively.

References

(1) Digital Television Storage and Video Redundancy Reduction MSc Report, Douglas E. Stell, Polytechnic Institute of Brooklyn, June 1969.

(2) Picture Coding, W. F. Schreiber, Proc. of IEEE, Vol. 55, No. 3, March 1967, pp 320-330.

Fig. 2. Sample Photograph after RECORDING and PLAYING Operations

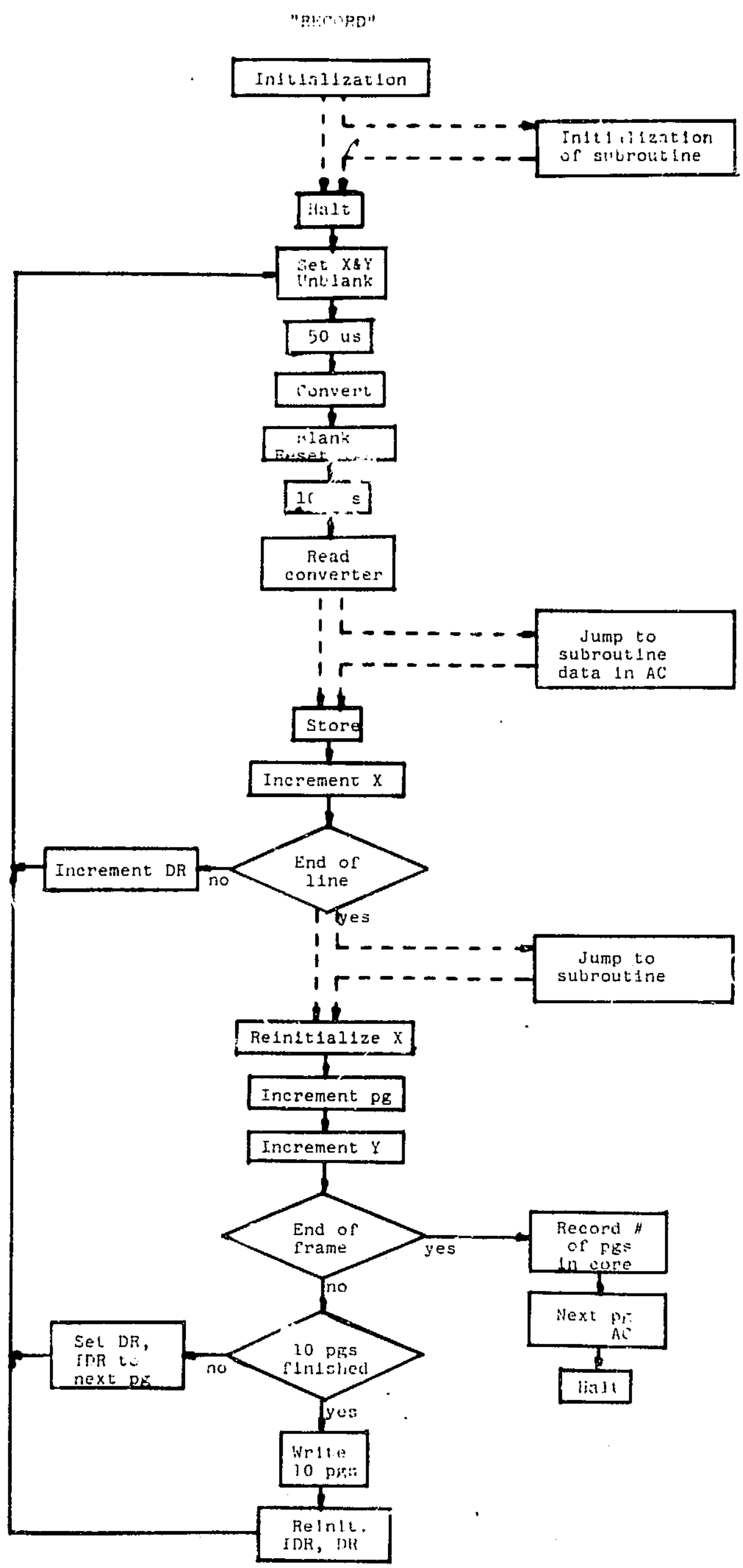

Fig. 3. Flow Chart for the RECORD Program

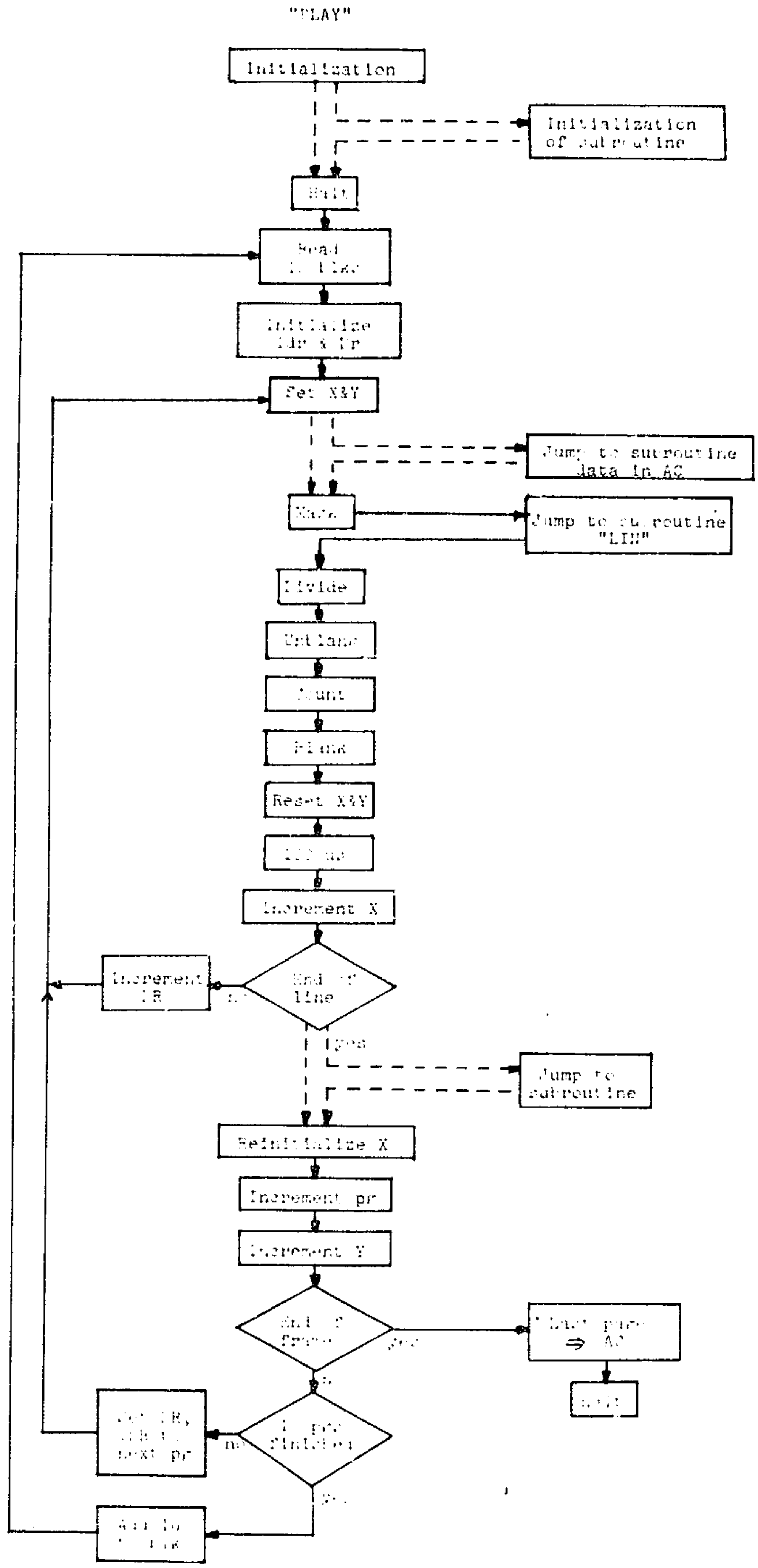

Fig. 4. Flow Chart for the PLAY Program

IV. A New, Recursive, Second Order Gradient Algorithm

Nomenclature

1) A vector is represented by: $\underline{x}$

2) Random quantities are represented by a tilde (~)

e.g., $\tilde{n}$

3) Components of a vector are represented by superscript in parenthesis. For example, the k^{th} component of $\underline{x}$ is:

$\underline{x}^{(k)}$

4) The stage of iteration will be indicated by a subscript:

$\underline{x}_i$ is the vector $\underline{x}$ evaluated at the i^{th} stage.

$x_i^{(k)}$ is the k^{th} component of $\underline{x}$ at the i^{th} stage.

5) The transpose of a matrix T is T^t.

6) The deterministic part of a quantity is represented by a Latin character; the random part by a Greek character, e.g.,

$$\tilde{\underline{g}} = \underline{g} + \tilde{\underline{\psi}}$$

7) Powers of a quantity are indicated in the standard manner, e.g., the i^{th} power of the matrix T is T^i.

8) The symbol $\rho(T)$ denotes the Spectral Radius of the matrix T. The symbol $R_S^*(k)$ denotes the sampled auto-correlation function of S(t) at time $t = kT$.

9) The norm of a matrix A is denoted by $||A||$. The norm of a vector $\underline{x}$, by $||\underline{x}||$.

Introduction

The equalization of data signals which have been transmitted through a dispersive channel has recently received new attention by virtue of the fact that a transversal (tapped delay line) structure lends itself readily to adaptive and iterative adjustments. In the presence of both dispersion and additive noise, an appropriate measure of the quality of equalization is the sum of the mean squared distortion due to intersymbol interference and the mean squared noise. This measure can be shown to be closely related to either the signal-to-noise ratio at the decision point or the average probability of digit error.

For a given set of transmitted signals and channel conditions, the mean squared distortion plus noise can be shown to be a positive definite quadratic function of the tap gains $x_1, x_2, x_3, \ldots x_n$. The basic transversal equalizer structure is shown in Figure 1. The input is periodically sampled after filtering and the samples are applied to the input of the transversal filter. For data equalization, the taps are ideally adjusted so that the output, y(k), has a maximum at y(o) [time being referenced to this point] while $y(k)\ k \neq 0$ is as small as possible. The departure from this condition is measured by the sum of the mean squared distortion plus the mean squared noise, $\overline{D}^2 + \sigma^2$. In Appendix I, we show that the mean squared error

$$\overline{e^2} = \overline{D}^2 + \sigma^2 + (\overline{e})^2 \tag{1}$$

can be expressed as a quadratic of the tap gains $\underline{x}$ as follows:

$$\overline{e^2} = \frac{1}{2}\,\underline{x}^t G\underline{x} - \underline{a}^t\,\underline{x} + V_r^2 \tag{2}$$

$(\overline{e})$ is the mean of the error, after equalization $(\overline{e})$ has a small, but non-zero value.

where

G = covariance matrix of sampled received signal

$\underline{a}$ = a vector whose components are proportional to the sample values of an isolated noiseless received pulse

V_r = peak level of reference signal.

The minimization of (2) can be accomplished by various iterative algorithms. If noiseless observations are available, the Fletcher-Powell[1] and Fletcher-Reeves[2] conjugate-gradient methods guarantee convergence in exactly N stages of iteration where N is the dimension of the vector $\underline{x}$. This performance is accomplished when truncation errors are negligibly small, or, equivalently, when signal-to-noise ratios are high.

On the other hand, when noise is appreciable, the adjustment algorithm commonly used is based on a gradient method or some variation of stochastic approximation[3].

The performance of conjugate-gradient methods in the presence of noise is not known. The analysis of this behavior in noise is difficult even if small noise is assumed because of the complicated way in which the direction of search at stage k depends on all (k - 1) directions. Furthermore, for moderate noise levels noise-noise cross products must be considered making the analysis still more difficult.

Gradient methods including stochastic approximation algorithms work well in the presence of noise in an asymptotic sense. The conditions for convergence can be stated. However, they tend to converge slowly.

Higher order gradient methods, which is the subject of this paper, makes use of stored values of gradients obtained in previous stages of iteration. The objective of using these higher order gradients are (1) to smooth the noisy observations and (2) to permit a more rapid convergence to take place.

Higher-Order Gradient Methods:

With $\underline{x}_i$, the tap gain vector at stage (i); $\underline{g}_k$, the gradient vector measured at stage (k), with α_0, α_1... some positive constants selected to guarantee convergence the iteration is as follows:

$$x_{i+1} = \underline{x}_i - \alpha_0 \tilde{\underline{g}}_i - \alpha_1 \tilde{\underline{g}}_{i-1} - \alpha_i \tilde{\underline{g}}_{i-2} \cdots - \alpha_M \tilde{\underline{g}}_{i-M}$$

The iteration starts at $\underline{x}_0$ selected arbitrarily. The initial gradient is $\tilde{\underline{g}}_0$ Heuristically, the advantage of the multi-stage gradient method is that it has some of the ridge seeking properties of the conjugate gradient methods. while being simpler to implement and analyzed. In addition, some smoothing of the random components of the gradients is expected to take place insuring good performance in presence of noise.

Figure 2 illustrates in a simple fashion why the higher order gradient algorithm is expected to have ridge seeking ability (i.e., fast convergence capability). Assume that the convex surface has a ridge. The gradients tend to follow the geodesic starting from point (1) if the first-order gradient method is used. For the second-order gradient method the direction of search at (2) is approximately along the resultant vector of the gradient, at points (2) and (1). This direction heads faster towards the ridge.

Figure 3 is a two dimentional projection of the contours of Figure 1. Two paths are sketched indicating the expected behaviour of a first-order gradient and a second-order gradient algorithm. The simple gradient algorithm converges "exponentially" to the minimum. The second-order gradient (S.O.G.) exhibits "damped oscillatory" behavior. Consequently, it should be able to converge faster than the simple gradient method. Computer simulation indeed reveals that the S.O.G. method can produce significant speed improvements. First a noiseless system is considered (i.e., the gradients are assumed noiseless). Conditions on α and β are given for stability. Proofs that the parameters $\underline{x}$ converge to the true minimum without bias are given. Then the gradient vectors $\underline{g}_i$ and $\underline{g}_{i-1}$ at the $i^{\underline{th}}$ stage and at the $(i-1)^{\underline{th}}$ stage are assumed corrupted by noise from a stationary random process. The noise samples are assumed independent. A bound on the asymptotic value of the mean-square error in $\underline{x}$ is given. The convergence of the first-order gradient algorithm is also studied for comparison. The speed of convergence of the two algorithms is investigated, putting in evidence the superiority of the S.O.G. in the presence of appreciable spread in the range of the eigenvalues of the system matrix G.

Convergence of the S.O.G. Algorithm with Noiseless Gradients

The iteration, which is designed to minimize the quadratic function (2) is given by:

$$\underline{x}_{i+1} = x_i - \alpha \underline{g}_i - \beta \underline{g}_{i-1} \tag{3}$$

when $\underline{g}_i$ is the gradient of the function at the $i^{\underline{th}}$ iteration ans is given by

$$\underline{g} = G\underline{x} - \underline{a} \tag{4}$$

Operating both sides of (3) by G and identifying the gradient terms, we obtain the recurrence relation

$$\underline{g}_{i+1} = [I - \alpha G]\, \underline{g}_i - \beta G \underline{g}_{i-1} \tag{5}$$

Now, since G is a symmetric positive definite matrix, it can be diagonalized by a norm-preserving transformation, P, which upon applying to both sides of (5) yields

$$\underline{W}_{i+1} = [I - \alpha\Lambda]\, \underline{W}_i - \beta\Lambda \underline{W}_{i-1}$$

where $\quad W_i = P\underline{g}_i$

and

$$G = P^{-1} \Lambda P \text{ defines } \Lambda.$$

The system (6) is completely decoupled in its components and the zeroes cf the characteristic polynomials of the system

$$F(z) = z^2 - [1 - \alpha \lambda_k] z + \beta \lambda_k$$

determine the stability and dynamic behavior. λ_k are the eigenvalues (assumed distinct for the moment) of the matrix G. For stability, the zeroes of F(z) must lie within the unit circle $|z| < 1$. An equivalent condition, the Schur-Cohn Criterion[4] states that the necessary and sufficient conditions for stability are: a) $F(1) > 0$, b) $F(-1) > 0$, c) $|\beta \lambda_k| < 1$. It will turn out that for our purposes it is necessary for α, β, > 0; then for stability we require

$$\beta < \frac{1}{\lambda_k}, \quad \text{all } k \tag{7}$$

$$(\alpha - \beta) < \frac{2}{\lambda_k}, \text{ all } k \tag{8}$$

The recurrence equation for the tap-weights after diagonalizing G by a the similarity transformation, is:

$$\underline{Z}_{i+1} = [I - \alpha\Lambda] \underline{Z}_i - \beta \Lambda \underline{Z}_{i-2} + (\alpha + \beta) \underline{b}$$

where

$$\underline{Z} = P\underline{x}$$

$$G = P^{-1} \Lambda P \quad ; \quad \underline{b} = P\underline{a}$$

The components of $\underline{Z}$ are decoupled. Using the State-Space representation one can express the recurrence equation fot the k^{th} components of $\underline{z}$ as the following first-order vector equation:

$$\underline{y}_{j+1} = T(\lambda_k)\,\underline{y}_j + (\alpha+\beta)\,D(\lambda_k)\,\underline{c}_o \tag{9}$$

where

$$\underline{y}_{j+1} = \begin{bmatrix} z_i(k) \\ z_{i-1}(k) \end{bmatrix}$$

(The superscripts identify the components of the vector, with $j = \frac{i+2}{2}$)

$$T(\lambda_k) = \left[\begin{array}{c|c} (1-\alpha\lambda_k)^2 - \beta\lambda_k & -\beta\lambda_k(1-\alpha\lambda_k) \\ \hline (1-\alpha\lambda_k) & -\beta\lambda_k \end{array}\right],$$

$$D(\lambda_k) = \left[\begin{array}{c|c} 1 & 1-\alpha\lambda_k) \\ \hline 0 & 1 \end{array}\right], \text{ AND}$$

$$\underline{c}_o = \begin{bmatrix} 1 \\ 1 \end{bmatrix}$$

Stability of the recurrence Equation (5) for the gradients guarantees the stability of Equation (9) for the tap-weights. Furthermore, Equation (9) is stable if the maximum eigenvalue of T is less than 1, i.e.,

$$\rho(T) \triangleq \max_k |\text{eigenvalue of } T(\lambda_k)| < 1 \tag{10}$$

$\rho(T)$ is the spectral radius of T.

<u>Rate of Convergence</u>

Iterating Equation (9), we get the solution:

$$\underline{y}_{j+1} = T^j\,\underline{y}_i + (\alpha+\beta)\,b^{(k)} \sum_{k=0}^{j-1} T^k D\,\underline{c}_o \tag{11}$$

Let the error vector $\underline{E}_{j+1}$ be defined as:

$$\underline{E}_{j+1} = \underline{Y}_{min} - \underline{Y}_{j+1}$$

where $\underline{Y}_{min}$ is the vector that yields the minimum **mean-square** error.

It can easily be shown that the square of the norm of $\underline{E}$ is bounded at each stage as follows:

$$||\underline{E}_{j+1}||^2 < \rho^{2(j-1)}(T)\, ||\underline{\delta}||^2 \qquad (12)$$

where $\underline{\delta}$ is a constant vector:

$$\underline{\delta} = \underline{Y}_{min} - {}^{T}\underline{Y}_1$$

$$\rho(T) = \text{spectral radius of } T.$$

From (11) we have $\rho(T) < 1$. The ratio of the norm of $\underline{E}$ at two consecutive stages is approximately:

$$||E_{j+1}||/||\underline{E}_j|| \approx \rho(T)\, ||\underline{\delta}|| \qquad (13)$$

Equation (13) yields the asymptotic rate of convergence. It shows that $\rho(T)$ must be made as small as possible for fast convergence.

If the roots of T are complex, then:

$$\rho(T) = |\beta\lambda_k| \qquad (14)$$

Therefore it becomes easy to set $\rho(T)$ by controlling only (β). The additional requirement which guarantees complex roots is:

$$4\beta\lambda_k > (1 - \alpha\lambda_k)^2 \qquad (15)$$

It is seen immediately that we must have $\beta > 0$. $\beta\lambda_k$ is bounded as follows (combining 14 and 15):

$$\frac{(1 - \alpha\lambda_k)^2}{4} < \beta\lambda_k < 1 \tag{16}$$

Equations 7, 8, 16 must be satisfied to guarantee good performance of the S. O. G.

Selection of (α) and (β) for Stability

Case of known G

When G is known it is easy to estimate λ_{max} ; we have [5]

$$\lambda_{max} \leq 1 \leq \max_{1} \leq n \sum_{j=1}^{n} |G_{i,j}|$$

Coefficients (α) and (β) are selected to satisfy equations (7) and (8) for λ_{max}. They are automatically satisfied by all the other eigenvalues. This technique for selecting (α) and (β) can be used in computer simulation. There is no need to calculate the eigenvalues.

Case of unknown G

For an adaptive system, G is generally unknown. In this case it is necessary to estimate λ_{max} by an initial search procedure. The search procedure is as follows: Start with an $\underline{x}_o$. Then a search is made along the steepest descent direction, i. e.:

$$\underline{x} = \underline{x}_o - k\underline{g}_o$$

$$k > 0$$

k is increased until a minimum of $\overline{e^2}$ is obtained. At that point we have:

$$k = \frac{\underline{g}_o^t \, \underline{g}_o}{\underline{g}_o^t \, G \underline{g}_o} \tag{17}$$

$$\frac{1}{\lambda_{max}} < k < \frac{1}{\lambda_{min}}$$

We than set $\alpha \simeq k$, $\beta \simeq \frac{k}{2}$. For systems where $\lambda_{max}/\lambda_{min} < 2$, the values of α and β so obtained will satisfy the stability requirements (7) and (8).

For systems with large $\lambda_{max}/\lambda_{min}$ ratio, there is a possibility that unstability might occur. In that case, one would start again at a new starting point, the procedure being repeated until proper values are found.

The search technique just indicated is exactly similar to the first stage of the Fletcher-Reeves [2] algorithm. This suggests that one could also use the first few stages of the F-R algorithm in the search for (α) and (β). The search is stopped when a stable combination is found.

S. O. G. with Noisy Gradients

In practical application of the S. O. G. algorithm to equalizers, the gradients are obtained by a correlation operation between the error signals and the appropriate delayed input. Under these circumstances,

$$\underline{\tilde{g}}_i = \underline{g}_i + \underline{\tilde{\Psi}}_i$$

where $\underline{\tilde{g}}_i$ is the noisy measurement of the gradient $\underline{g}_i$ corrupted by a noise vector, $\underline{\tilde{\Psi}}_i$ which is assumed to have zero mean $E\|\tilde{\Psi}_i\|^2 = \sigma^2$, and independent of each i. It is further assumed that $\underline{\tilde{\Psi}}_i$ is independent of the tap gains $\underline{x}$. Then substituting these noisy gradients into the algorithm (3) yields, after collecting terms,

$$\underline{x}_{i+1} = (I - \alpha G)\,\underline{x}_i - \beta G x_{i-1} + (\alpha + \beta)\underline{a} - \alpha\,\underline{\tilde{\epsilon}}_i \tag{18}$$

where

$$\underline{\tilde{\epsilon}}_i = (\underline{\tilde{\Psi}}_i + \frac{\beta}{\alpha}\,\tilde{\Psi}_{i-1}) \tag{19}$$

whence

$$E|\underline{\tilde{\epsilon}}_i|^2 = E\,|\underline{\tilde{\Psi}}_i|^2 \left[1 + (\frac{\beta}{\alpha})^2\right] \tag{20}$$

Equation (18) may be decoupled, by applying the diagnolization transformation, P as above. Writing the result as a first order equation, we obtain an equation similar to (9) driven by a random sequence. Iterating this equation, one obtains an equation similar to (10).

$$\underline{y}^{(k)}_{j+1} = T^j \underline{y}_1 + (\alpha + \beta) b^{(k)} \sum_{k=0}^{j-1} T^k DC_o + \alpha \sum_{k=0}^{j=1} T^k D\tilde{f}_k \tag{21}$$

where $\tilde{f}_k$ is a random sequence linearly related to $\tilde{\epsilon}_k$. Now since $\rho(T) < 1$,

$$\sum_{k=0}^{j=1} T^k = [I - T^{j-1}][I - T]^{-1} \quad .$$

The non-random component $\underline{\tilde{\theta}}_j$ of $\underline{y}_j$, obtained by subtracting the mean, is

$$\underline{\tilde{\theta}}_j = -\alpha \sum_{k=0}^{j-1} T^k D \underline{\tilde{f}}_k \tag{22}$$

we will show in Appendix (II) that the near squared value of $\underline{\tilde{\theta}}_2$ is bounded as follows when the eigenvalue of T are distinct

$$E||\underline{\tilde{\theta}}||^2 < \frac{2\alpha^2\sigma^2}{N}\left[1 + \left(\frac{\beta}{\alpha}\right)^2\right] \frac{\rho(D^tD)}{1 - \rho^2(T)} \quad , \quad \alpha \neq 0 \tag{23}$$

The matrix T is a 2 x 2 matrix and its eigenvalues are distinct except for the rare situation when the discriminant $(1 - \alpha\lambda_k)^2 - 4\beta\lambda_k = 0$, all λ_k. The S.O.G. gradient, in fact exhibits its best performance when the eigenvalues of T are complex. Consequently Equation (23) is valid for all practical situations and the only condition required to maintain the right hand side finite for any N is that $\rho(T) < 1$. But this condition, as was shown, is equivalent to the Shur-Cohn criterion for dynamic convergence. Hence, dynamic convergence insures stochastic boundedness.

Computer Simulation

The performance of the S. O. G. is investigated by simulation on a digital computer for a system where S(t) is a raised-cosine pulse defined as

$$S(t) = \frac{h}{2} \left(1 + \cos 2\pi \frac{t}{L}\right) \qquad -\frac{L}{2} < t < \frac{L}{2}$$

$$S(t) = 0 \qquad |t| > \frac{L}{2}$$

The pulse has peak level (h) and width L. The raised-cosine pulse is very convenient for simulation because of its finite width. This pulse is also used in practical data communications[6].

The results for the simulation for noiseless observations are shown on Figures 4 through 7 for an 11-tap equalizer. It has been shown by Coll[7] that an 11-tap equalizer yields a performance close to optimum, when the isolated pulse S(t) is a raised-cosine.

For all curves the rate of convergence is plotted with respect to the coefficient (α). The coefficient (β) is treated as a parameter. In the F.O.G. algorithm β is equal to zero.

The rate of convergence is the number of iterations, required to equalize within a given accuracy of the final SNR. The starting point is the same in all cases, namely, the center-tap weight is set equal to unity, all other tap-weights are set to zero.

The intersymbol interference distortion is classified as small

$$\left(\frac{\lambda_{max}}{\lambda_{min}} \leq 2\right), \quad \text{moderate} \left(\frac{\lambda_{max}}{\lambda_{min}} \approx 5\right), \quad \text{and large} \left(\frac{\lambda_{max}}{\lambda_{min}} > 10\right).$$

This classification is from the point of view of the equalizability of the channel. When the ratio $\frac{\lambda_{max}}{\lambda_{min}}$ is as large as 20, it turns out that the spectral radius of the T matrix corresponding to the smallest eigenvalue λ_{min} is very close to unity. This is caused by the fact that (α) and (β) cannot be made too large for stability reasons. In fact, in practice we have $\alpha\lambda_{max} < 2$, $\beta\lambda_{max} < \rho$. In the expression for $\rho(T)$ a small value of $\alpha\lambda$ yields a $\rho(T)$ close to unity. Consequently when the ratio is greater than 20 the channel is practically unequalizable.

Figure 8 shows that equalized and the equalized SNR versus $\frac{T}{L}$. The data rate is $\frac{1}{T}$. The simulation is performed for various values of $\frac{T}{L}$. The intersymbol interference increases when $\frac{T}{L}$ decreases. Table-1 is a tabulation of the eigenvalues of G for various $\frac{T}{L}$. The ratio of $\frac{\lambda_{max}}{\lambda_{min}}$ is greater than 20 for $\frac{T}{L}$ equal to or less than 0.3. Figure 8 shows that the SNR starts dropping rapidly above 0.3.

The final SNR accuracy for the moderate and large distortion cases is 0.5 db (10%). For the small distortion case is is 0.1%.

The important points of the simulation are:

1. The S.O.G. is quite insensitive to variations in (α).

2. The behaviour of the S.O.G. at moderate and large distortion is different from its behaviour at low distortion.

At low distortion, there is an optimum (β) just as predicted by the analysis. At moderate and large distortion large (β) tend to give better performance. This could be explained by the fact that the S.O.G. tends to locate a ridge and ride along it towards the minimum. In these situations the asymptotic formula for the rate of convergence is not quite applicable. Improvements in rates of convergence vary from 1.25 to about 2/1 for the large distortion, and from 1.5 to 3/1 for the moderate distortion case.

<u>Performance with Noisy Observations</u>

The rates of convergence with noisy observations was also investigated for the low distortion cast ($T/L = 0.4$). The noise component in the gradient corresponds to and initial SNR in the largest component of about 40 db. In the S. O. G. α and β were set equal to 0.01. In the F. O. G. α was set equal to 0.02. This was done in order to have the situation where the effective corrective action would be about the same strength in the absence of noise. The criterion for convergence was that the SNR should be within 0.2 db (5%) for the final value for more than 90% of the time. The results tabulated in Table 2 show that the S. O. G. is 5 times faster than the F. O. G.

Appendix I

Referring to Figure 1, at the input to the equalizer we have:

$$\tilde{v}(t) = \sum_n \tilde{\theta}_n S(t - nT) + \tilde{\eta}(t)$$

where $\tilde{\theta}_n = \pm 1$ represents the independent sequence of binary symbols 1, or 0 constituting the data bit-stream.

$\eta(t)$ is the noise procedd into the TDL.

The error at sampling instants is

$$\tilde{e} = \tilde{\theta}_o V_R - \tilde{y}(o) = \tilde{\theta}_o V_R - \sum_j x^{(j)} \tilde{v}(j)$$

where V_R is the peak reference voltage.

The mean-square error is, assuming that the data symbols are uncorrelated and that the noise and data processes are uncorrelated:

$$\overline{e^2} = E\{\tilde{e}^2\} = V_R^2 + \frac{1}{2} \underline{x}^t G \underline{x} - \underline{a}^t \underline{x}$$

The matrix T is the correlation matrix of input signal and noise:

$$G(i, j) = 2 \sum_n R_S^*(-j - n) R_S^*(-k - n) + 2 R_\eta^*(-j - k)$$

$R_S^*(k)$ = sampled autocorrelation function of isolated pulse S(t).

$R_\eta^*(k)$ = sampled autocorrelation function of the noise process.

The components $a^{(k)}$ of the vector $\underline{a}$ is:

$$a^{(k)} = 2 V_R S(-k)$$

The mean-square error $\overline{e^2}$ can be expressed as follows by a simple manipulation of the expression shown previously:

$$\overline{e^2} = (\overline{e})^2 + D^2 + N_o$$

where:

$\bar{e}$ = mean of the error = $V_R - \sum_j x^{(j)} R_S^*(-j)$

D^2 = mean-square distortion (intersymbol interference)

$$D^2 = \sum_{h \neq 0} \sum_j \sum_k x^{(j)} x^{(k)} R_S^*(-j-n) R_S^*(-k-n)$$

N_o = Output noise power

$$N_o = \sum_j \sum_k x^{(j)} x^{(k)} R_\eta^*(j-k)$$

Signal-to-Noise Ratio:

The output signal-to-noise ratio is defined as:

$$SNR = \frac{(\overline{\vartheta_o y(o)})^2}{D^2 + N_o} = \frac{(V_R - \bar{e})^2}{\overline{e^2} - (\bar{e})^2}$$

When $\overline{e^2}$ is minimum, we have, assuming G is nonsingular,

$$\underline{x} = G^{-1}\underline{a}$$

$$\overline{e^2}_{min} = V_R^2 - \frac{1}{2}\underline{a}^t G^{-1}\underline{a}$$

$$\bar{e} = V_R - \frac{1}{2V_R}\underline{a}^t\underline{x} = \frac{\overline{e^2}_{min}}{V_R} - 1$$

The SNR corresponding to the minimum is:

$$SNR = \frac{V_R^2}{\overline{e^2}_{min}} - 1$$

Appendix II $\quad$ Bound on $E||\tilde{\theta}||^2$

The random component $\tilde{\underline{\theta}}_j$ of $\underline{y}_j$ is

$$\tilde{\underline{\theta}}_j = -\alpha \sum_{k=0}^{j-1} T^k D \tilde{\underline{f}}_k \tag{II. 1}$$

Let $D \tilde{\underline{f}}_k \triangleq \tilde{\underline{\mu}}_k$, then $E||\tilde{\underline{\theta}}_i||^2$ is bounded if $E||T^k \tilde{\underline{\mu}}_k||^2$ decrease faster than $(\frac{1}{k})$.

Now, $$E||\tilde{\theta}_j||^2 = \alpha^2 E \sum_{i,k} (T^i \tilde{\underline{\mu}}_i)(T^k \tilde{\underline{\mu}}_k) \tag{II. 2}$$

where $E\{\tilde{\underline{\mu}}_i^t \tilde{\mu}_k\} = \delta_{ik} E||\tilde{\underline{\mu}}_k||^2$

then

$$E||\tilde{\underline{\theta}}_j||^2 = \alpha^2 \sum_k E\{\tilde{\underline{\mu}}_k^t B_k \tilde{\underline{\mu}}_k\} < \alpha^2 \rho(B_k) E||\tilde{\underline{\mu}}_k||^2 \tag{II. 3}$$

where

$$B_k = (T^k)^t T^k \tag{II. 4}$$

and

$$\rho(B_k = \max_i (\ell_i), \quad \ell_i \text{ an eigenvalue of } B_k$$

Now

$$E||\underline{\mu}||^2 < \rho(D^t D) E||\tilde{\underline{f}}_i||^2 \tag{II. 5}$$

$$D^t D = \begin{bmatrix} 1 & a \\ a & (a^2+1) \end{bmatrix} \quad \text{and has eigenvalues } \frac{a^2+2}{2} \pm \frac{|a|}{2}\sqrt{a^2+4}$$

where $\quad a \triangleq (1 - \alpha\lambda_k)$

hence for the range $|\alpha| < 1$, (the conditions for dynamic stability)

$$1 < \rho(D^t D) < \frac{3+4\sqrt{5}}{2}$$

next,

$$E||\tilde{\underline{f}}_i||^2 = 2E||\tilde{\underline{\psi}}_i||^2 \left[1 + (\frac{\beta}{\alpha})^2\right] = \frac{2\sigma^2}{N}\left[1 + (\frac{\beta}{\alpha})^2\right] \tag{II. 6}$$

Then

$$E\,||\underline{\theta}_i\,||^2 < \frac{2\alpha^2\sigma^2}{N}\left[1 + \left(\frac{\beta}{\alpha}\right)^2\right]\rho\,(D^tD)\sum_k \rho\,(B_k) \tag{II. 7}$$

It remains to express $\rho(B_k)$ in terms of T. But it is apparent that the eigenvalues of B_k are simply the squares of those of T. Hence $\rho(B_k) = \rho^2(T)$ and substituting into (II. 7) we get:

$$E\,||\underline{\theta}_i||^2 = \frac{2\alpha^2\sigma^2}{N}\left[1 + \left(\frac{\beta}{\alpha}\right)^2\right]\frac{\rho(D^tD)}{1 - \rho^2(T)} \tag{II. 8}$$

which is equation (23).

EIGENVALUES

T/L =	0.2			0.3			0.325			0.35	
1	0.1905623E	03	1	0.9182054E	02	1	0.7680396E	02	1	0.6413972E	02
2	0.1250777E	03	2	0.8206992E	02	2	0.6956519E	02	2	0.5896867E	02
3	0.1627129E	03	3	0.6868138E	02	3	0.5964699E	02	3	0.5188040E	02
4	0.5220184E	02	4	0.5983728E	02	4	0.5339320E	02	4	0.3202762E	02
5	0.8600641E	02	5	0.4647359E	02	5	0.4315642E	02	5	0.4767342E	02
6	0.1233392E	02	6	0.3372678E	02	6	0.3326416E	02	6	0.4009033E	02
7	0.2756798E	02	7	0.2316492E	02	7	0.2477571E	02	7	0.2338210E	02
8	0.4509062E	01	8	0.1492329E	02	8	0.1799931E	02	8	0.2454019E	02
9	0.1375841E	01	9	0.9222512E	01	9	0.1242232E	02	9	0.1656314E	02
10	0.6194134E	00	10	0.5740190E	01	10	0.7532462E	01	10	0.1424158E	02
11	0.5543146E	00	11	0.3934752E	01	11	0.9451706E	01	11	0.1133326E	02

T/L =	0.4	
1	0.4571059E	02
2	0.4329649E	02
3	0.3897430E	02
4	0.4072165E	02
5	0.3014349E	02
6	0.3740820E	02
7	0.2789381E	02
8	0.2909106E	02
9	0.2457819E	02
10	0.2284688E	02
11	0.2121237E	02

Table 1 Eigenvalues for Various Values of T/L

	α	β	No. of Iterations
S. O. G.	0. 01	0. 01	22
F. O. G.	0. 02	0. 0	110

Table 2 Convergence with Noisy Observations.
$T/L = 0.4$, Initial SNR = 40 db.

References

1. Fletcher, R. and M. J. D. Powell, "A Rapidly Convergent Descent Method for Minimization" Computer Jl. Vol. 6, No. 2, pp 163-168, April 1963.

2. Fletcher, R., C. M. Reeves, "Function Minimization by Conjugate Gradients" Computer Jl. Vol. 7, No. 2, pp 149-154, July 1964.

3. Chang, Y. H., and F. B. Tuteur, "Methods of Stochastic Approximation Applied to the Analysis of Adaptive Tapped Delay Line Filters", Yale Univ. Rpt. CT-17, Nov. 1967.

4. Freeman, H., <u>Discrete Time Systems</u>, John Wiley, 1965, p. 176.

5. Varga, R. S., <u>Matrix Iterative Analysis</u>, Prentice-Hall, 1962.

6. Bennet, W. R. and J. R. Davey, <u>Data Transmission</u>, McGraw-Hill, New York 1965.

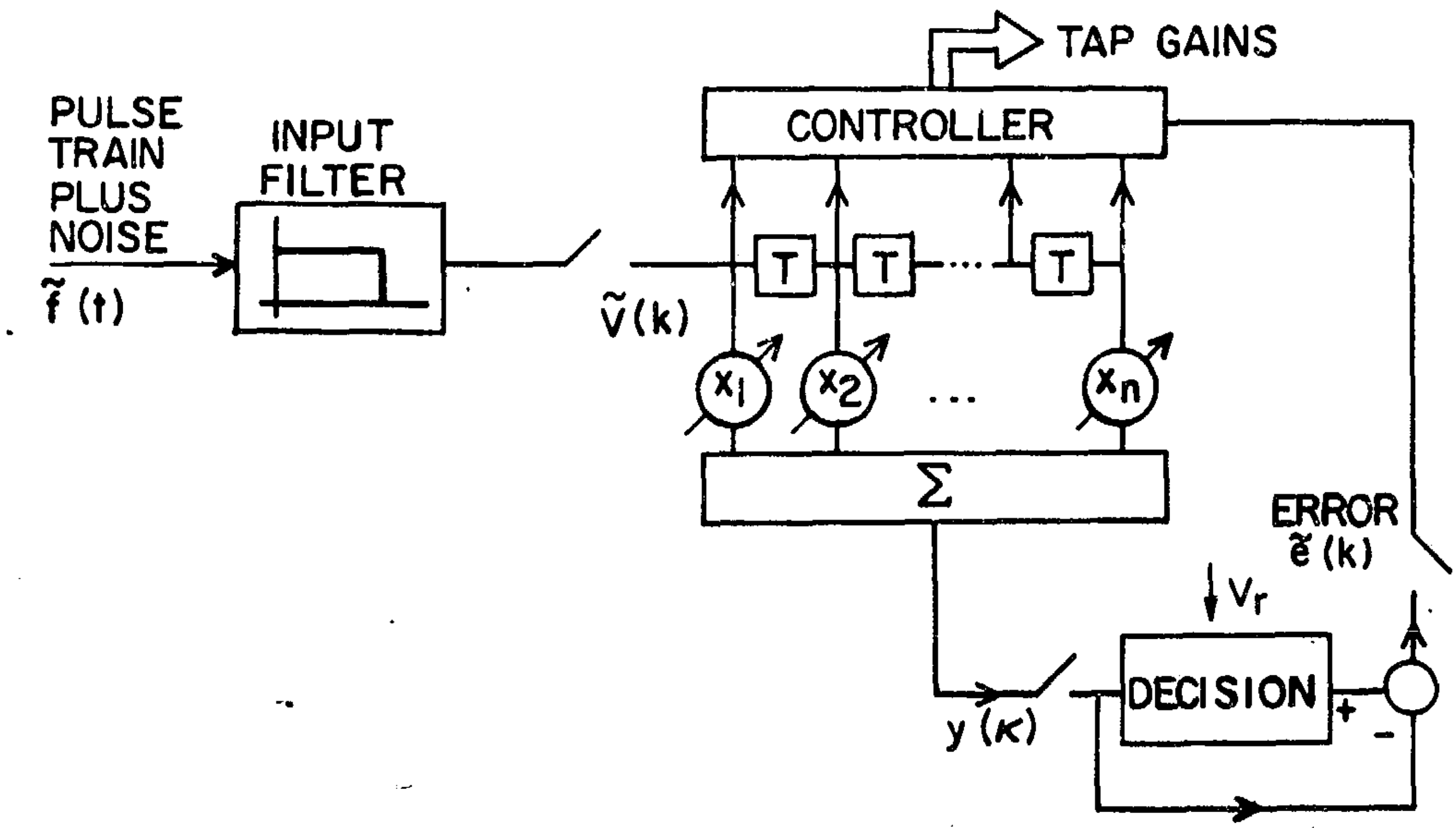

Fig. 1 Basic Equalizer

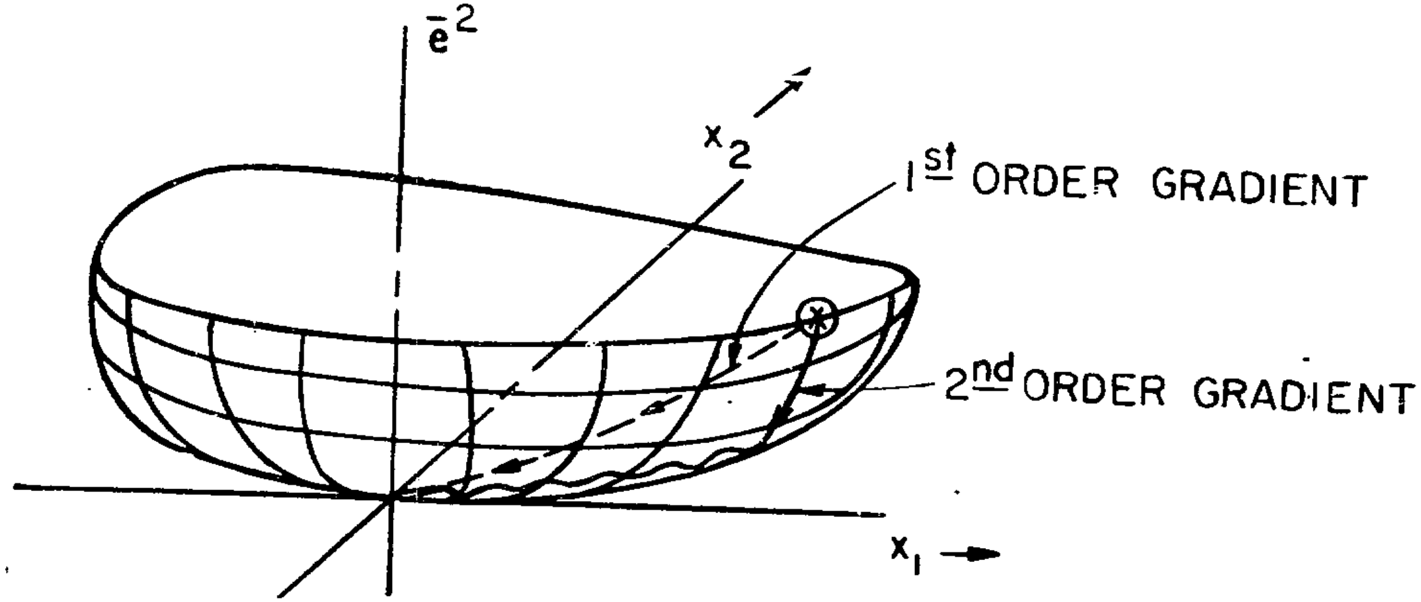

Fig. 2 Convex Surface with a Ridge

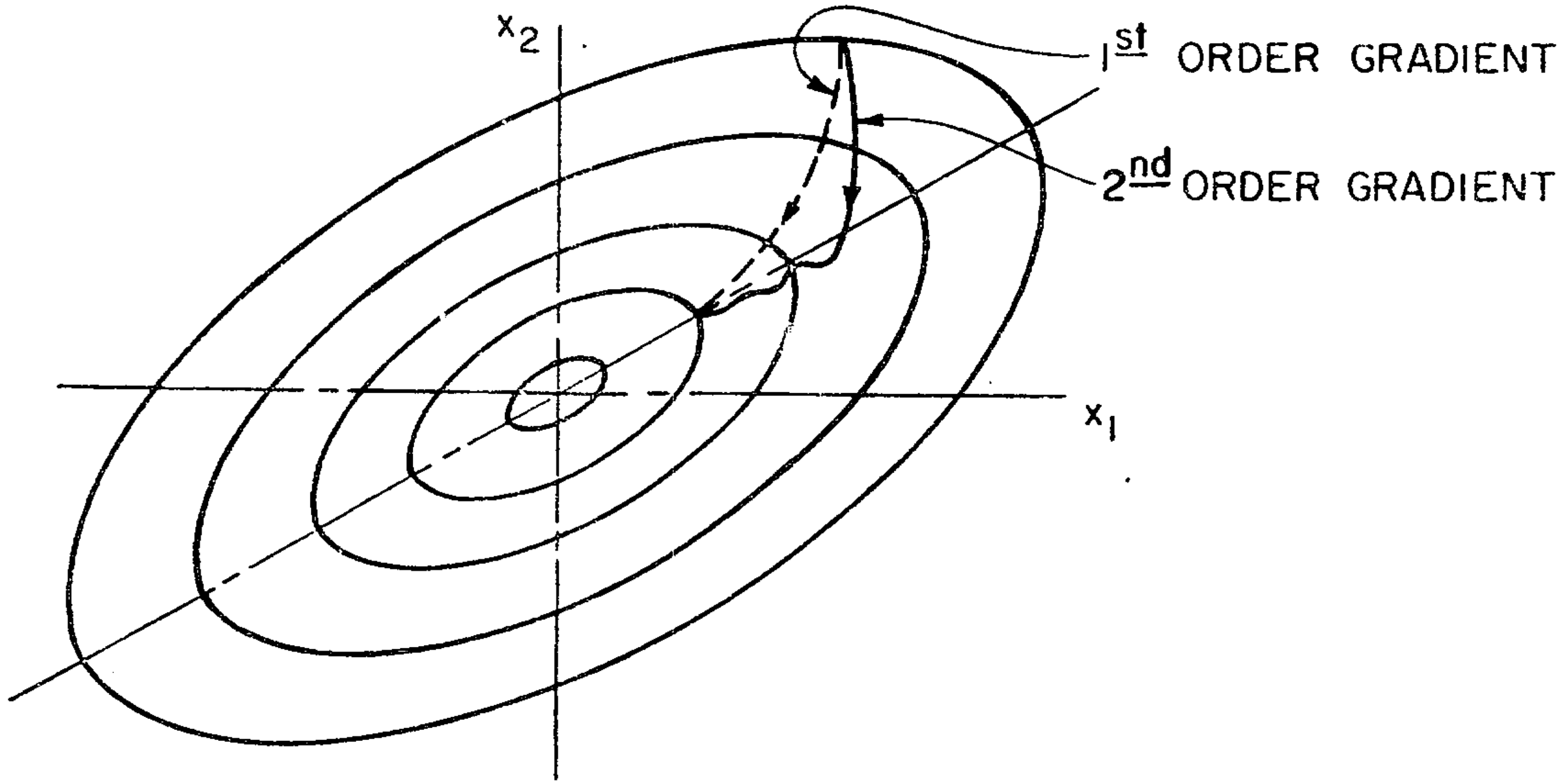

Fig. 3 Profiles of 1st and 2nd Order Gradient

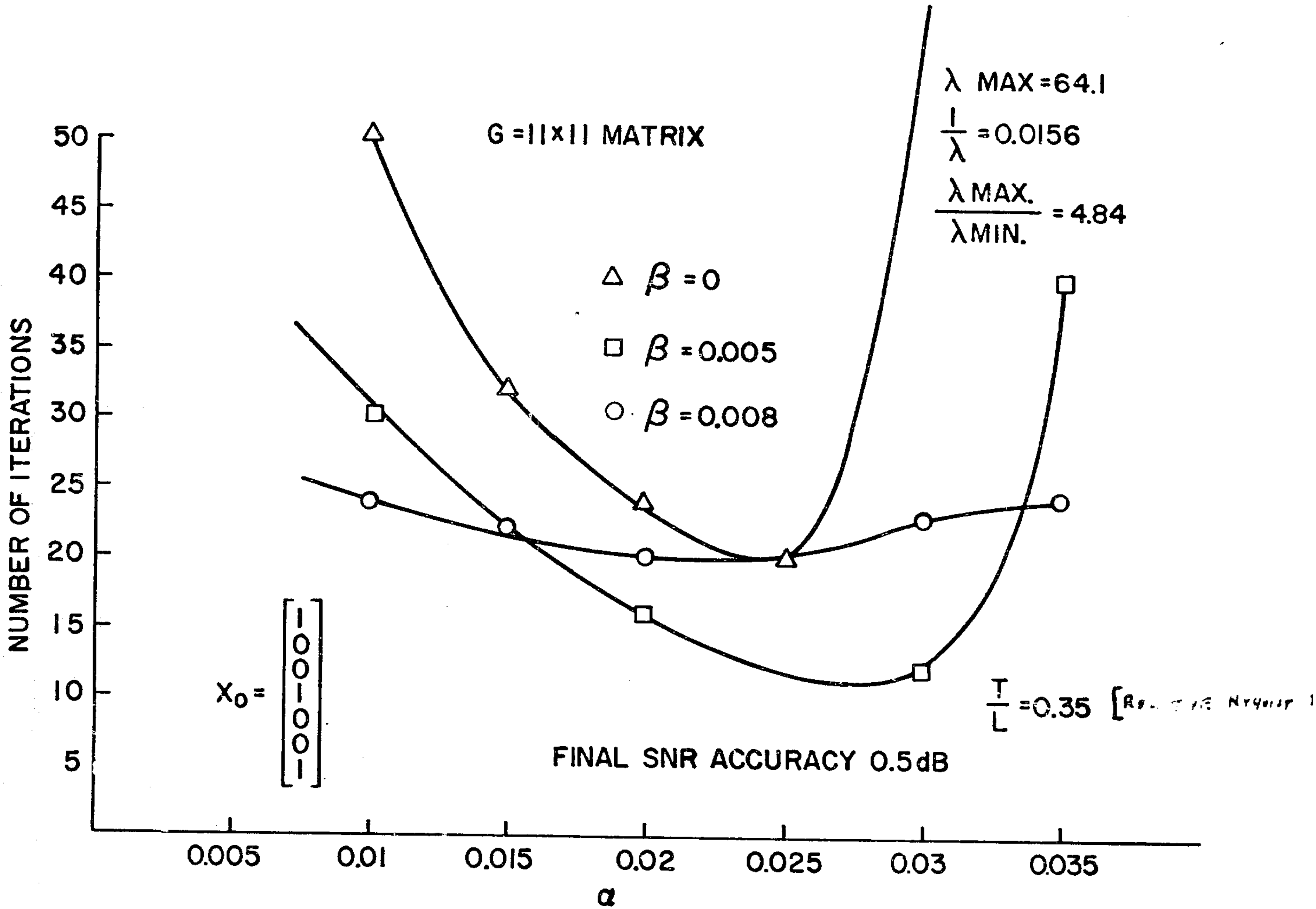

Fig. 4 Rates of Convergence; Moderate Distortion

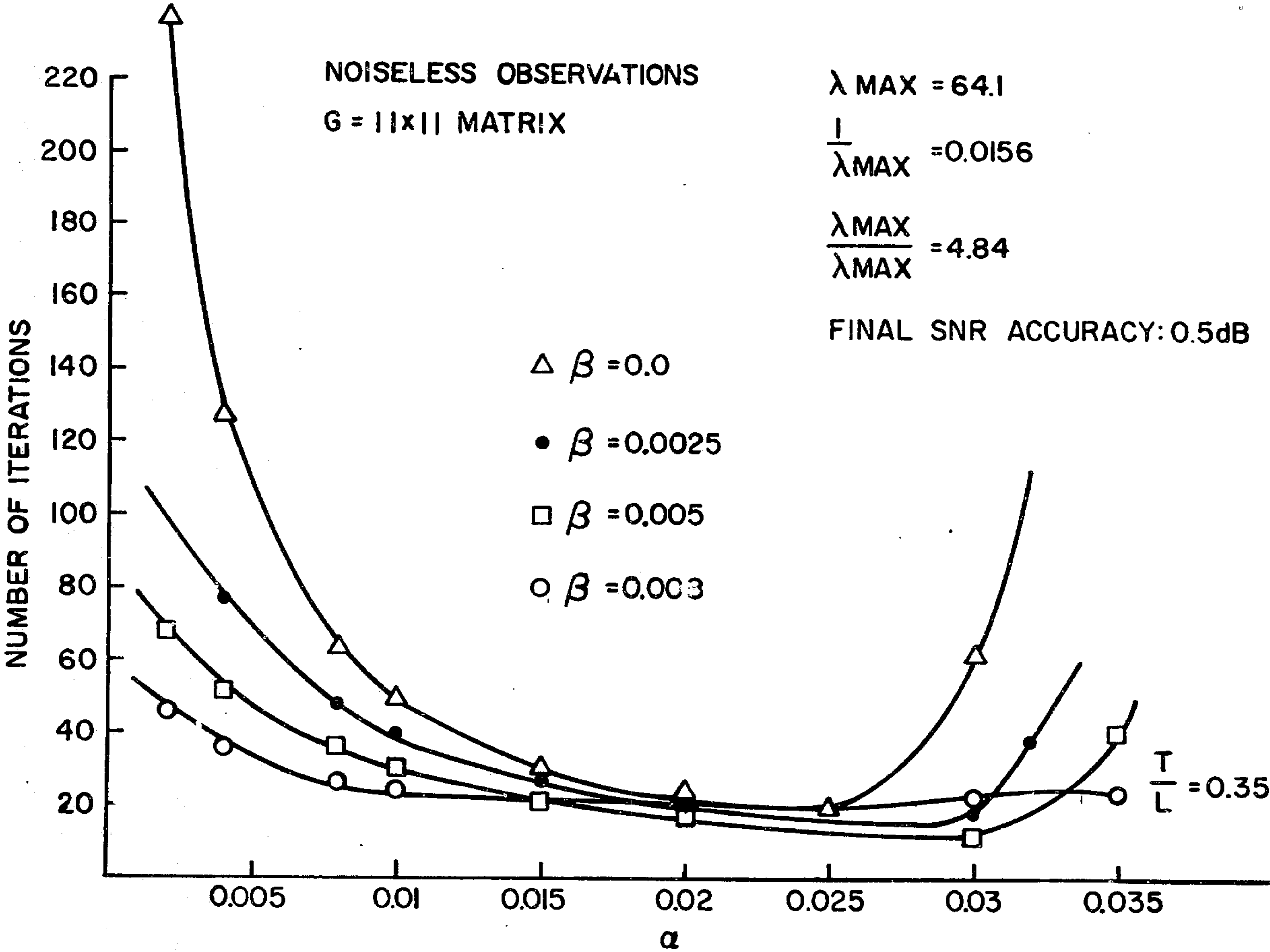

Fig. 5 Rates of Convergence; Moderate Distortion

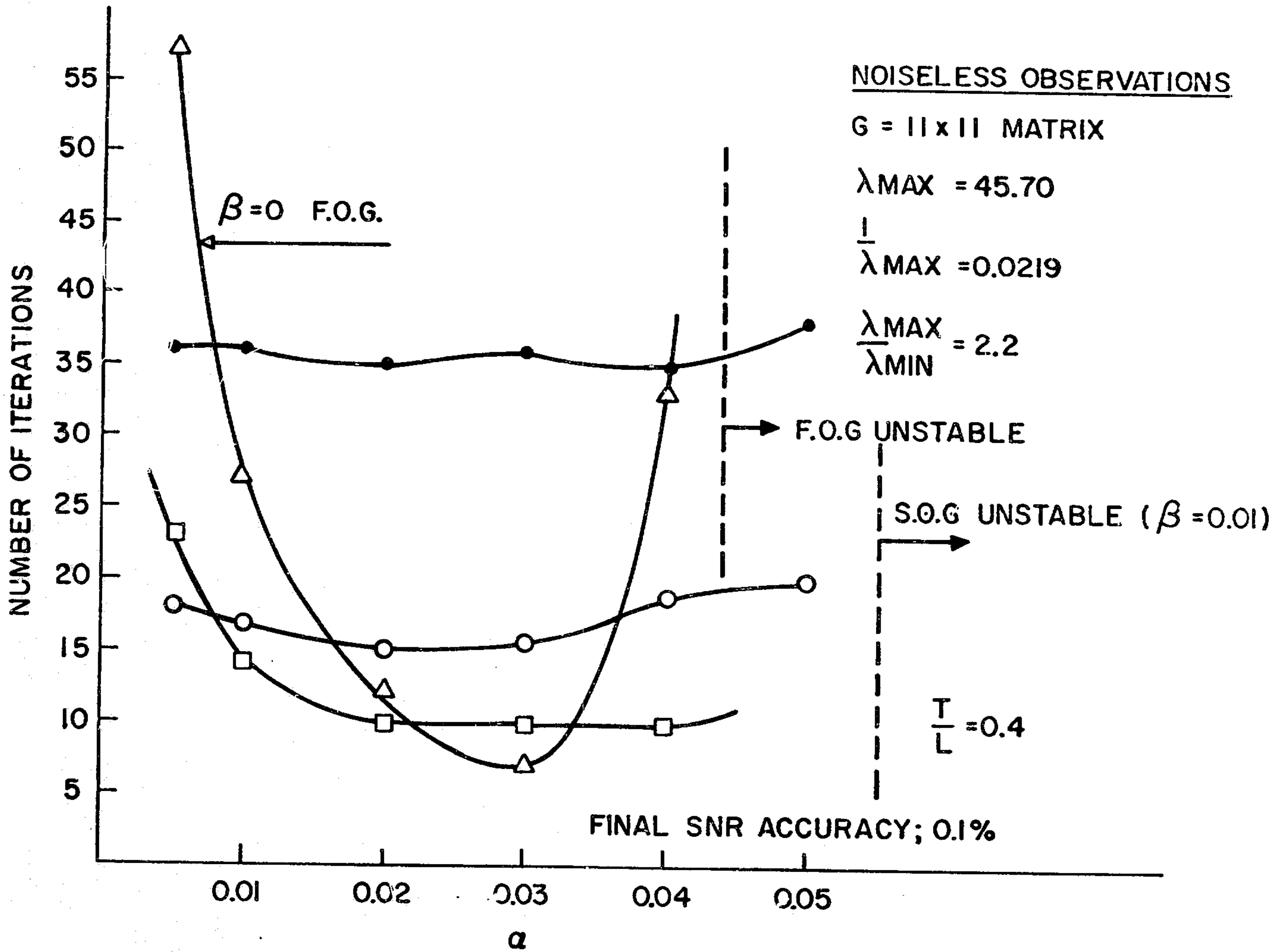

Fig. 6 Rates of Convergence; Small Distortion

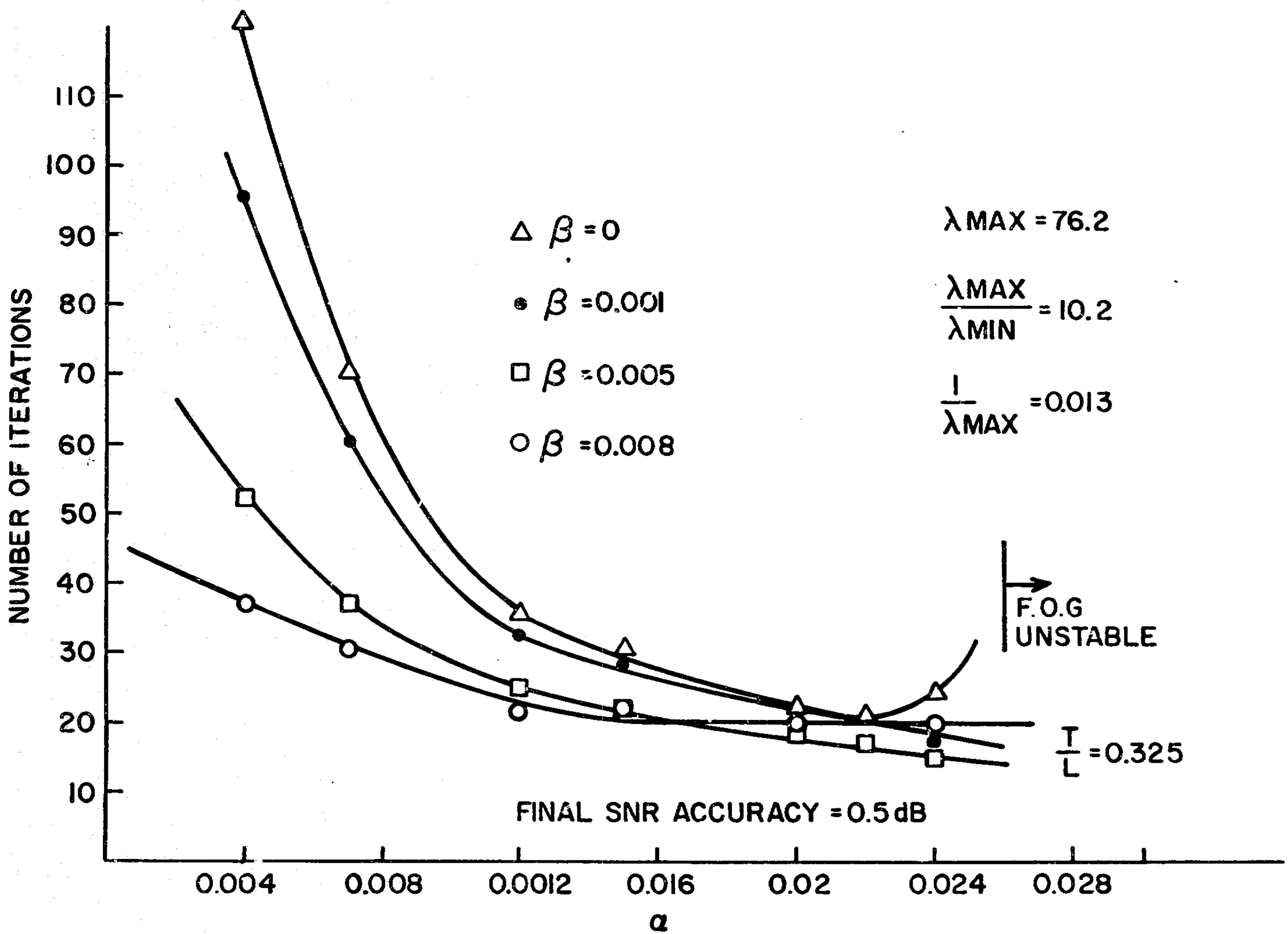

Fig. 7 Rate of Convergence; Large Distortion

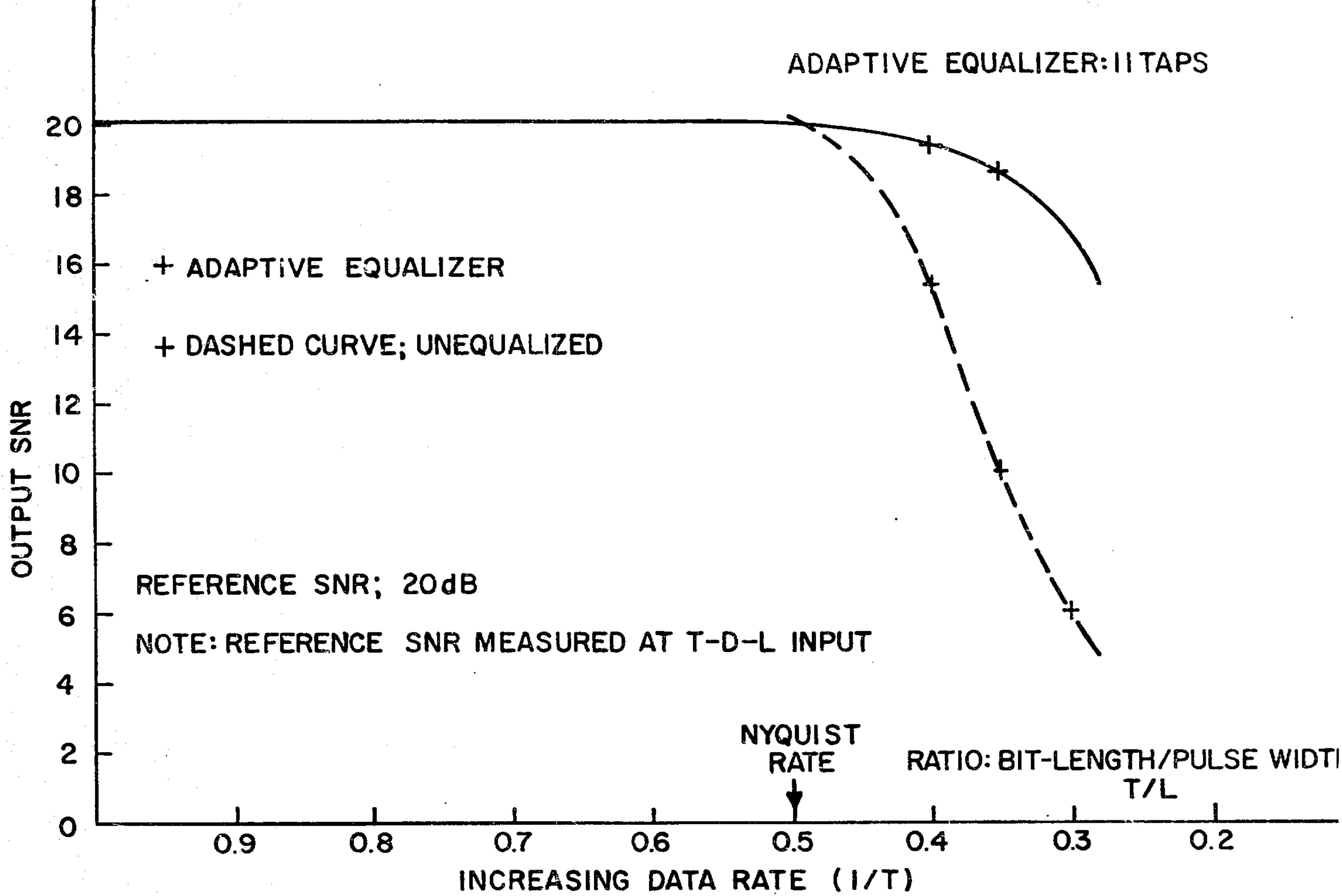

Fig. 8 Output SNR of Adaptive Equalizer and Matched Filter Equalizer

Papers Published

1. " Expected Number of Spikes in Phase Locked Loops", D. L. Schilling and P. Osborne, International Telemetering Conference, October 1968.

2. " Performance of Binary PSK Communication Systems, " D. L. Schilling and J. Oberst, International Telemetering Conference October 1968.

3. " Output Signal-to-Noise Ratio of an FM Discriminator with Nonideal Limiting, " D. L. Schilling and J. Refi, International Telemetering Conference, October 1968.

4. " Robust Detection Using Extreme Value Theory, " D. L. Schilling, L. Milstein and J. Wolf, IEEE Transactions on Information Theory, May 1969.

5. " Threshold Extension Using the FMFB", D. L. Schilling and E. Hoffman, ICC Conference Record, June 1969.